Beyond the Shikimate pathway: The novel role of photosynthetic electron transport in mediating hormesis and lethal responses to glyphosate

JON-PAUL ANTHONY DUNNE

Beyond the Shikimate pathway: The novel role of photosynthetic electron transport in mediating hormesis and lethal responses to glyphosate

Jon-Paul Anthony Dunne

Thesis Submitted for the Degree of Master of Science by Research in Biological Sciences

Supervisor: Dr. Steve Chivasa
Co-supervisor: Dr. Chris Greenwell

Department of Biosciences, Durham University

Submitted March 2022

Abstract

Glyphosate is the most widely used herbicide in agriculture, with a truly global market dominance. The existence of a range of glyphosate-resistant crops has led to a surge in glyphosate usage in countries where genetically modified crops are deregulated. This makes glyphosate a key environmental chemical pollutant sourced from agriculture and understanding its impact on non-target organisms is paramount. With this high level of usage, an inevitably increasing number of glyphosate-resistant weeds emerged over the past few decades. Therefore, there is pressing need to design appropriate countermeasures for controlling such weeds to protect food production systems. This requires a clear understanding of how glyphosate kills cells. Glyphosate inhibits the shikimate pathway, resulting in aromatic amino acid depletion and subsequent protein starvation. However, recent studies identified a clear link between glyphosate toxicity and exposure to high levels of light, suggesting that glyphosate-induced cell death involves mechanisms far more complex than imagined previously. This presents a key research question, what is the mechanism underpinning glyphosate toxicity? Remarkably, shikimate pathway-possessing organisms bereft of chloroplasts have very high glyphosate lethal dose concentration, in comparison to equivalent organisms with chloroplasts. Therefore, our group proposed the hypothesis that glyphosate inhibition of the shikimate pathway activates cell death through generation of damaging reactive oxygen species (ROS) triggered by constricting photosynthetic electron transport (PET) in the presence of light. To test this hypothesis, we used two model organisms (*Synechocystis sp.* PCC 6803 and *Chlamydomonas reinhardtii* CCAP 11/32B) to evaluate the impact of glyphosate on cell growth. Growth assays revealed two distinct responses to glyphosate viz. (i) hormesis, characterised by activation of growth at sublethal glyphosate concentrations and (ii) growth arrest and cell death at lethal doses. Crucially, whether cells responded by hormesis or cell death was controlled by the presence of as yet unidentified extracellular signals secreted by cells into the growth medium. To unravel the molecular basis for the hormetic and lethal responses, a global proteomic analysis of glyphosate-treated *Synechocystis* cells was conducted using isobaric tags for relative and absolute quantitation (iTRAQ) technology. This highlighted the key proteins differentially-expressed in the two responses. Gene ontology analysis revealed that a majority of the identified proteins are photosynthetic proteins located in thylakoids. The overall pattern emerging from the protein data is that the lethal response was associated with a collapse in the abundance of key components of the electron transport chain, while in hormesis the same components remained unaffected or were increased. Furthermore, the protein profile in the hormetic response was consistent with redirecting fixed carbon away from the inhibited shikimate pathway to re-establish photosynthetic electron transport flow to prevent reduction of O_2 and ROS generation. This study has revealed the light driven mechanism of glyphosate toxicity. This entails excessive ROS generation by the photosystems regulated by complex metabolic feedback signalling centred around reconfiguration of metabolite distribution from the Calvin-Benson cycle. The implications of this research are 3-fold. First, redirecting Calvin-Benson cycle metabolites to alternative pathways constitutes a viable escape from toxicity and may be a potential mechanism of glyphosate resistance in agriculture. Secondly, hormesis driven by secreted extracellular signals could be the basis for pollution-induced algal blooms, which have far-reaching environmental consequences. Finally, these results could be exploited in industrial algal cultivation to generate biomass for commercial applications.

Table of Contents

List of Figures

List of tables

List of abbreviations

µg	Microgram
µL	Microlitre
µmol	Micromolar
1,3-BPGA	1,3-bisphosphoglycerate
^{1}Chl*	Excited state chlorophyll
2PG	2-phosphoglycolate
^{3}Chl*	Triplet state chlorophyll
3GP	Glycerate 3-phosphate
3OC12-HSL	N-3-oxododecanoyl homoserine lactone
3-PGA	3-Phosphoglyceric acid
ABC	ATP binding Cassette
ACAC	Acetyl coenzyme-a carboxylase
ACCase	Acetyl coenzyme a carboxylase
ACN	Acetonitrile
ADP	Adenosine diphosphate
Ald	Aldolase
AMPA	A-amino-3-hydroxy-5-methyl-4-isoxazolepropionic acid
ANOVA	One-way analysis of variance
APCB	Allophycocyanin beta chain
ARTO	Alternative respiratory terminal oxidase
ATP	Adenosine triose phosphate
ATPβ	ATP synthase beta subunit
B_6	Vitamin B_6
BEH	Ethylene bridged hybrid
BG_{11}	Blue green
BLAST	Basic local alignment search tool
BSA	Bovine serum albumin
C4-HSL	N-butanoyl-L-homoserine lactone
c_6	Cytochrome c_6
C8-AHL	N-octanoyl-homoserine lactones
CAT	Catalase
CC	Cellular Component
CcmK	Carbon dioxide-concentrating mechanism protein
cDNA	Complementary DNA
CHAPS	3-((3-cholamidopropyl) dimethylammonio)-1-propanesulfonate
CI	Chloroform:Isoamylalcohol
CID	Collision-induced dissociation
CoA	Coenzyme-A
COX	Cytochrome C oxidase
CS	Chorismate synthase
CUR	Curtain gas
cyd	Cytochrome d
Cyt	Cytochrome
DAHP	3-deoxy-d-abarino-heptulosonate-7-phosphate
DAHPS	3-deoxy-d-abarino-heptulosonate-7-phosphate synthase
DHQ	3-dehydroquianate dehydratase

DHQS	3-dehydroquianate synthase
DMSO	Dimethyl sulfoxide
DNA	Deoxy-ribonucleic acid
DNase	Deoxyribonuclease
e^-	Electron
E4P	Ethyrose-4-phosphate
EDTA	Ethylenediaminetetraacetic acid
$EDTANa_2$	Ethylenediaminetetraacetic acid disodium salt dihydrate
EPSP	5-enolpyurvylshikimate 3-phosphate
EPSPS	5-enolpyurvylshikimate 3-phosphate synthase
ESI	Electrospray ionization
F-1,6-BP	Fructose 1,6-biphosphate
F-6-P	Fructose-6-phosphate
FBPase	Fructose 1,6-biphosphatase
Fd	Ferredoxin
Fe-SOD	Iron superoxide dismutase
Flv	Flavodiiron
FNR	Ferredoxin-NADP reductase
FQR	Ferredoxin-PQ reductase
FRP	Fluorescence recovery protein
FtsH	ATP-dependent zinc metalloprotease
FUM	Fumarate
g	Gravitational force equivalent
G3P	3-phosphoglycerate
GADPH	Glyceraldehyde 3-phosphate dehydrogenase
GC	Guanine or cytosine
GO	Gene ontology
h	Hour
H_2ase	Hydrogenase
HILIC	Hydrophilic interaction liquid chromatography
HSD	Tukey's honestly significant difference
HTL	Hydrothermal liquefaction
hv	Energy
iTRAQ	Isobaric Tags for Relative and Absolute Quantification
kDa	Kilodalton
LasR	Transcriptional activator protein lasr
LC-MS	Liquid chromatography-mass spectrometry
m	Metres
M	Molar
m/z	Mass/charge
ME	2-mercaptoethanol
mg	Milligram
min	Minute
mL	Millilitre
mM	Millimolar
mm	Millimetre
MMTS	Methyl methanethiosulfonate

MOPS	3-(n-morpholino)propanesulfonic acid
MS	Mass spectrometry
MS-MS	Tandem mass spectrometry
MTT	3-(4,5-dimethylthiazol-2-yl)-2,5-diphenyltetrazolium bromide
NAD^+	Oxidised Nicotinamide adenine dinucleotide
NADH	Reduced Nicotinamide adenine dinucleotide
$NADP^+$	Oxidised Nicotinamide adenine dinucleotide phosphate
NADPH	Reduced Nicotinamide adenine dinucleotide phosphate
NCBI	National Centre for Biotechnology Information
NDH	NAD(P)H-quinone oxidoreductase
NDH1	NAD(P)H-quinone oxidoreductase subunit I
nm	Nanometres
nM	Nanmolar
NPQ	Non-photochemical quenching
OCP	Orange carotenoid-binding protein
PC	Plastocyanin
PCI	Phenol:Chloroform:Isoamylalcohol
PCR	Polymerase chain reaction
PET	Photosynthetic electron transport
PETC	Photosynthetic electron transport chain
PetC2	Cytochrome b6-f complex iron-sulphur subunit 2
PGK	3-Phosphoglyceric acid Kinase
PHB	Polyhydroxybutyrate
PPase	Inorganic pyrophosphatase
PQ	Plastoquinone
PQH_2	Plastoquinol
PRK	Phosphoribulokinase
pro-AIP	Precursor autoinducing peptides
PRPPK	Ribose-phosphate pyrophosphokinase
PRX	Peroxidase
PsaA	Photosystem I P700 chlorophyll a apoprotein A1
PsaF	Photosystem I reaction centre subunit III
PsbE	Cytochrome b559 subunit alpha
p-value	Probability value
qPCR	Quantitative polymerase chain reaction
Qtrap	Quadrupole linear ion traps
R-5-P	Ribose-5-phosphate
RBCL	Rubisco large subunit
RBCS	Rubisco small subunit
RNA	Ribonucleic acid
RPE	Ribose-5-phosphate Epimerase
RPI	Ribose-5-phosphate isomerase
RRM	RNA recognition motif
rRNA	Ribosomal ribonucleic acid
Ru-5-P	Ribulose-5-phosphate
Rubisco	Ribulose-1,5-bisphosphate carboxylase-oxygenase
RuBP	Ribulose-1,5-biphosphate

s	Seconds
S-7-P	Sedoheptulose-1,7-bisphosphate
SAM	S-adenosylmethionine
SBPase	Sedoheptulose-1,7-bisphosphatase
SD	Standard deviation
SDH	Succinate dehydrogenase
SDH2	Succinate dehydrogenase Fe-S subunit
SDS	Sodium dodecyl sulphate
SDS-PAGE	Sodium Dodecyl Sulphate-polyacrylamide gel electrophoresis
SPE	Solid phase extraction
SPSS	Statistical Product and Service Solutions
SUC	Succinate
TAE	Tris-acetate-EDTA
TCA	Tricarboxylic acid
TCEP	Tris(2-carboxyethyl)phosphine
TEM	Transmission electron microscopy
TK	Transketolase
TM	Thylakoid membrane
TNA	Total nucleic acid
Tris	Tris(hydroxymethyl)aminomethane
Tris-HCL	Tris(hydroxymethyl)aminomethane hydrochloride
UV	Ultraviolet
V	Volt
w/v	Weight/volume ratio
Xyl-5-P	Xylulose-5-phosphate
YbjN	Putative sensory transduction regulator

Declaration

I declare that the material contained in this thesis has not been previously submitted, in whole or in part, for a degree in Durham University or any other institution. Except where states otherwise by reference or acknowledgment, the work presented is entirely my own and supervisor's which has been generated by us as the result of original research.

Statement of Copyright

Acknowledgements

I would like to express my deepest gratitude to my supervisor Dr Steve Chivasa (PhD) who not only took a chance by offering me this project despite the change of field. But also provided me with invaluable research skills and helped me become a better scientist. I am deeply thankful to him for readily incorporating my own ideas into our research which helped shape this project and the conclusions drawn from it.

I am deeply thankful to Professor Chris Greenwell (PhD) for being a great Co-Supervisor and helping to arrange this research opportunity. I would also like to thank the all the academic staff and fellow researchers within Durham Biosciences department who have helped shape my ideas and provided feedback on my work and research progress.

Thanks to Dr Adrian Brown (PhD) and Dr Rachael Dack (PhD) for collaborating with this project and carrying out the iTRAQ and mass spectrometric analysis respectively.

Special thanks to Annabel Hollins, an excellent lab technician and good friend who not only assisted in my learning and lab work but was also a pillar of support throughout this project.

I would also like to give special thanks to all the friends and family who've supported me during my course throughout this tumultuous period. Especially those who were in my support bubble throughout the pandemic.

Dedication

This work is dedicated to my dear departed mother, Susan Dunne.

1.0 Introduction and literature review

1.1 Introduction

Innovations in plant biotechnology and the development of agrochemicals, such as chemical fertilisers and pesticides, have enabled the production of vast amounts of crops which improve food security and support numerous economically important global value chains (Kovalenko & Ulez'ko, 2020). Herbicidal active ingredients are an important part of modern chemical technologies used in farming, and glyphosate based herbicides have been the global market leader (Duke & Powles, 2008). The use of glyphosate in products such as Roundup and Touchdown (Monsanto-ag., 2019) has played a positive role in the current global transition to lower tillage farming methods, which has contributed to lowering soil erosion (Benbrook, 2016; Perry et al., 2016). This has established it as the dominant herbicide active ingredient in 21st century agriculture. In 2014 global glyphosate usage had risen almost 15-fold after the introduction of resistant transgenic crops in 1996. The usage of glyphosate-based herbicides has been so essential in modern industrialised agriculture that it represented over 70% of herbicide usage in the USA's soybean production in 2014 (Benbrook, 2016). However, the use of glyphosate is under threat for two main reasons. Firstly, because of emerging concerns regarding the impacts of glyphosate on both the environment and human health. Secondly, because of the emergence and spread of glyphosate-resistance in weeds (reviewed in Heap & Duke, 2018).

Although there is no conclusive data on the effects of glyphosate on human health, glyphosate has been shown to alter gut microbiomes in rats due to shikimate pathway inhibition (Mesnage et al., 2019). This effect could also occur in human gut microbiomes, as many human gut microbes appear to have sensitivity to glyphosate (Mesnage & Antoniou, 2020). Glyphosate's main degradation product α-amino-3-hydroxy-5-methyl-4-isoxazolepropionic acid (AMPA) along with several adjuvants present in glyphosate-based herbicides, have been demonstrated to possess harmful qualities in various organisms, both independently and in various combinations (Séguin et al., 2017; Mesnage et al., 2013). As an environmental pollutant, glyphosate usage has increased rapidly to a level that can influence the free phosphorus content of soils and freshwater via its degradation products (Hébert, Fugère & Gonzalez, 2019). The true scale of the impact glyphosate-derived P has on ecosystems remains uncertain.

The efficacy of glyphosate and other herbicides is being eroded by development of resistance in weeds. Understanding the mechanisms of herbicide phytotoxicity and generally how biological systems respond and adapt to xenobiotics is crucial in developing strategies to overcome herbicide resistance. There is currently a very limited number of new compounds in the research and development pipelines of major agrochemical companies (Sparks & Lorsbach, 2017), necessitating the search for countermeasures to overcome herbicide resistance. Naturally sourced alternatives could be utilised as herbicides if the mechanisms of synthetic herbicide lethality were better understood. While aromatic amino acid starvation caused by inhibition of the shikimate pathway has been broadly accepted as the mechanism of glyphosate phytotoxicity, our laboratory generated evidence indicating that this may not be the case at the recommended glyphosate field application rates (Chivasa, personal communication). Therefore, this project was initiated to investigate the

mechanisms of glyphosate toxicity using unicellular photosynthetic model microorganisms - *Synechocystis* and *Chlamydomonas reinhardtii*. Because these organisms are naturally abundant in fresh water and marine environments, the results obtained in the research could be extrapolated to the potential impact of glyphosate on the aquatic environment.

This literature review chapter first explores the environmental impact of glyphosate to provide a broad overview of off-target consequences of the herbicide beyond its agricultural use. This is particularly significant given that the research organisms (*Synechocystis* and *Chlamydomonas reinhardtii*) are used for environmental monitoring purposes. This is followed by a review of the biochemical and metabolic impacts of glyphosate inhibition of the target shikimate pathway to contextualise the proposed experiments. As application of herbicides aims to inhibit weed growth or kill weeds, how glyphosate affects photosynthesis across many organisms is discussed. Given that our preliminary findings suggest that the mechanism of glyphosate phytotoxicity is not aromatic amino acid starvation, alternative non-shikimate pathway targets of glyphosate reported in different organisms are discussed prior to setting out the hypothesis and specific objectives of this project.

1.2 Glyphosate in the environment

Monsanto has denoted glyphosate as an "environmentally benign herbicide", stating on their website that the shikimate pathway only occurs in plants and microorganisms, thereby not affecting "higher lifeforms such as mammals, birds, fish and insects" (Monsanto-ag, 2019). This statement however does not account for possible glyphosate effects on shikimate pathway-possessing organisms in the surrounding ecosystems. It has been reported that glyphosate has both a high sorption and retention, and low mobility in clay and loam soils (Okada et al., 2016; Ortiz et al., 2017). Despite this its effects are widespread, as glyphosate and its metabolite AMPA have been found frequently in both US and South American soils, surface water, ground water, blown material and precipitation (Vera et al., 2010; Battaglin et al., 2014; Berman et al., 2018). Glyphosate's strong adsorption to clay soils can cause it to accumulate over time, particularly in colder areas with non-acidic soils (Bento et al., 2016; Crick, 2016). Its degradation product AMPA, is also known for being toxic to earthworms (Domínguez et al., 2016).

AMPA dissolves in water during heavy precipitation and travels into riparian groundwater in urban catchments (Van Stempvoort et al., 2014). The degradation of glyphosate and its competitive adsorption to soil can also increase the level of PO_4^{3-} being exported to freshwater (Hébert et al., 2019) (Figure 1). Glyphosate accumulation can also make non-target plants more susceptible to disease, increasing the level of soil-borne pathogens, thus posing a threat to newly planted glyphosate-resistant crops (Hammerschmidt, 2018; Kao et al., 2019). Glyphosate can even be spread via manure (Muola, 2020), potentially resulting in exposure of pastoral land to glyphosate if cattle are fed glyphosate-treated crops. A study by Druille et al. (2013) found arbuscular mycorrhizal fungi, which assist plants in acquiring important minerals and micronutrients, had their spore viability and root colonisation negatively impacted by glyphosate, demonstrating an overall negative effect of glyphosate on clay/loam soil ecosystems.

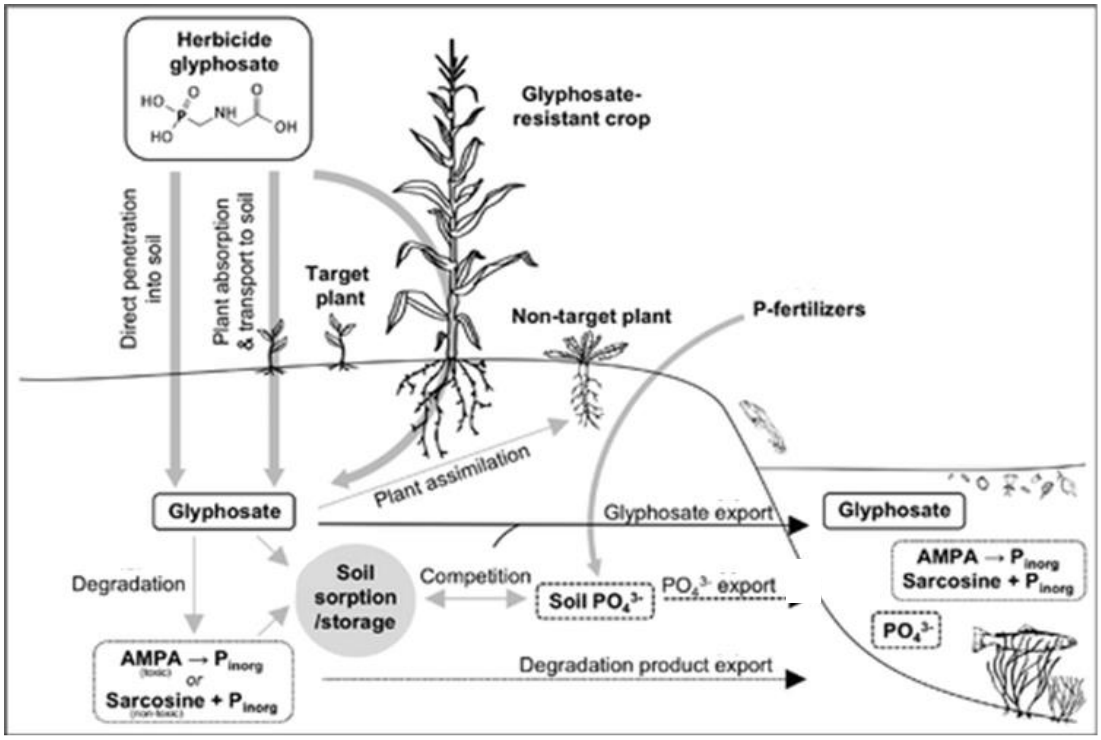

Figure 1.1. Schematic diagram showing the transport and degradation of glyphosate through the soil into freshwater ecosystems. Adapted from Hébert er al. (2019).

In sandy soils, glyphosate rapidly washes out, causing it to travel into surrounding areas via runoff and throughflow, such as wetlands and other water bodies (Liang et al., 2020). This can significantly reduce the biomass and productivity of algae, periphyton and macrophytes of exposed areas (Sura et al., 2012; Vera et al., 2012). These are important indicators for freshwater ecosystem health (Wu et al., 2017), and the effects may be exacerbated by the fact that glyphosate can accumulate in biofilms, increasing concentration by magnitudes of 2 or 3 compared to the surrounding water (Beecraft & Rooney, 2021). Glyphosate and its associated herbicides can alter aquatic ecosystems in a similar manner to how it alters gut microbiomes. Cyanobacteria and microalgae have a long-established high glyphosate tolerance (Fernández et al., 2021), with many species able to metabolise it (Forlani et al., 2008; Powell et al., 1991). However, this resilience is not evenly distributed among microorganisms. This can in turn cause an imbalance in ecosystems as less tolerant organisms, such as brown algae and diatoms, may not die directly from glyphosate treatment but will instead be outcompeted by more glyphosate tolerant cyanobacteria and green algae (Sylwestrzak et al., 2021). This effect would be further exacerbated if cyanobacterial growth is already boosted by the eutrophication of phosphate and nitrogen-based compounds that are currently sourced from agricultural run-off (Chakraborty et al., 2017; Carvalho, 2013).

Glyphosate and AMPA have even been documented in estuaries (Skeff et al., 2015), posing a potential threat to coastal and marine life. Glyphosate is known to harm non-photosynthetic marine organisms, studies of which often use mussels as a model organism for marine fauna due to their diet of microalgae, a foundational organism in the marine ecosystem. Golden mussels (*Limnoperna fortunei*) that were exposed to commercial formulation of glyphosate with surfactants via contaminated microalgae (*Scenedesmus vacuolatus*) showed significant increase in alkaline-phosphatase activity after 21 days, likely

in response to the accumulation of an organophosphate (glyphosate) in their haemolymph and hepatopancreas (Lummato, 2018). The mechanism which triggers this response is unclear though alkaline phosphatase has been closely linked to the immune response of bivalves (Lummato, 2018). In a different mussel species *Mytilus galloprovincialis*, glyphosate was shown to increase haemolymph pH and decrease circulating Haemocyte (immune cell) count after 7 days exposure and lower Haemocyte membrane stability (Matazzo, 2018). This phenomenon could play a role in altering the immune response across species.

A similar trend was found across honeybees in which glyphosate exposure altered the expression of genes associated with the adaptive immune system as well as altering the composition of the gut microbiota, in which *Snodgrassella alvi* was almost entirely wiped out (Castelli et al., 2021). This microbe colonises the ileum and modulates the honeybee immune system (Kwong et al., 2017). The microbiome is now being recognised as an important component of adaptive immune response and homeostasis in animals (Gopalakrishnan et al., 2018; Honda and Littman, 2016). Glyphosate in conjunction with AMPA was able to significantly reduce the total bacterial load of the *Mytilus galloprovincialis* gut microbiome after 7 days exposure (Lori et al., 2020). Species richness, measured in 16s RNA analysis, was affected across all treatments with members of the Vibrio genus increasing their dominance upon treatment. Once again demonstrating the varied effects of glyphosate on organisms with differing tolerance (Lori et al., 2020). Glyphosate can also be adsorbed by microplastics which then adsorb onto, and accumulate on, microalgae cell walls, resulting in toxicity further up the food web (Zhang et al., 2018). Glyphosate has also been shown to stimulate toxin release, as well as the release of other intracellular contents in *M. aeruginosa,* which could in turn pose an additional threat to surrounding organisms (Yu et al., 2021; Wu et al. 2016).

The additional abiotic stresses posed by glyphosate have also been linked to an altered immune response and a rise in opportunistic bacteria in gut microbiomes observed in honeybees and rats (Castelli et al. 2021; Mesnage et al., 2019). This phenomenon can be observed on the terrestrial ecosystem level in glyphosate-treated fields and woodland soils (Kao et al., 2019; Hammerschmidt, 2018; Ratcliff et al., 2006). It is therefore possible that in a similar manner to how pathogens may colonise and dominate a weakened microbiome or terrestrial ecosystems, more resilient cyanobacteria or microalgae could dominate glyphosate-polluted aquatic ecosystems and trigger more frequent algal bloom events as result (Lurling and Rosselink, 2006). This phenomena has already been hypothesized for photosynthesis inhibiting herbicides. This becomes increasingly likely when factors such as climate change already boost the likelihood of bloom events (Paerl & Huisman, 2009). Agricultural run-off has long since been attributed to harmful algal blooms in marine ecosystems (Beman et al., 2005), however given the prevalence of herbicides in modern agriculture, perhaps it is time to consider the potential effects glyphosate may have on marine ecosystems. Therefore, studying the impact of glyphosate on microalgae and cyanobacteria could also provide important information on the fate and impact of glyphosate to the environment.

1.3 Glyphosate inhibition of the shikimate pathway

The primary metabolic pathway targeted by glyphosate is the shikimate pathway (Amrhein et al., 1980). This metabolically essential pathway remains relatively unaltered throughout all recorded species which utilise it, like plants and bacteria (Schmid & Amrhein, 1995; Tzin et al., 2012; Aristilde et al., 2017). This is what makes glyphosate so effective as a herbicidal active ingredient, as it can inhibit production of the pathway's key outputs; aromatic amino acids (Amrhein et al., 1980), folate (vitamin B_9), which is crucial in DNA synthesis and repair, plastoquionone, which transports electrons from photosystem II (PSII) to cytochrome b_6f complex, and enterobactin, a compound used for acquiring iron (Bongaerts et al., 2011; Figure 2). Unfortunately, surprisingly little research has been done on the effect of glyphosate in relation to these metabolites, other than aromatic amino acids. The shikimate pathway begins with the dephosphorylation of phosphoenolpyruvate (PEP) and condensation of ethyrose 4-Phosphate, which are then combined to form 7P-2-dehydro-3-deoxy-D-arabino-heptonate, in the shikimate pathway commitment reaction catalysed by 3-deoxy-d-abarino-heptulosonate-7-phosphate synthase (DAHPS) (Kloosterman, 2003). A series of dephosphorylation, dehydration and hydrogenation reactions catalysed by the enzymes 3-dehydroquianate synthase (DHQS), 3-dehydroquianate dehydratase (DHQ), shikimate 5-dehydrogenase (SDS) then occur sequentially to form the aromatic compound shikimate (Aristilde et al., 2017).

What follows is the chorismate-formation stage of the pathway. A phosphate group taken from ATP is added to shikimate's 3rd carbon atom via shikimate kinase to form shikimate 3-phosphate. The enzyme 5-enolpyurvylshikimate 3-phosphate (EPSP) synthase then cleaves a phosphate group from PEP and binds the pyruvate (enol-form) to shikimate 3-phosphate. Glyphosate acts as a molecular mimic of PEP, allowing it to competitively bind to EPSP synthase and inhibit EPSP production (Figure 1.2). This prevents the final stage of the

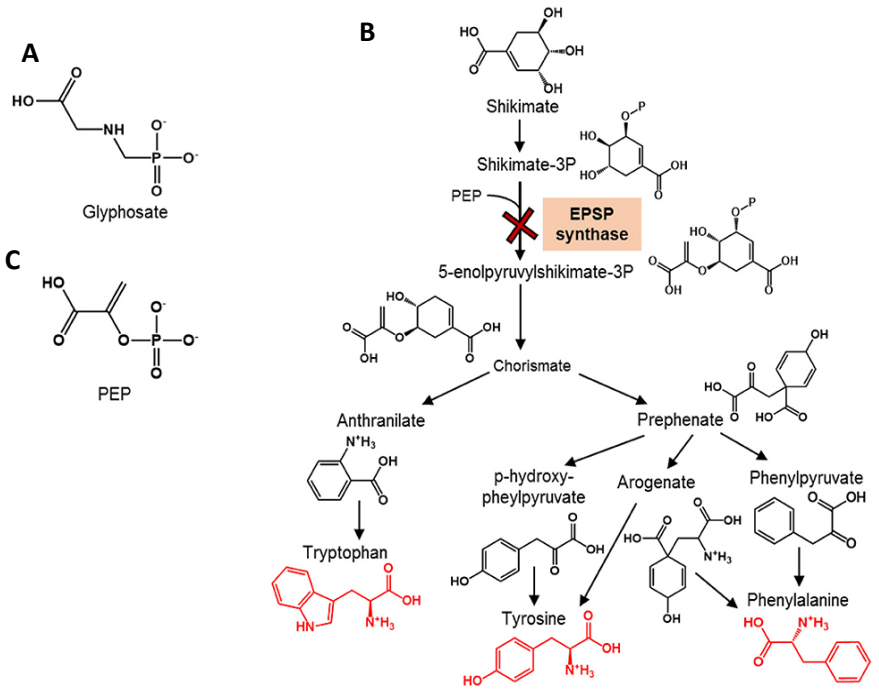

Figure 1.2. Glyphosate interaction with the shikimate pathway. (A) Chemical structure of glyphosate; (B) Site of glyphosate inhibition on the chorismate formation stage of the shikimate pathway; (C) Chemical structure of phosphoenolpyruvate (PEP). Red denotes aromatic amino acids. Taken from Aristilde et al. (2017*)*.

pathway, where chorismate synthase cleaves the remaining phosphate group to form chorismate. Chorismate is an important branch-point metabolite in autotrophs, as it is the precursor to aromatic amino acid synthesis and several other secondary metabolites, thus accounting for around 30% of the carbon fixed via photosynthesis (Tohge et al., 2013). Inhibition of the shikimate pathway by glyphosate is characterised by the accumulation of shikimic acid and other upstream metabolites (Steinrücken & Amrhein, 1980; Singh & Shaner 1998; Henry et al., 2007). Exposure of plants to pure glyphosate or commercially available formulations, such as Roundup and Touchdown, is attended by the cessation of growth and death of the treated plants. Furthermore, the breakdown product of glyphosate, AMPA is toxic across various non-target organisms (Bonnet et al, 2007; Domínguez et al., 2016) and directly interferes with biosynthesis of important plant and bacterial compounds (Gomes et al., 2016; Figure 2). A study on three *Escherichia coli* strains showed glyphosate- or AMPA-induced expression of proteins associated with iron uptake and responses to iron-limiting conditions (Stenger, 2019). It's possible therefore that other shikimate pathway products such as Enterobactin, which plays a role in iron uptake may play a role in glyphosates lethal mechanism then their production is limited.

1.4 Mechanisms of glyphosate resistance

The number and prevalence of glyphosate resistant weeds has increased dramatically in the past few decades. The threat posed by resistance to agriculture has led to extensive research of the underlying mechanisms. This has led to discovery of multiple methods of resistance, with the best understood relating to the EPSPS mutation or gene duplication. Several weed species have evolved more effective EPSPS active site alterations than what is operational in genetically modified crop specifies (Perrotti et al., 2019). For example, a biotype of Argentinian *Amaranthus hybridus* developed high resistance to glyphosate via a triple amino acid substitution (Perrotti et al., 2019). This strategy of resistance is not limited to plants, having been observed in some fungi. Members of the fungal genus *Acremonium* have displayed similar EPSPS active site mutations with multiple amino acid substitutions that confer very high resistance to glyphosate (Liu & Cao., 2018). Amplifying the number of EPSPS genes has evolved as a glyphosate resistance mechanism in several other weed species. This increases the concentration of glyphosate required to fully inhibit the shikimate pathway. This is a common method seen in prevalent glyphosate-resistant weeds, such as waterhemp (Dillon et al., 2017) and *Amaranthus palmeri* (Gaines et al., 2010), which has some resistant strains possessing over 160-fold more *EPSPS* gene copies.

Other modes of resistance not directly related to the EPSPS gene or enzyme have been reported. Certain weeds are able to utilise aldo-keto reductase enzymes in order to metabolise glyphosate, as is seen in deccan grass *Echinochloa colona* (Pan et al., 2019). Another important aspect of glyphosate resistance appears to be the cell wall, as was shown in a study on *Saccharomyces cerevisiae* (yeast) strains, in which resistant strains adapted to long term glyphosate exposure through the upregulation of genes related to cell wall thickening (Ravishankar et al., 2019). Demonstrating that resilience can easily be conferred by making it less easy for glyphosate to enter a cell. Organisms can also become resilient to glyphosate by transporting it either out of the cell or into a compartment, storage organ or vacuole (reviewed in Sammons and Gaines, 2014; Rong-Mullins et al., 2017). *Saccharomyces cerevisiae* has been shown to import glyphosate into cells using aspartic acid transport proteins and consequentially export it using ABC pleiotropic drug transport proteins, which in turn confers resistance when these proteins are respectively

up and down regulated (Rong-Mullins et al., 2017). Glyphosate-resistant *Conyza canadensis* (horseweed) rapidly sequesters glyphosate into the vacuole, thus avoiding chloroplast entry and inhibition of EPSPS (Ge et al., 2010).

Despite extensive research on glyphosate resistance in weeds, the full range of mechanisms is unknown. In five separate glyphosate resistant *Poa annua* (annual bluegrass) populations, EPSPS gene number amplification was identified as the mechanism of resistance in only one, while the mechanism in the other four remains enigmatic (Barua et al., 2019). These populations with unknown mechanisms of glyphosate resistance had previously displayed resistance to multiple herbicides with different modes of action, including PSII, acetolactate synthase, and acetyl coenzyme A carboxylase (ACCase) inhibitors (Barua et al., 2019). Glyphosate effectiveness in weed control is altered by both the time of application and the circadian rhythms of the plants (Mohr et al., 2007). Glyphosate is most effective when applied at dawn (Belbin et al., 2019). This indicates that exposure to light after application may increase the lethality of glyphosate and raises the need for analysis on glyphosates potential impacts on the photosynthetic apparatus.

Recent research has shown that prolonged incubation of glyphosate-treated plant tissues in the dark inhibits cell death (Van Horn et al., 2018; Chivasa & Gonzalez-Torralva, 2019). A study on glyphosate-resistant *Ambrosia trifida* demonstrated varying levels of resistance across phenotypes that were not associated with the EPSPS gene or enzyme, nor the rapid sequestration of glyphosate into a vacuole (Van Horn et al., 2018; Moretti et al., 2018). *Ambrosia trifida* exhibited a H_2O_2-associated rapid response to treatment which was energy dependent, stemming from either exogenous sucrose or light, and mitigated by the addition of aromatic amino acids (Moretti et al., 2018). Such a rapid response indicates that the mechanism of glyphosate-induced cell death does not stem from the inability to synthesise proteins. Instead, it implicates photosynthesis as a crucial factor (Geiger et al., 1986) and might be related to the production of reactive oxygen species (Moretti et al., 2018), pointing to a possible role of chloroplasts and photosynthetic systems in the lethal mechanisms of glyphosate.

1.5 Glyphosate stress on the photosynthetic machinery

Current research demonstrates several proteins and plant pigments required for photosynthesis are sensitive to glyphosate treatment, which is likely to be the cause of generation of reactive oxygen species (ROS) (Huang et al., 2012; Soares et al., 2020). In eukaryotic photosynthesis, the light-harvesting complexes (LHC) funnel photons into photosystem II (PSII) reaction centre to facilitate the water-splitting reaction. The P_{680} reaction centre of PSII is composed of a manganese cluster and the special protein pairs D1, D2, CP43 and CP47 (Vinyard et al., 2013). The light energy is used to produce $½O_2$, two protons and two electrons from H_2O. The electrons are transferred to plastoquinone (PQ) which forms plastoquinol (PQH_2), electrons are then transferred to the cytochrome b_6-f complex . PQH_2 is then oxidised and the electrons in the complex are used to pump one proton each into the thylakoid space, before being passed on to plastocyanin. Plastocyanin transports the electrons to photosystem I (PSI), which uses light energy to transfer them to ferredoxin in the stroma. The enzyme complex ferredoxin-$NADP^+$ reductase then cleaves electrons from ferredoxin to produce NADPH. Meanwhile, ATP synthase pumps protons out of the now excited thylakoid space to phosphorylate ADP, thus producing ATP (Figure 1.3). Both ATP and NADPH are essential energy carriers and electron doners in the reduction

phase of the Calvin-Benson cycle which converts 3-phosphoglycerate to the sugar G3P, a precursor to glucose and other organic compounds such as shikimate.

At higher or sudden increases in light intensity, the flow of electrons can cause ATP/NADPH supply to exceed demand from the Calvin-Benson cycle. Combined with the limited rate of PQH_2 oxidation by the cytochrome b_6-f complex, this can lead to diminished capacity of the electron transport chain to accommodate more electrons. As a result, excited reaction centre chlorophyll molecules (^{1}Chl*) will be converted to the triplet state (^{3}Chl*), which can release photon energy that alters the electron spin of O_2 forming singlet oxygen ($^1O_2$), an extremely damaging ROS. ROS accumulation is then intensified due to proton accumulation in the thylakoid space exceeding ATP production causing the lumen to acidify (Carbonera et al., 2012). This can cause proteins of specific LHCs, such as LHCSR (light harvesting complex stress related) to be protonated causing energy-dependent quenching (qE) to activate (Wobbe & Remacle, 2015; Tian et al., 2019). This protonation alters the positions of LHCs surrounding PSII, reducing the rate of energy transfer to the reaction centre. More light is thereby dissipated as heat, reducing $^1O_2$ production due to chlorophyll spending less time in its excited state (^{1}Chl*) (Wobbe & Remacle 2015; Tian et al., 2019)(Figure 1.3).

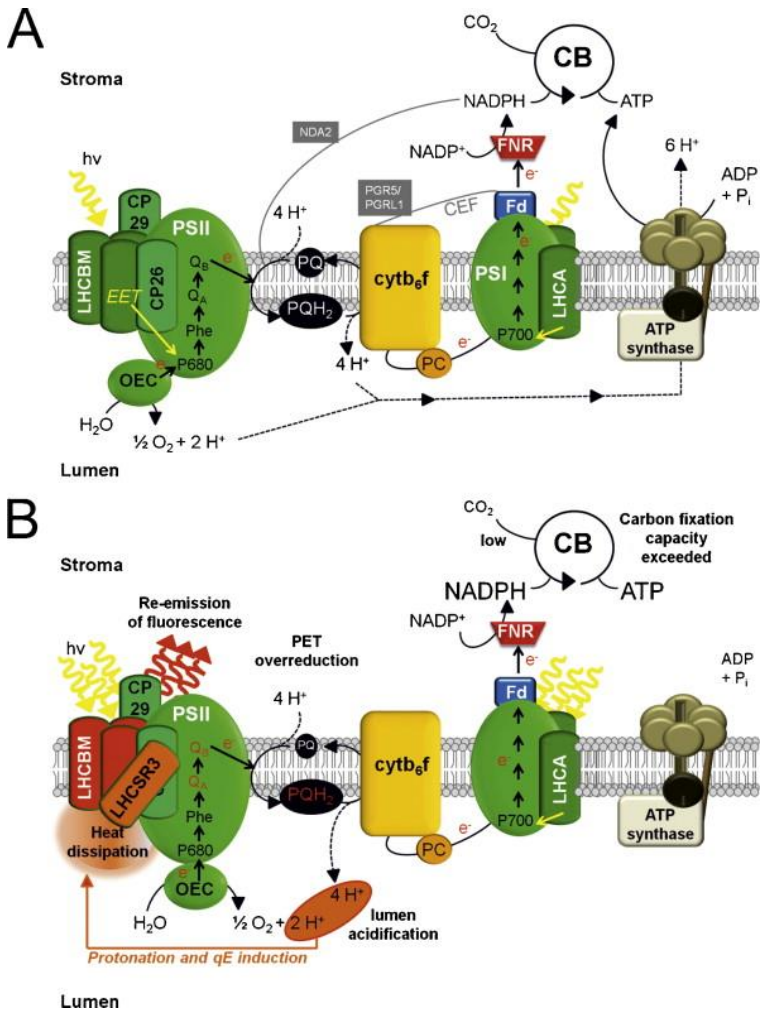

Figure 1.3. The photosynthetic electron transport chain of *Chlamydomonas reinhardtii* at: (A) sub-saturating light intensity; (B) over-saturating light intensity. Taken from Wobbe & Remacle (2015).

A similar response to sudden changes in light intensity also occurs in photosynthetic bacteria, albeit via a slightly different mechanism. Instead of LHC proteins being situated around the photosystem, Cyanophyta (Blue-Green algae) and Rhodophyta (red algae) possess antenna complexes known as phycobilisomes. The core of the phycobilisome is composed of phycobiliproteins, known as allophycocyanin, which are connected to the photosystem via a terminal pigment, which also transfers light energy to the attached photosystem. Situated on top of these proteins are chromophorylated proteins such as OCPs (Orange Carotenoid-binding proteins) and stacks of the phycobiliprotein phycocyanin connected via linker proteins. Rhodophyta antenna complexes additionally possess phycoerythrin. In response to sudden exposure to high light, the OCP photoprotective mechanism activates, where high irradiance stimulates photoconversion of OCP^o to its red active form (OCP^r), causing channelling of light energy to be diverted to it instead of the terminal pigment. The energy is subsequently dissipated as heat, a safe strategy to divert excess light energy away from the photosystems where damaging ROS can be synthesised. Regular light harvesting is restored by the fluorescence recovery protein (FRP), which is active in both light and dark conditions. This protein restores OCP^r to its inactive form OCP^o, thus resuming normal light harvesting capability (Figure 1.4).

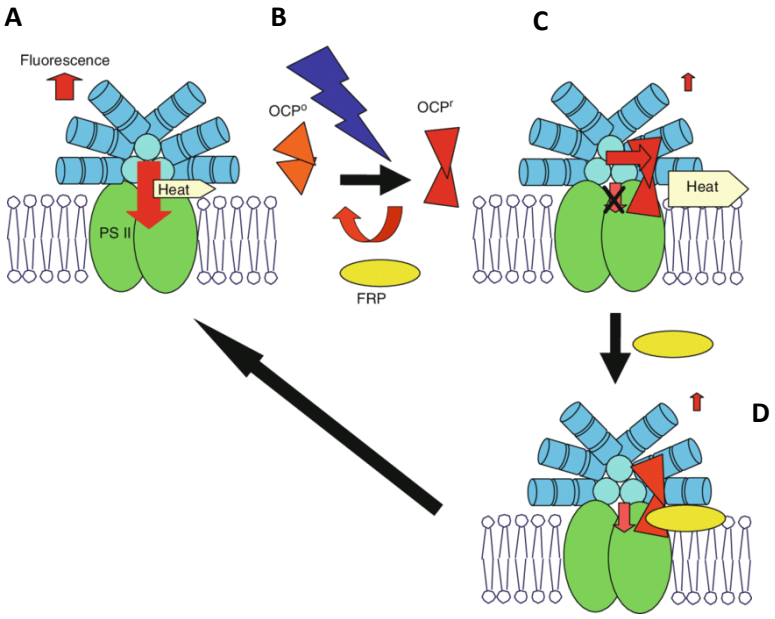

Figure 1.4. OCP photoprotective mechanism in cyanobacteria. Light blue circles represent allophycocyanin, blue segmented cylinders represent phycocyanin. The photoprotective mechanism proceeds as follows: (A) Normal light harvesting conditions, light energy travels down the terminal pigment to PSII (or PSI); (B) Irradiance from high light exposure activates OCP^o converting it to OCP^r; (C) Light energy is channelled to OCP^r and dissipated as heat; (D) FRP converts OCP^r back to OCP^o, light harvesting resumes. Taken from Kirilovsky et al. (2014).

In consistent high light, it would be unsustainable for the phycobilisome to be continuously deactivated by OCP, thus prompting a more permanent alteration of antenna complex structure via gene expression to acclimate to consistently high light conditions (Hihara et al. 2001). A study on *Synechocystis sp.* PCC 6803 showed that within roughly 15 minutes exposure to consistent high light, the genes for both Photosystem I, II and the antenna complex structural and phycobilli proteins were down regulated, whilst Rubisco alongside

ROS scavenging and antioxidant enzymes such as Fe-superoxide dismutase were permanently upregulated (Hihara et al. 2001). One outlier gene in the photosystems was the D1 protein, which alongside genes for NAD(P)H dehydrogenase, showed significant upregulation at 15 minutes before subsequent down regulation (Hihara et al. 2001)

Figure 1.5 schematically illustrates changes in gene expression associated with transfer of *Synechocystis* cells from normal light to excessively high light (Hihara et al., 2001). These responses are accounted for by the difference in the level of light available to the photosystems between normal light and excessive light regimes. In excessive light, oversaturation of the electron transport chain leads to heightened ROS production, triggering upregulation of the antioxidant response. After ~12 hours: Fe-SOD gene expression lowers; allophycocyanin is upregulated and returns to pre-exposure levels; phycocyanin remains suppressed; Rubisco and the carbon-concentrating mechanism proteins remain highly expressed. This demonstrates the cell is altering the structure of the phycobilisome by removing phycocyanin to make it less sensitive to lower wavelengths of light (below 600nm). In the first 15 minutes, the upregulation of D1 acts as a protective measure against photoinhibition (Rintamäki et al., 1994), whereas NAD(P)H-quinone oxidoreductase (NDH-1) works in conjunction with photosystem I to maintain cyclic electron flow, thus mitigating ROS formation caused by excess electrons (Tan et al., 2020). This increased photosynthetic capacity allows for the cells to upregulate protein synthesis and thereby grow and reproduce faster (Figure 1.5).

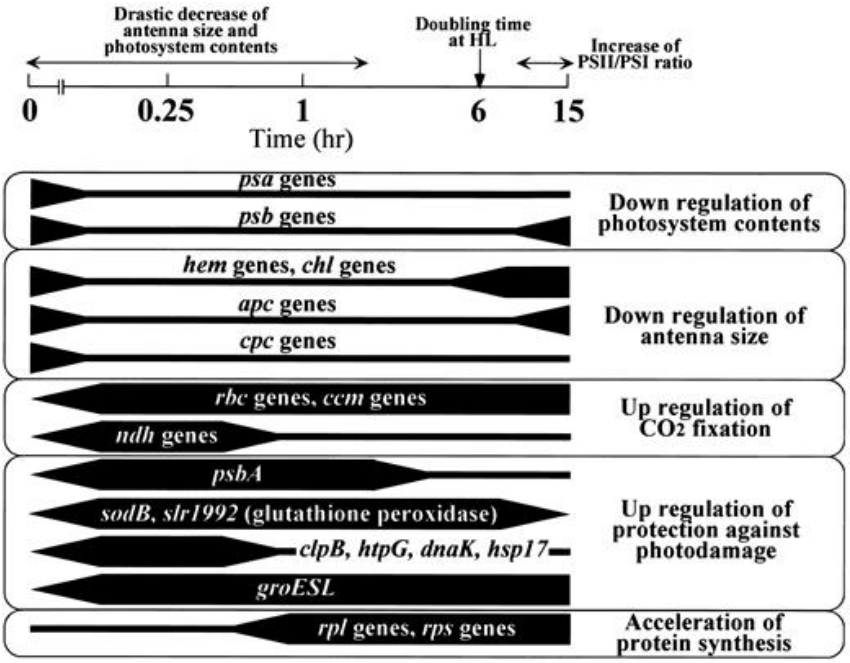

Figure 1.5. Summary of DNA microarray analysis results of *Synechocystis* gene expression in response to consistently high light. Full explanation of the results is given in the text. Taken from Hihara et al. (2001).

Given glyphosate's blockage of the shikimate pathway could have the potential to limit the production of plastoquinone, which is a necessary component of the photosynthetic electron transport chain (Liu & Lu, 2016). This could pose a more urgent threat to photosynthetic organisms as upscaling plastoquinol production is a necessary component of acclimation to

higher light intensities (Ksas et al., 2015). This in turn could explain the photoinhibition observed in glyphosate treated *Salix miyabeana* cultivar SX64 (Willow) caused by decreased photochemistry and subsequent ROS generation (Gomes et al., 2017). The mechanism behind the induction of oxidative stress needs to be illuminated to understand the true scope of glyphosate's impact on organisms and the ecosystem they inhabit. Given that ROS generation primarily occurs as a result of overloading the electron transport chain, it is therefore necessary to monitor the expression of genes encoding the protein components of the photosynthetic machinery during exposure to glyphosate. Glyphosate also alters the distribution of fixed carbon across multiple species, including the production of polysaccharides and sugars in both higher plants and microalgae, particularly when applied at a hormetic dose (Lummato et al., 2019; Pincelli-Souza et al, 2020; Zhao et al., 2020; de Almeida Silva et al, 2022).

1.6 Effects of glyphosate on non-photosynthesis metabolism

1.6.1 Respiratory electron transport chain

Interactions between glyphosate and the respiratory machinery of photoautotrophs is under-researched as most studies have been done in animal systems. There is a clear difference between the effects of glyphosate, AMPA and additional herbicide adjuvants on the TCA cycle and oxidative phosphorylation (Mesnage, 2015; Benachour and Séralini, 2009; Piexoto, 2005). This is likely due to the interactions between AMPA and herbicide adjuvants on cell membranes (Piexoto, 2005). Glyphosate's impact on the respiratory function is thought to arise from direct interactions with the electron transport chain, resulting in mitochondrial dysfunction and subsequent ROS generation (Bailey et al., 2018).

High concentrations of glyphosate-based herbicides completely suppress succinate dehydrogenase activity, leading to a loss of cell viability, as has been observed in organisms exposed to the herbicide Touchdown (Bailey et al., 2020; Burchfield et al., 2019). This has led some to the hypothesis that glyphosate inhibits succinate dehydrogenase, also known as complex II of the respiratory electron transport chain. This hypothesis is supported by a model-based experiment, which demonstrated that glyphosate could interact with the succinate binding site of succinate dehydrogenase (Ugarte, 2014), likely due to similarities in their chemical structure (Figure 1.6).

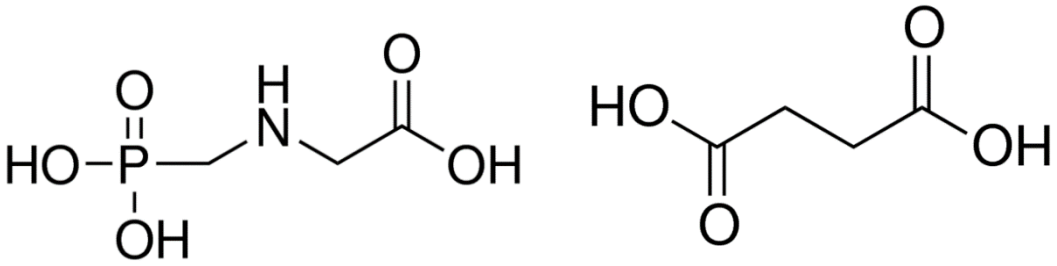

Figure 1.6. Chemical structure of glyphosate and succinic acid.

Further evidence was reported from a study on TM4 Sertoli cells, which showed that both succinate dehydrogenase activity and cell viability were lowered in the presence of pure glyphosate (Vanlaeys et al., 2018). It appears this interaction only results in oxidative stress as the various flux modes and shunts of the TCA cycle can ensure fumarate is still produced (Steinhauser et al., 2012; Araújo et al., 2011; Sweetlove et al., 2010). This hypothesis also correlates with observed increases of complex I activity, which could help counteract the

decreased flow of electrons stemming from complex II (Aristilde et al., 2017; Mesnage, 2015). This theory has been confirmed in a study of *Caenorhabditis elegans,* in which glyphosate-based herbicide treatment directly reduced succinate dehydrogenase activity, proton gradient integrity and thereby ATP production (Burchfield et al., 2019). Hydrogen peroxide concentrations in cells of these worms rose in conjunction with complex II inhibition, as did complex IV activity (Burchfield et al., 2019).

Interestingly, Gomes and Juneau (2016) found that glyphosate also inhibited electron transport chain function in *Lemna minor* (duckweed) via oxidative stress and hypothesized glyphosate inhibited complex III in plants in a similar manner to antimycin A. However, the mechanisms underpinning this observation are unknown. This makes cyanobacteria an interesting choice of model organism for understanding glyphosate induced stress, as they possess integrated photosynthetic and oxidative respiratory electron transport chains, which link across several membranes (Cooley and Vermaas, 2001; Leah-Smith et al., 2013). Despite differences in the structure of their respiratory complexes, cyanobacteria possess many homologous subunits with eukaryotes (Chadwick et al., 2018). If the hypotheses posed in previous literature are to be assumed correct, glyphosate should have two additional targets: succinate dehydrogenase, the hypothesized primary non-photosynthetic electron doner to cyanobacterial electron transport (Cooley and Vermaas, 2001) and the cytochrome B_6f complex, which has been hypothesized as the antimycin A-sensitive component of cyclic electron transfer, due its similarity with mitochondrial complex III (Breyton, 2000). Taking the unique aspects of cyanobacterial electron transport into account could help provide new insights into glyphosate toxicity

1.6.2 Antioxidants and other free enzymes

Arachis hypogaea (peanut) leaves sprayed with 360 and 720 g per hectare of glyphosate increased superoxide dismutase (SOD) activity by 105% and 275% respectively, alongside marked increases in other antioxidant-associated enzymes (Radwan and Fayez, 2016). At concentrations of 4 mg/L glyphosate and above SOD, catalase (CAT) and glutathione-*S*-transferase activity decreases in *Scenedesmus vacuolatus,* despite evidence of higher levels of ROS generation (Iummato et al., 2019). It has been speculated that glyphosate's metal-chelating properties allow it to bind with divalent cations necessary to form the quaternary structures of antioxidant enzymes, such as SOD and CAT, but evidence for this has not yet been found (Mertens et al., 2018).

In *C. elegans*, sample worms showed unchanged levels of superoxide and hydroxyl radicals, but significant increases in Hydrogen peroxide levels in response to concentrations recommended for agricultural use (Burchfield et al., 2019). Given that the primary response to glyphosate in all other species has been to upregulate SOD, it can be speculated that the singular increase in H_2O_2 is because the cells are adept at scavenging and detoxifying any superoxide that may form from restricted electron transfer. In piglets, glyphosate activated the Nrf2-mediated defence response, the Nrf2 transcription factor promotes gene expression of antioxidant and stress-related enzymes in the presence of ROS (Qui et al., 2020). The root cause of this response, however, remains unclear. What is a clear cause of interest, is the highly varied impact glyphosate has on the antioxidant response of different organisms.

1.6.3 Glyphosate-induced cell damage

A study by Benachour and Séralini (2009) found the herbicide Roundup to be toxic to human uterine cells. However, the damage to cell outer membranes was caused not only by the active ingredient glyphosate, but also the adjuvant polyethoxylated tallow amine (POEA). In the same study, AMPA was found to damage cell membranes both synergistically with roundup ingredients and individually. The study also suggested that POEA is able to increase permeability of human cell membranes to enhance glyphosate uptake and toxicity (Benachour and Séralini, 2009). Exposure of rat liver cells to Roundup increased mitochondrial membrane permeability to Ca^{2+} ions and acted as a translocator of H^{+} into the matrix, contributing to dysfunction and oxidative stress (Mesnage et al., 2015). Increased vacuolisation of hepatopancreas cells in decapod crustaceans (*Macrobrachium potiuna*) exposed to a glyphosate-based herbicide has also been observed (de Melo., 2019). Whether these effects were caused by glyphosate itself, an adjuvant or a combination of both is unclear, prompting the need for studies comparing effects of pure glyphosate and glyphosate-based herbicide on cell ultrastructure.

A study by Iummato et al (2019) explored the ultrastructural changes in the microalga *Scenedesmus vacuolatus* during exposure to a glyphosate formulation. There was marked increases in (1) cell wall thickness, (2) vacuole size, (3) total volume, (4) bleaching and (5) alterations in thylakoid stacking patterns. One of the most interesting aspects of this change in cell ultrastructure was the accumulation of starch encompassing the pyrenoids, indicating that large quantities of sugars were being produced. Additionally, the level of chlorophyll *a* and *b* was lowered and cell growth rate declined in response to glyphosate. This provides further evidence that glyphosate affects not only the photosynthetic electron transport chain, but also the Calvin cycle (Iummato et al., 2019) and could provide a valuable lead toward the primary mode of action in glyphosate treated plants.

1.7 Research Question and Hypothesis

The broad research question addressed in this project was - What is the mechanism of glyphosate-induced cell death in photoautotrophs? In plants, glyphosate toxicity is associated with shikimate pathway inhibition since the expression of an EPSPS protein with reduced affinity for glyphosate in transgenic crops confers protection against concentrations used in agriculture (Bakhsh et al., 2020). While depletion of aromatic amino acids has been proposed as the main mechanism of activating cell death in plants, research from our lab showing that dark-incubated plant tissues avoid glyphosate injury (Chivasa and Gonzalez-Torralva, 2019) negates this notion. Moreover, other forms of plant cell death activated by a mycotoxin (Asai et al., 2000) or heavy metal ions (Wang et al., 2013) are similarly inhibited by incubation in darkness. This suggests the existence of a core cell death pathway that integrates signalling from biotic and abiotic stress stimuli activating different primary targets.

Our hypothesis is that light-driven generation of damaging reactive oxygen species in the chloroplast is the main cause of stress-induced cell death in plants. According to this hypothesis, the balance between energy transfer from LHCs to the photosystems and utilization rates of ATP and reducing power by the Calvin-Benson cycle is the central switch that can be triggered to activate cell death. When flux through the Calvin-Benson cycle slows beneath the rate at which reducing power and ATP are generated, cell death is activated by reduction of molecular oxygen to the highly damaging singlet oxygen. Under high ATP and NADPH levels, when the electron transport chain is fully saturated, LHCs continue to

intercept and transfer light energy to the reaction centre chlorophylls. Failure of excited singlet state chlorophylls (^{1}Chl*) to discharge their energy via photochemistry leads to further energy absorption and conversion to the excited triplet state (^{3}Chl*), which transfers the energy to oxygen and formation of the singlet oxygen radical (Carbonera et al., 2012). Cyclic electron flow pathways also become overloaded, resulting in electrons derived from the water splitting reaction being transferred to O_2, forming superoxide. Both of these damaging reactive oxygen species can then either disrupt cell functions or react with oxygen and protons to form other damaging ROS such as hydroxyl radicals and hydrogen peroxide. A high enough accumulation of ROS can then cause damage to DNA and induce ROS mediated cell death.

According to our hypothesis, glyphosate activates cell death by oversaturating the photosynthetic electron transport indirectly via reducing flux through the Calvin-Benson cycle. The Calvin-Benson cycle fixes carbon and acts as the distribution centre of organic precursors to the main metabolic pathways that generate cellular building blocks, such as synthesis of amino acids, simple sugars and complex carbohydrates, nucleic acids and fatty acids. As the shikimate pathway is a major carbon sink responsible for over 30% of fixed carbon (Tohge et al., 2013)(Figure 1.7), its inhibition by glyphosate leads to a build-up of Calvin-Benson cycle intermediates and slowing down of the cycle. This triggers light-dependant ROS production, which kills plant cells.

Most of the research on the mechanisms of glyphosate-induced cell death has been carried out on plants. In this study, however, we used the cyanobacterium *Synechocystis sp.* PCC 6803, and the microalga *Chlamydomonas reinhardtii* CCAP11/32B as model organisms. These organisms were selected for multiple reasons. Firstly, they possess the same core metabolic pathways as higher plants, including the shikimate pathway, the primary site of glyphosate inhibition. Secondly, these organisms have the added benefits of high multiplication rates, a small genome, less complex cellular structure, and minimal biological variation during growth and response to stress. This enables us to generate large datasets, which are easy to interpret, within a short space of time. Additionally, cyanobacteria and microalgae are frequently found in habitats polluted by glyphosate, such as soil and freshwater habitats. Therefore, new insights into the wider effects of glyphosate on these environments can be obtained through research, so that clear scientific understanding can be used to inform policy-making for environmental protection.

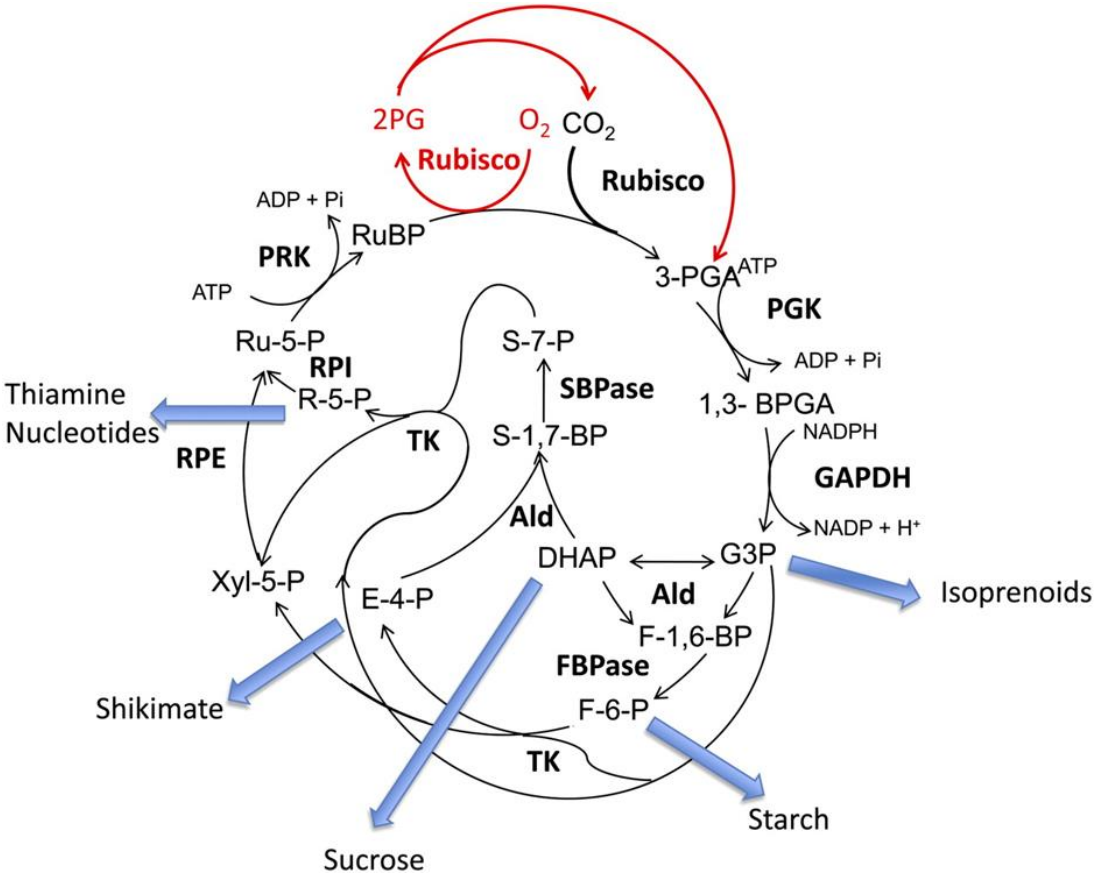

Figure 1.7. The Calvin-Benson cycle. Carbon is fixed to ribulose biphosphate (RuBP) via rubisco catalysis, forming an unstable intermediate that splits into two molecules of 3-PGA. The cycle then enters it reduction phase, in ATP and NADPH are consequently used alongside 3-PGA kinase (PGK) and GAPDH to convert 3-PGA into 1,3-BPGA and then G3P, which can either be used to produce isoprenoids or continue along the cycle. The regenerative phase is then initiated, in which G3P can either be catalysed by aldolase (Ald) or transketolase (TK). Aldolase catalysed reactions can either yield sucrose derived from DAHP or trigger subsequent reactions catalysed by aldolase and either SBPase or FBPase to yield S-7-P or F-6-P respectively. F-6-P can then be used to produce starch. If G3P metabolism is catalysed by Transketolase however the Ethyrose-4-Phosphate is formed, which can then be used in the shikimate pathway. Otherwise transketolase participates in subsequent sets of reactions alongside R-5-P isomerase (RPI) or ribulose-5-P epimerase (RPE) to form Ru-5-P (Ribulose-5-phosphate) or Thiamine Nucleotides. ATP is then used in conjunction with phosphoribulokinase (PRK) to convert Ru-5-P to RuBP. This completes the Calvin-Benson cycle and allows rubisco to either fix O_2 to form 2-phosphoglycolate (2PG) for photorespiration or fix CO_2 to repeat the cycle. Taken from Raines (2011).

1.7.1. Specific Objectives

1. **Establish the impact of glyphosate on the growth and viability of *Synechocystis spp. PCC6803* (cyanobacterium) and *Chlamydomonas reinhardtii* (microalga).**
   Dose-response experiments should establish sub-lethal and lethal doses of glyphosate under different light conditions. In addition to providing detailed understanding of how these organisms behave under glyphosate stress, the results should reveal the appropriate glyphosate concentration to use in subsequent experiments.
2. **Conduct proteomic analysis to establish the metabolic response of cyanobacterial cells to glyphosate.**
   Use of unbiased global protein analysis should identify all the major metabolic and signalling pathways activated in response to glyphosate. Inclusion of sublethal and lethal glyphosate doses provides an excellent filter to identify specific changes associated with toxicity.
3. **Investigate the response of selected metabolic pathways to glyphosate via analysis of gene expression.**
   To test the hypothesis, expression analysis key genes in the photosynthetic electron transport chain and Calvin-Benson cycle should reveal if photosynthesis is central to glyphosate toxicity. In addition, evaluation of the response of selected shikimate pathway genes and respiratory genes provides comparators.
4. **Evaluate the role of secreted signals on the glyphosate response of cyanobacterial and algal cells.**
   Secreted signals have been found to control the light-dependent cell death activated by the mycotoxin fumonisin B1 (Chivasa and Goodman, 2020). Since glyphosate-induced death is similarly light-dependent, investigating if it is also regulated by secreted signals should help to understand the shared core death pathway between biotic and abiotic stresses.

2.0 Materials and Methods

2.1 Cyanobacterial and microalgal cell growth and treatment

The organisms used in this study comprised of the cyanobacterium *Synechocystis sp. PCC6803* and the eukaryotic microalga *Chlamydomonas reinhardtii* CCAP 11/32B. *Synechocystis sp.* PCC 6803 was provided by Professor Norio Murata (National Institute for Basic Biology, Japan). *Synechocystis sp.* was originally isolated in 1968 from a freshwater lake in Oakland, California by R. Kunisawa. The isolate of *Synechocystis sp.* submitted to the Pasteur Culture collection of Cyanobacteria and given the strain number PCC 6803. *Chlamydomonas reinhardtii* CCAP11/32B was obtained from the Culture Collection of Algae and Protozoa. It was isolated by G. M. Smith in 1945 from a soil sample taken from a potato field in Amherst, Massachusetts, USA. Its equivalent strains from other culture collections include SAG 11-32a, UTCC 84 and UTEX 89.

While *Synechocystis sp.* PCC 6803 has a fully sequenced genome, the genome of *Chlamydomonas reinhardtii* CCAP11/32B has not been sequenced. Therefore, proteomics and gene expression analysis experiments were confined to the cyanobacterium, while only physiological experiments were conducted on the microalga.

Cell cultures were cultivated using Blue-Green$_{11}$ (BG_{11}) medium, originally developed by Stainer et al. (1971). BG_{11} is comprised of the following concentrations of compounds: 17.6mM $NaNO_3$; 229.6µM K_2HPO_4; 304.3µM $MgSO_4 \cdot 7H_2O$; 242.9µM $CaCl_2 \cdot 2H_2O$; 31.2µM citric acid; 22.8µM ferric ammonium citrate green; 2.7µM $EDTANa_2$; 188.8µM Na_2CO_3; 46.5µM H_3BO_3; 9.1µM $MnCl_2 \cdot 4H_2O$; 0.8µM $ZnSO_4 \cdot 7H_2O$; 1.6µM $Na_2MoO4 \cdot 2H_2O$; 320nM $CuSO_4 \cdot 5H_2O$ and 170nM $Co(NO_3)2 \cdot 6H_2O$. BG_{11} medium was adjusted to pH 7.1 and sterilised by autoclaving. Cells were initially sub-cultured then grown/bulked-up in autoclaved flattened glass flasks containing 500ml of sterile BG_{11}. The cultures were kept sterile by capping the flasks with a foam bung through which a sterile glass tube inserted from the top, delivered filter-sterilised compressed air to the bottom of the flask. The widened top-end of the glass tube was packed with sterilised cotton lint to prevent dust entering the tube. The cultures were incubated in a temperature-controlled growth chamber at 30°C with continuous illumination at 33.58µmol.m^{-2}.s^{-1} for 5 days and then 1.37µmol.m^{-2}.s^{-1} for 2 days.

2.2 Glyphosate treatment of cell cultures

Stock solutions of 50 mM glyphosate in water were prepared, adjusted to pH 5 using KOH, and stored at -20°C in small aliquots to prevent repeated freeze-thaw cycles. The pure Glyphosate powder was stored at -20°C to prevent degradation that can occur at room temperature (Garcia-Muñoz et al., 2020). Cell cultures were treated with an appropriate amount of filter-sterilized glyphosate to final concentrations ranging from 0.1mM to 10mM, depending on each specific experiment. Treated cells were in sterile glass conical flasks that were then placed on an orbital shaker (120 revolutions per minute) at 23°C. Depending on the experiment, some treated cell was incubated in complete darkness, while others were incubated in a 16 h-photoperiod(~80 µmol.m^{-2} s^{-1}).

2.2.1 Effects of glyphosate on freshly inoculated cell culture growth (Growth curve experiments)

A culture of *Synechocystis sp. PCC6803* cells at an optical density (OD) of 0.06 at 600nm were used to inoculate 30 mL of fresh BG_{11} medium containing a final concentration of 0 mM, 0.25 mM, 0.5 mM, 1 mM and 2 mM glyphosate. Similarly, a culture of *Chlamydomonas reinhardtii* cells at a density of 0.02 at 600 nm was used to inoculate 30 mL fresh BG_{11} spiked with glyphosate to a final concentration of 0 mM, 1 mM and 2 mM. Each treatment was replicated 4 times for both organisms. Aliquots of 800 µL were immediately withdrawn from each replicate flask and subsequently every 24 hours. The optical density of these aliquots was spectrophotometrically measured against a BG_{11} blank at wavelength 600nm in a (Ultrospec 500 Pro, Amersham Biosciences, Amersham, UK). The optical density average values were plotted against time and the standard deviation used as error bars.

2.2.2 Effects of glyphosate on mature dense cell cultures (Single timepoint experiments)

Highly density cell cultures (OD of 0.6 – 1 at 600nm) grown previously in the absence of glyphosate stress were used for these experiments. To 7 mL cell culture aliquots were added 2 mL of 5X BG_{11} and an appropriate volume of glyphosate to give the desired final concentration (provided in Results section for specific experiments) in a final volume of 10 mL, in triplicates samples. The cultures were incubated in complete darkness for 24hrs and then moved to the light-dark cycle for a 24-72hrs, depending on the experiment. At the time of harvesting, the samples were photographed before processing for metabolic activity (section 2.5.2), protein extraction (section 2.3.1), or RNA extraction (section 2.4.2). Samples for protein and RNA extraction were inactivated metabolically prior to further processing. To achieve this, per 10 mL of cell culture samples, 1.25 mL of ice cold (-20°C) 5% (w/v) phenol in ethanol were added. Samples were centrifuged for 20 minutes at 10000 x ***g*** to pellet the cells. The cell pellet was resuspended in 1 mL of ice cold 5% (w/v) phenol in ethanol and then stored at -20°C until further processing.

2.3 Proteomic analysis

2.3.1 Protein extraction and quantification

Four-replicate cyanobacterial cultures treated with 0 mM, 1 mM, or 2 mM glyphosate and incubated in complete darkness for 24 h followed by 24 hours high light, were metabolically inactivated (section 2.2.2) and used for protein extraction. Metabolically inactivated cells suspended in 5% (w/v) phenol in ethanol were centrifuged for 10 minutes (10000 x ***g***) and the supernatant discarded. Cell pellets were homogenized in 200 µL of dimethyl-sulfoxide (DMSO) using plastic pestles. Protein in the homogenate was precipitated by adding 5 µL of 1.5 M Tris-HCl (pH 8.8) and 800 µL acetone. Samples were then incubated at -20°C for 24 hours for full protein precipitation. The precipitates were pelleted by centrifugation (17000 x ***g***, 10 mins) and washed 3 times by repeated resuspension in 500 µL 80% acetone and centrifugation (5 minutes, 17000 x ***g***). After washing, the protein was extracted from the pellets in 200 µL lysis solution (9 M urea, 2 M thiourea, 4% (w/v) CHAPS, 30 mM Tris-HCl, pH 8.8).

The protein concentration was quantified using a modified Bradford assay (Bradford, 1976). A calibration curve was generated using standards with 0, 1, 2, 4, 8 or 10 µg/mL of Bovine

Serum Albumin (BSA) in a final reaction volume of 1ml containing: 90 mM urea; 20 mM thiourea; 0.04% CHAPS; 0.3 mM Tris; 1 mM HCl; and 900 µL of a 4-fold dilution of BioRad protein assay dye (Bio-Rad Laboratories, Watford, UK). The reactions for assaying protein samples did not have BSA, which was substituted with 1 µl of intracellular protein. The absorbance of the calibration standards and samples were measured against a reagent blank at wavelength 595nm in a spectrophotometer (Ultrospec 500 Pro, Amersham Biosciences, Amersham, UK). This was done within the linear range of the reaction, which is between 5-30 minutes of addition of the BioRad dye. A calibration curve was constructed and protein sample concentration interpolated from the linear regression of the calibration data points.

2.3.2 Protein labelling and gel electrophoresis

To check protein quality, 50 µg from each protein sample were fluorescently labelled and analysed by sodium dodecylsulphate-polyacrylamide gel electrophoresis (SDS-PAGE). Protein samples were labelled with Cy3 or Cy5 (cyanine NHS ester minimal) dye at a ratio of 800 picomoles label to 50 µg protein in a final volume of 49 µL in thelebelling buffer: 9 M urea; 2 M thiourea; 4% (w/v) CHAPS; 30 mM Tris-Cl; pH 8.5. The reaction was initiated by addition of the dye, proceeded in complete darkness with incubation on an ice-water bath for 30 minutes, and stopped by addition of 1 µL of 10 mM lysine. Aliquots with 2.5 µg protein were mixed with protein loading buffer (62.4 mM Tris-HCl (pH 6.8); 10% glycerol; 2% (w/v) SDS; 1% (w/v) dithiothreitol; 0.01% bromophenol blue) in a final volume of 10 µL. Samples were boiled at 100°C for five minutes and centrifuged (17000 x ***g*** for 10 minutes). The protein samples were loaded into Invitrogen NuPAGE 12% bis-tris gels (Thermo-Fisher Scientific, Loughborough, UK) for electrophoresis using a tris-glycine buffer (25 mM Tris-HCl, 190 mM glycine and 0.1% SDS). A Cy2-labelled BenchMark protein ladder (Thermo Fisher Scientific Loughborough, UK) containing 1 µg protein was loaded alongside the samples to serve as molecular weight markers. The gels were run at 100 V until the bromophenol blue dye-front had travelled to the bottom of the gel. At the end of the run, the gels were fixed in 10% acetic acid/40% methanol for 30 min before imaging with the Typhoon 9400 scanner (GE Healthcare, Amersham, UK).

After the gel-based quality control, samples were then prepared for mass spectrometric analysis. Proteins samples were labelled with isobaric tags for relative and absolute quantification (iTRAQ) using the following method. Aliquots of 12.5 µg protein from each sample were precipitated in 80% acetone by making up the sample volume to 100 µL with deionized water and adding 5 µL of 1.5 M Tris-HCL (pH8.8) followed by 400 µL acetone. After vortex-mixing, the tubes were incubated overnight at -20°C. The protein precipitates were centrifuged for 10 minutes (17000 x ***g***) and the supernatant carefully removed. Protein pellets were then processed using the iTRAQ Reagent Multiplex Buffer Kit (Sigma-Aldrich, Merck KGaA, Darmstadt, Germany). To the pellet was added 4 µL of 1% SDS solution and incubated at 60°C for 1 hour. Samples were then mixed with 48 µL of dissolution buffer and left on a rotary shaker at room temperature for 1 hour. After pulse-centrifuged to remove bubbles and bring sample to the bottom of the microfuge tube, 1 µL of reducing agent (TCEP) was added. After incubation at 60°C for 1 hour, 0.5 µL of blocking agent (MMTS) were added and samples incubated at room temperature for 10 minutes. The samples were then digested by mixing with 2 µL of 0.5 µg/ µL trypsin gold (Promega, Southampton, UK) and incubating overnight at 37°C.

After digestion, samples were freeze-dried for 4 hours and the powder stored at -20°C. The peptides where then labelled using the iTRAQ Reagents Multiplex Kit (Merck KgGa, Darmstadt, Germany). Samples were resuspended in 50 µL of deionized water and the pH adjusted to pH7.5 by addition of 5 µL of dissolution buffer. Samples were then mixed with 20 µL aliquots of ITRAQ label as follows: the 4-replicate control samples were labelled with tags of molecular weight 113, 114, 115, or 116, while the 4-replicate 1 mM glyphosate-treated samples and 4-replicate 2 mM glyphosate-treated samples were labelled with tags of molecular weight 117, 118. 119, or 121. The reaction proceeded at room temperature (21°C) for 2 hours. Because duplicate control samples had been generated, the 1 mM glyphosate-treated replicates were pooled with a set of controls while the 2 mM glyphosate-treated replicates were pooled with the second control set. The pooled samples were then freeze dried.

Samples were submitted the Biosciences Proteomics Facility for mass spectrometric analysis by Dr Adrian Brown using the following standard protocol. Pooled labelled peptides originating from 50 µg of protein were dissolved in 75 µL formic acid:acetonitrile solution (0.1% formic acid, 3% acetonitrile). Samples were then mixed with 150 µL 0.3 M ammonium formate (pH 3) and the pH was adjusted to 3 using trifluoroacetic acid. Samples were clarified via centrifugation at 10,000 x **g** for 10 minutes, and subsequently mixed with 1275 µL acetonitrile (ACN). Buffer solution salts and untagged labels were removed and discarded from samples using HILIC SPE cartridges (PolyLC Inc., Columbia, USA) containing 300 mg of 12 µm polyhydroxyethyl-A. Aliquots of 1.5 mL of sample were added to SPE cartridges and the flow through was readministered for a second passage after centrifugation. Initial preparation of cartridges before sample clarification involved washing them with 3 mL of peptide release buffer (5% ACN, 30 mM ammonium formate pH 3.0) for a total of four washes. This was followed by a further 4 washes with 3 mL binding buffer (85% ACN, 30 mM ammonium formate pH 3.0). After clarification, columns were washed twice using 2 mL of binding buffer each round, after which 2X 1 mL aliquots of peptide release buffer were used to elute sample peptides. Eluted peptides were then freeze-dried and dissolved in 3% ACN, 0.1% formic acid. Samples were then analysed via Liquid Chromatography-Mass Spectrometry (LC-MS).

2.3.3 Mass spectrometric analysis

Samples were separated and analysed via Liquid Chromatography Mass Spectrometry (LC-MS) using an in-house TripleTOF 6600 mass spectrometer (AB Sciex, Warrington, UK) alongside an Eksigent 425 LC system 425 (AB Sciex) Nanospray III source. Salts and non-peptides were removed from the samples using a trap column (Triart C18 column 1/32'', 5 µm, 5 x 0.5 mm) purchased from YMC (Kyoto, Japan). The remaining peptides were then segregated using a Triart C18 column 1/32'', 3 µm, 150 x 0.3 mm (YMC) with a programmed flow rate of 5 µL/min. The program utilised two buffer systems: buffer A (aqueous 0.1% FA) and buffer B (0.1% FA in ACN). The following Linear gradients of buffer solutions were then applied as follows: 3-5% buffer B for 2 minutes; 5- 30% buffer B for 66 minutes; 30-35 % buffer B for 5 minutes; and 35-80% buffer B for 2 minutes. The column was then washed with 80% buffer B for 3 min. Three percent buffer B was then reapplied to the column over 1 min and held for equilibration for 8 mins. Analysis via the TripleTOF MS was then initiated, with a gradient initiation over 85 minutes. Data-dependent MS-MS acquisition of the top-30 ions was selected with the ion collision energy set for peptides with iTRAQ label tags. Precursor-ion scans of 250 ms within the range 400-1600 m/z yielded up to 30

multiply-charged ions (>500 cps) selected over 50 ms for CID fragmentation and MS/MS spectrum and subsequent acquisition (m/z 100-1500). Cycle times were set at 1.8 sec with 15 seconds rolling precursor exclusion to limit multiple fragmentation of the same peptide. Spectrometer data in a raw.wiff format was obtained using the Analyst TF 1.7.1 instrument control and data processing software (AB Sciex).

2.3.4 iTRAQ data analysis

A *Synechocystis sp.* database downloaded from the Uniprot database (https://www.uniprot.org/) in May 2020 was used to process the raw.wiff files obtained from LC-MS via the ProteinPilot™ 5.0.1 version 4895 software, integrating the Paragon™ Algorithm 5.0.1.0.4874 (AB Sciex). The following parameters for data processing were selected: iTRAQ 8-plex Paragon method allowing for trypsin digestion; MMTS-blocked thiol groups on cysteine residues; 1 missed cleavage; and TripleTOF 6600 spectrometer instrument. The 'Run False Discovery Rate Analysis' option was selected and a correction for label bias applied, with "Unused ProtScore Confidence" being set as a 0.05 threshold for protein detection (Ngcala et al,. 2020). Filtered data files for were converted to an Excel format, which contained both peptide and protein analysis sheets. Data were then filtered for significance, by excluding all peptides identified with confidence level below 95% and excluding proteins identified on the basis of less than two peptides with a significance level ≥ 95% (Ngcala et al,. 2020). A second filter was then applied to the data to remove protein duplicates with no quantitative. The average fold-change in protein expression and associated standard deviation were calculated across the 4 replicates. A Student's T-test was performed to identify statistically significant fold-changes in protein abundance between control and glyphosate treatments. Proteins that remained after applying the filter were used for bioinformatic analysis.

2.3.5 Bioinformatics

The gene list analysis tool on Pantherdb.org (accessed 12/09/21) was used to perform a statistical overrepresentation test for the following annotations: GO biological process; GO cellular component; and GO molecular function. The protein list from the ITRAQ data that had been filtered to retain only proteins with a significant fold-change in abundance were compared against the genome data to assess trends of over-expressed functional groups both for the 1mM and 2mM glyphosate-treated samples. Significant trends were identified using Fisher's exact test with the raw *p*-value corrected by calculating the false discovery rate to eliminate false positives.

2.4 Gene expression analyses

2.4.1 Primer design

Synechocystis sp. PCC6803 proteins from selected metabolic pathways were identified by BLAST-search of the Cyanobase database (http://genome.microbedb.jp/blast/blast_search/cyanobase/genes). Functionally verified, known enzymes of either *Escherichia coli* or *Chlamydomonas reinhardtii* that were retrieved from the National Centre for Biotechnology Information (NCBI) database (https://www.ncbi.nlm.nih.gov/) or Phytozome database version 13 (https://phytozome-next.jgi.doe.gov/), were used as bait sequences in BLAST analyses to identify appropriate *Synechocystis* proteins. The cDNA sequences were retrieved and used for primer design. Primers for selected *Synechocystis sp*. genes were designed using the NCBI primer-BLAST tool (https://www.ncbi.nlm.nih.gov/tools/primer-blast/), which accepts design parameters

from the user: amplicon length 75-150 base and 1 GC clamp in the primers. The primers were then commercially synthesised by Integrated DNA Technologies (Leuven, Belgium). The full list of gene sequences and primers used in this project can be found in APPENDIX III.

2.4.2 RNA extraction and quantification

Metabolically inactivated cells suspended in 5% (w/v) phenol in ethanol were centrifuged for 10 minutes (10000g) and the supernatant discarded. Cells were then resuspended in 500 µL of resuspension buffer (20 mM Tris-HCl, 5 mM EDTA and 0.5% SDS). An aliquot of 500 µL acidic phenol solution (pH 4.5) was added and the tubes vortex mixed. Samples were snap-frozen in liquid nitrogen and then transferred to a heating block set at 70°C for 2.5 minutes. After vortex-mixing, the heating block temperature was reduced to 65°C and the samples incubated for a further 10 minutes, with brief vortex-mixing at 2.5-minute intervals. The freeze-thaw cycle was repeated a second time.

From this point onwards, samples were stored in an ice bath at all times. Samples were centrifuged at 17000 x ***g*** for 10 minutes and the aqueous phase (top phase ~500 µL) was transferred to a fresh 1.5 mL microfuge tube. An aliquot of 500 µL phenol:chloroform:isoamylalcohol (PCI) solution with a ratio 25:24:1 was added to the samples and the mixture was vortexed for 10 seconds. Samples were then centrifuged (17000 x ***g*** for 5 minutes) and the aqueous top phase (~500µl) was transferred to a 2.5 mL microfuge tube. The total nucleic acid was then precipitated by adding a tenth volume of 3 M sodium acetate pH 5.2 (50 µL) and 2.5-fold volumes of ice-cold ethanol (1250 µL). After mixing, the tubes were stored at -20°C for a minimum of 24 h. Samples were centrifuged (17000 x ***g*** for 10mins) and the supernatant was discarded.

The RNA samples were then purified using the Spectrum Plant Total RNA Kit (Sigma Aldrich, London, United Kingdom) (https://www.sigmaaldrich.com/GB/en) as per manufacturer's instructions with minor deviations. To each sample was added 500 µL of lysis solution/2-mercaptoethanol (2-ME) mixture (1 µL 2-ME per 1 mL lysis solution). After vortexing for 30 seconds, the samples were incubated at room temperature for a maximum of 3 minutes. Samples were centrifuged (17000 x ***g*** for 3 minutes) and the clarified solution carefully pipetted into filtration columns seating in a 2-mL collection tube. After centrifugation (17000 x ***g***, 1min), the filtrate was mixed with 500 µL binding solution. The mixture was centrifuged (17000 x ***g***, 1min) through a binding column, which retained the nucleic acids. The binding column wash washed by centrifuging (17000 x ***g***, 1min) through 300 µL wash solution. A mixture of DNase and DNase digestion buffer at a 1:7 (v/v) ratio was prepared and 80 µL added to the membrane of the binding column and left to incubate at room temperature for 15mins. After completion of DNase digestion, the samples were sequentially washed with 500 µL of wash solution-I followed by wash solution-II, with centrifugation (17000 x ***g***, 1min) in-between. After drying the columns via a minute centrifugation (17000 x *g*), RNA was eluted in 50 µL of sterile deionised water. RNA concentration was quantified using a Nanodrop ND-1000 Spectrophotometer (Thermo Fisher Scientific, Waltham, Massachusetts, USA). The samples were stored at -20°C.

2.4.3 RNA gel electrophoresis and cDNA synthesis

RNA quality was checked by gel electrophoresis. Aliquots containing 300 ng RNA were mixed with 5 µL RNA loading buffer: 64% (v/v) formamide, 8.2% (v/v) formaldehyde, 130 mM MOPS, 130 µg/mL ethidium bromide, 0.1% (w/v) Orange G. Samples were then

incubated at 65°C for 10 minutes and loaded into 1.2% (w/v) agarose gels made with MOPS buffer (20 mM MOPS, 5 mM sodium acetate, 1 mM EDTA, pH 7). Gels were made by mixing agarose and MOPS buffer in a glass conical flask and heating in a microwave until the agarose was fully dissolved. The gel mixture was left to cool to ~50°C and carefully poured into the casting tray with combs inserted. The gels were then polymerised at room temperature. Gels were placed in an electrophoresis tank and submerged in 1X MOPS buffer before RNA samples were loaded into the wells. Gels were run at 50 V for around 1h and 15 minutes.

After confirming RNA integrity by visualisation with a UV transilluminator (signified by crisp rRNA bands with no smearing), RNA was used to synthesise cDNA using the qPCRBIO cDNA Synthesis Kit (PCR Biosystems Ltd., London, UK) . For each sample, ~630 ng RNA was placed in a 500 µL microfuge tube and 2.5 µL of 5X CDNA synthesis mix (with reaction buffer, the 4 deoxy-nucleotides, oligo-(dT), reverse transcriptase, and RNase inhibitor) added and made up to a final volume of 10 µL with water. The reaction was incubated in a G-STORM thermal cycler (GS1, G-Storm, Somerton, UK) with the following programme: 25°C for 5 min; 42°C for 30 min; and 85°C for 5 min.

2.4.4 PCR analysis and DNA gel electrophoresis

Polymerase chain reactions (PCR) to test primer specificity were carried out using the SensiFAST SYBR No-ROX mix (Bioline, Nottingham, UK). Reactions were performed in sterile, flat capped 200 µL PCR tubes in a final reaction volume of 20 µL containing: 5 µL of 100-fold diluted cDNA; 8.4 µL of deionised H_2O; 100 nM each of both the forward and reverse primers; and 5 µl of 2x SensiFAST SYBR No-ROX mix. Samples were mixed by pipetting and the tubes placed in a G-STORM thermal cycler (GS1, G-Storm, Somerton, UK) set to the following programme: 112 °C heated lid and 3-minute 95°C hot start; 40 cycles of 30 seconds of denaturation at 95°C, 15 seconds of annealing at 56°C, and 15 seconds of extension at 72°C. PCR samples were then stored at 4°C until they were loaded into gels.

DNA electrophoresis gels were made by mixing agarose into TAE buffer [40 mM Tris base, 20 mM glacial acetic acid, 1 mM EDTA, pH 8.3) at a 3.5% v/w ratio, into a conical flask and dissolving by heating in a microwave. The gel mixture was left to cool down to ~50°C, after which 5 µL of 10 mg/mL ethidium bromide was added per 100 mL of gel solution. The mixture was then carefully mixed and poured into gel casting trays with combs inserted. The gels were then left to polymerise at room temperature. Gels were placed in an electrophoresis tank and submerged in TAE buffer. PCR samples were prepared for loading by mixing 10 µL of PCR products with 2 µL Orange G loading buffer solution (final concentration: 40 mM Tris-HCl, 20 mM acetic acid, 1 mM EDTA, pH 8.3, 3% (w/v) glycerol, 0.2% (w/v) Orange G). Samples were loaded into gels alongside a well loaded with 2 µL of HyperLadder V 25-500bp DNA ladder (Bioline, Nottingham, UK). Gels were run at 80 V for approximately 1 hour before visualisation with a UV-transillumination.

2.4.5 Quantitative PCR analysis

Quantitative PCR was conducted using cDNA samples generated as described in section 2.4.3. Each reaction was in final of 20 µl containing: 5 µl of 100-fold diluted cDNA, 8.4µl of deionised H_2O, 100 nM each of both the forward and reverse primers, and 5 µl of 2x SensiFAST SYBR No-ROX mix. Each sample was replicated twice to have 2 technical replicates on top of the 3 biological replicates built-in the experiment. Reaction tubes were then placed in a Real Time PCR Cycler Rotor Gene 3000 (Rotor-Gene 3000, Qiagen, Hilden,

Germany). A programme was selected with a 3-minute 95°C hot start followed by 40 cycles of: 10 seconds of denaturation at 95°C, 15 seconds of annealing at 56°C, 25 seconds of annealing at 72°C. QPCR data were analysed with REST 2009 Software (Qiagen) using the 16S rRNA gene as a constitutive reference control.

2.5 Evaluating the impact of extracellular signals on glyphosate toxicity

2.5.1 Treatment of cultures with whole or fractionated conditioned medium

To investigate the effects of extracellular signals on the response of cyanobacteria and microalgae to glyphosate, dense cultures of both organisms grown without glyphosate stress were used. Cell culture samples of 10 mL each were aliquoted into sterile 50 mL Falcon tubes and centrifuged (3000 x ***g***, 15mins) to pellet the cells. To test the effects of removal of extracellular signals, the medium was discarded and replaced with 7.5 mL of fresh BG_{11} and made up to 10 mL with glyphosate and sterile water to give the desired final concentration. To test the effects of secreted signals, the cells were resuspended in 7.5 mL of the original medium that they grew in (containing secreted signals) and 1.5 mL of 5X BG_{11} added to raise the nutrients to the same level with fresh medium. The volume was made up to 10 mL using sterile water and glyphosate to the desired final concentration. The latter treatment contained unfractionated conditioned medium i.e., conditioned medium is medium in which cells have grown previously and so contains secreted signals. Further treatment containing fractionated conditioned medium were generated by adding equivalent amounts of fractionated medium with 5X BG_{11} and glyphosate. Cell-free conditioned medium was centrifuged (4000 x ***g*** , 60 mins) through Sartorius Vivaspin molecular weight cut-off filters (Stonehouse, UK) of 10,000 Da or 5,000 Da to produce the 10 kDa and 5 kDa fractionated conditioned medium, respectively. The specific experimental details for the two organisms are as follows:

For *Synechocystis* – a dense culture with an optical density at 600 nm of 0.65 was used to generate six sample types: control cultures with conditioned medium, 1 mM glyphosate-treated cultures in conditioned medium, untreated cultures in fresh medium, 1 mM glyphosate-treated cultures in fresh medium, 1 mM glyphosate-treated cultures in 10 KDa fractionated conditioned medium, and 1 mM glyphosate-treated cultures in 5 KDa fractionated conditioned medium.

For *Chlamydomonas* – six sample types were selected with a similar culture density to *Synechocystis*: control cultures in conditioned medium, 2 mM glyphosate-treated cultures in conditioned medium, control cultures in conditioned medium spiked with 5X fresh BG_{11}, 2 mM glyphosate-treated cultures in conditioned medium supplemented with 5X fresh BG_{11} untreated cultures that were pelleted and resuspended in an equal volume of fresh BG_{11}, and 2 mM glyphosate-treated cultures that were pelleted and resuspended in an equal volume of fresh BG_{11}.

2.5.2 Assay for glyphosate via mass spectrometry

Triplicate 1 mM glyphosate treated *Synechocystis sp.* PCC6803 cell cultures were generated and 1 mL samples withdrawn at 0, 24, 48, and 72 after treatment. The samples were centrifuged at 17000g for 10 minutes and 800 µL transferred to fresh microfuge tubes. The clarified samples were flash-frozen in liquid nitrogen and stored at -20 C. The samples were submitted for analysis by Dr Rachel Dack in the Biosciences BioAnalytics Facility by tandem Liquid Chromatography-Mass Spectrometry (LC-MS) using an in-house Sciex 6500 Qtrap

(Sciex, Massachusetts, United States) coupled to a Shimadzu Nexera LC (Kyoto, Japan). Samples and 50 mM glyphosate stock solution were diluted 1:1000 in 95:5 H2O:MeCN. The diluted stock solution was used to prepare 0.05-5µM standards to generate a calibration curve. Five microlitres of sample were injected into an Atlantis Premier BEH C18 AX 2.1x100mm 1.7 µm column (Waters, Milford, MA, USA) held at 40°C. The auto sampler was set to 4°C. The program utilised two solvent systems: solvent A (aqueous 0.1% Formic Acid) and solvent B (MeCN and 0.1% formic acid). Analytes were separated at a flow rate of 0.2mL/min with the following gradient: 0-2 minutes: 5% B; 2-7 minutes : 5-95% B; 7-8.9 minutes : 95% B; 9-12: minutes 5% B, followed by 2 mins re-equilibration prior to injecting the next sample.

Identification and quantitation of glyphosate was then carried out using the Sciex 6500 Qtrap with the ESI operated in negative ionisation mode. The ionization source was operated with the following settings: ion spray voltage, -4.5KV; temperature (TEM), 500°C; curtain gas (CUR) flow rate, 40 arbitrary units; collision gas, medium; ion source gases, 40 and 50 arbitrary units. The primary degradation product of Glyphosate, AMPA (α-amino-3-hydroxy-5-methyl-4-isoxazolepropionic acid) was also tested for using the published transitions outlined by Fritz-Wallace et al (2020) as no standard was available in-house. Analyte specific parameters for glyphosate were optimized by infusion, followed by optimisation of source parameters, GS1 (40) and GS2 (50), TEM and CUR, gas via multiple injections. The specific parameters utilised for glyphosate and AMPA analysis are detailed in Table 1. Standards and samples were injected in duplicate. Samples were randomised with blanks interspersed. Standards used to prepare the calibration curve were injected at the beginning and end of the run and used to calculate glyphosate concentration in µM. Sample data was analysed using Sciex Analyst software, version 1.7 (Massachusetts, USA). The concentrations of the 0hr samples were then set as 100% to calculate percentage change in subsequent timepoints using T-Test to determine significance.

ID	Q1 m/z	Q3 m/z	Time (ms)	DP(V)	CE (V)	CXP
Glyphosate 1	168	150	50	-40	-16	-15
Glyphosate 2	168	124	50	-40	-24	-15
AMPA 1	110	78.9	50	-40	-28.7	-15
AMPA 2	110	63.0	50	-40	-20.1	-15

2.5.3 Analysis of secreted versus intracellular proteins

Cell-free conditioned medium from 50 mL of dense *Synechocystis* culture was generated by centrifugation (17000g, 10minutes) and transferring 30 mL of the supernatant to 3 50 mL Falcon tubes, 10 mL in each. To this conditioned medium were added 50 µL of 1.5 M Tris-HCl (pH 8.8) and 40 mL acetone. The samples were mixed and incubated overnight at -20 °C for protein precipitation. The precipitates were centrifuged (3000 x ***g***, 10minutes) and washed 10 10 mL 80% acetone 3 times. The protein pellets were finally dissolved in 200 µL of lysis buffer (LB) [9 M urea, 2 M thiourea, 4% (w/v) CHAPS, 30 mM Tris-HCl, pH 8.8]. Protein concentration was quantified using the modified Bradford assay (Bradford, 1976; see section 2.3.1). Aliquots with 15 µg of intracellular (see section 2.3.1) and extracellular protein samples were fluorescently labelled using cyanine5 NHS ester minimal dye (Cy5)

purchased from Lumiprobe (Hannover, Germany) according to the method described in section 2.3.2.

2.6 Cell viability assay (MTT)

Sample preparation for MTT assay involved incubating 10 mL of cell culture with 200 µL of 5mg/mL 3-(4,5-dimethylthiazol-2-yl)-2,5-diphenyltetrazolium bromide (MTT) solution overnight. The cell cultures were photographed as necessary prior to quantitative analysis. Three technical replicate 50 µL cell culture aliquots from each of 3 biological replicates were sampled from each culture flask, placed in a 1.5 mL microfuge tube and centrifuged at 17000 x ***g*** for 10 minutes. The supernatant was removed and the cells in the pellet disrupted using 1 mL dimethyl sulfoxide (DMSO). The tubes were centrifuged at 17000 x ***g*** for 10 minutes to pellet cellular debris. A volume of 800 µL was carefully taken from the top and the optical density at wavelength 470 nm measured against a DMSO blank in a spectrophotometer (Ultrospec 500 Pro, Amersham Biosciences, Amersham, UK).

2.7 Statistical analysis and reproducibility of results

A combination of quantitative and qualitative results we're obtained from these experiments. Qualitative studies were carried out using three technical replicates and were repeated on several occasions to ensure reproducibility of response. Figures for qualitative results will show no annotations for significance. All Quantitative analyses carried out in this experiment were done using a minimum of three biological replicates. One-way analysis of variance (ANOVA) and Tukey's Honestly Significant Difference (HSD) post-hoc test were used for statistical analysis of gene expression data and physiological experiments that evaluated cell viability, cell density and cell culture glyphosate concentration. The software packages used for statistical analyses were SPSS 28 (version 0.1.1) and Minitab 21 (version 2.0).

3.0 Results

3.1 Effects of glyphosate on cell growth

3.1.1 Effects of glyphosate on the growth of cell cultures

To prepare cell cultures for use in experiments, bulk cultures of *Synechocystis* and *Chlamydomonas* were generated by inoculating 500 mL of BG_{11} medium in specialised "flattened" glass flasks and incubating at 30°C with 33.58 $\mu mol.m^{-2}.s^{-1}$ light for 5 days and then 1.37$\mu mol.m^{-2}.s^{-1}$ for a further 2 days. These grew to very dense green cultures (Figure 3.1) that were stored at room temperature on the bench until they were used in experiments. When left for several months at room temperature, the cells retained their healthy green colour, but remained dormant without further multiplication. Cell growth and multiplication could be activated by addition of more nutrients, incubating at the growth temperature and bubbling compressed air or placing on a rotary shaker for aeration. The ability to stay dormant but alive for prolonged periods of time when stored without aeration at room is in contrast to plant cell suspension cultures, which die within a few days if aeration is stopped.

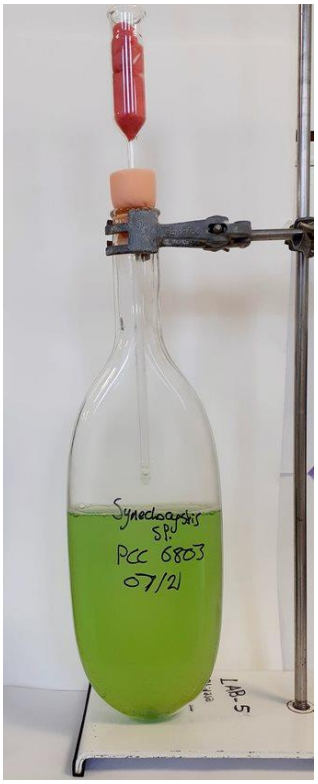

Figure 3.1. Appearance of a bulk culture of *Synechocystis sp.* PCC 6803 cells in a 500 mL flask. Photo taken in October 2021.

To investigate the effects of glyphosate on *Synechocystis* cell culture growth, triplicate flasks each containing 30 mL BG11 with 0 mM, 0.25 mM, 0.5 mM, 1 mM or 2 mM glyphosate were inoculated with cells to a final optical density of 0.061 (at 600 nm wavelength). Samples were withdrawn every 24 h for measurement of the optical density, and growth curves were generated by plotting mean optical density values as a function of time as shown in Figure 3.2. Growth of *Synechocystis* cells treated with 0.25 mM and 0.5

mM glyphosate was indistinguishable from the controls. Due to the high level of inoculum added, there was a no noticeable flat-lined lag phase but a progressive entry into the exponential growth phase that was in full swing as the cells entered day 3. These results indicate that, at concentrations ≤ 0.5 mM, glyphosate does not affect the growth of *Synechocystis* cell cultures. On the contrary, 1 mM and 2 mM glyphosate completely inhibited growth throughout the 7 days of the experiment. This result indicates that ≥ 1 mM glyphosate effectively suppresses *Synechocystis* cell multiplication.

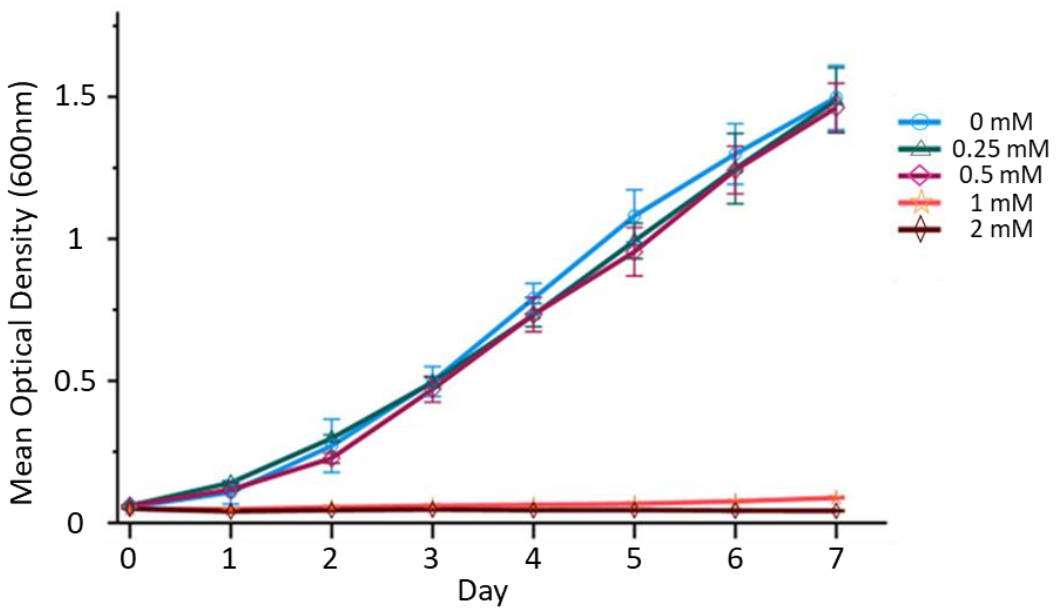

Figure 3.2. Dose-response effects of glyphosate on *Synechocystis sp.* PCC 6803 growth. Fresh growth medium flasks with the indicated final concentrations of glyphosate were inoculated with cyanobacterial cells and optical density measured at 24 h intervals. Bars represent mean ± SD (*n* = 3).

A similar experiment was conducted using *Chlamydomonas* inoculated to a final optical density of 0.021 (at 600 nm wavelength) into fresh medium with final glyphosate concentrations of 0 mM, 1 mM or 2 mM. At this inoculation density, there was a lag phase that lasted for 3 days in the untreated control cultures. After 3 days, the untreated cells entered the exponential phase that lasted for the duration of the subsequent 4 days. At both the 1 mM and 2 mM concentration, glyphosate totally suppressed algal cell multiplication (Figure 3.3). These results provide the glyphosate concentrations that effectively block *Chlamydomonas* cell culture growth. Additionally, the starting inoculum density was low enough for a significant lag phase, which presumably could be avoided by using a higher inoculum density for the cultures to immediately enter the exponential growth phase. Taken together, these results provide the glyphosate concentrations that suppress cyanobacterial and algal cell culture growth.

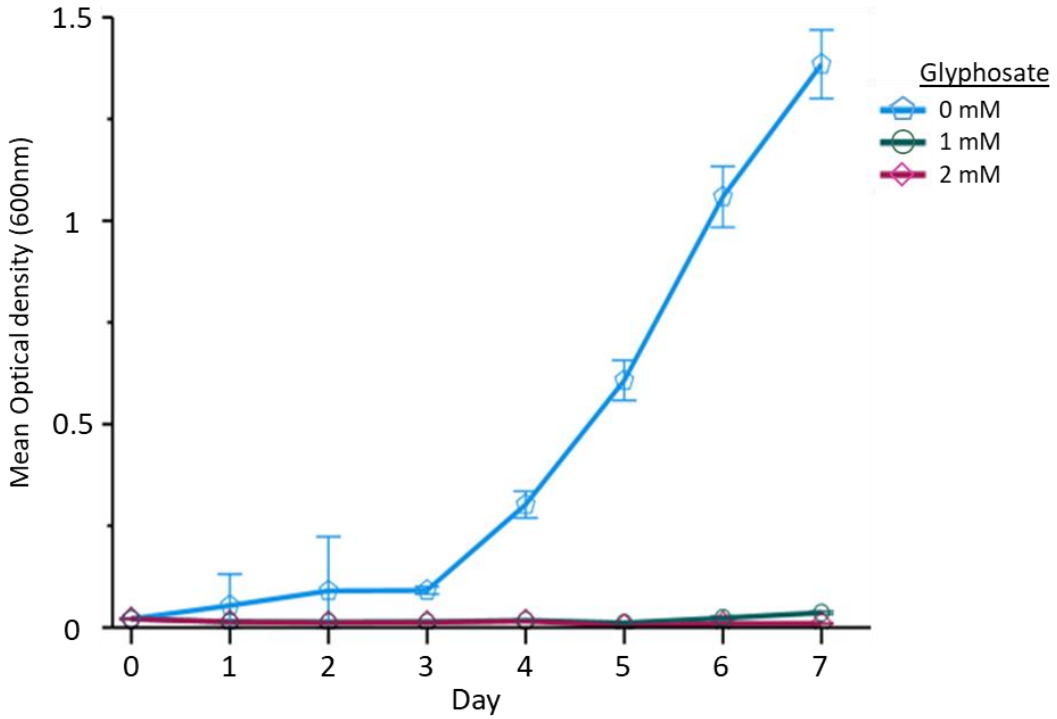

Figure 3.3. Effects of glyphosate on the growth of *Chlamydomonas* cell cultures. Legend denotes concentration of glyphosate treatment. Fresh growth medium flasks with the indicated final concentrations of glyphosate were inoculated with microalgal cells and optical density measured at 24 h intervals. Bars represent mean ± SD (*n* = 4).

3.1.2 Effects of glyphosate on cell metabolic activity

The previous section revealed the effects of glyphosate on cell culture growth, but not the effects of the herbicide on the metabolic activity of the cells. To investigate the latter, dense cell cultures of *Synechocystis sp.* and *Chlamydomonas reinhardtii* were treated with a range of glyphosate concentration. The cultures were immediately incubated in complete darkness for 24 h and then transferred to a 16 h photoperiod for the subsequent 72 h. Figure 3.4 shows the appearance of glyphosate-treated *Synechocystis* cultures at the end of the 72 h incubation period in the light-dark cycle. Cells treated with 0.5 or 1.0 mM glyphosate appeared greener than control cells, while higher glyphosate concentrations caused progressive chlorosis (Figure 3.4). To assess the metabolic activity of these cultures, MTT solution was added to each flask and cellular conversion of MTT to formazan allowed to proceed over 24 h. Photographs of the reactions showed cell metabolic activity at all glyphosate concentrations, with the exception of 5 mM glyphosate (Figure 3.4). The MTT assay is a colorimetric measure of cell viability, where the yellow tetrazole compound is reduced to a purple coloured formazan by cellular reductase and dehydrogenase enzymes. This provides an indication of the relative number and metabolic status of cells present within a sample. Cells without any metabolic activity will remain yellow, while the intensity of purple is proportional to cell viability. The absorbance at 570 nm of formazan extracted

from control cells is arbitrarily considered as 100% viability, which is used to calculate viability in other treatments proportionally.

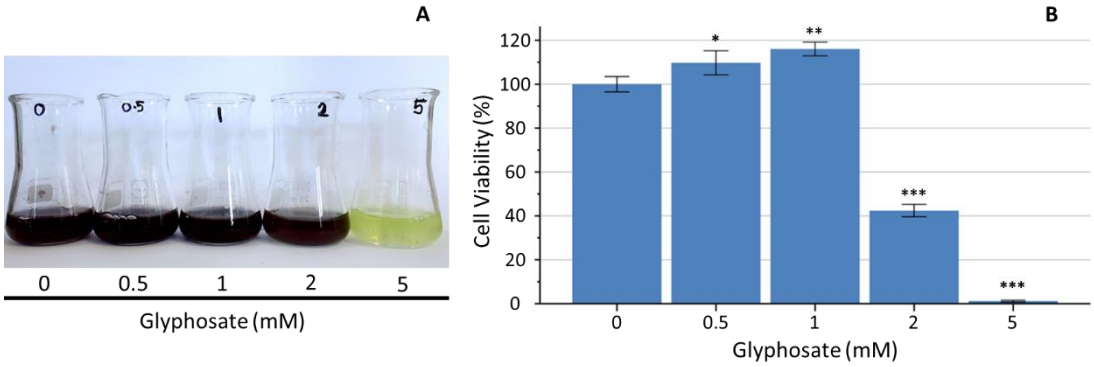

Figure 3.4. Effects of glyphosate on *Synechocystis* cell metabolic activity. Cell cultures were treated with the indicated glyphosate concentrations: (**A**) Appearance of cells treated with glyphosate for 72 h and incubated with MTT solution over the subsequent 24 h (**B**) Quantitative analysis of cell viability was performed with technical replicates. Bars represent mean ± SD (*n* = 3). Significant differences between means are denoted by one (P<0.05), two (P<0.01) or three (P<0.001) asterisks.

These results revealed that 5 mM glyphosate completely shut down metabolic activity, indicating that the cultures were dead. Extraction and spectrophotometric quantification of the formazan accumulated in the cells provided a measure of the level of cell viability relative to control cells assumed to have 100% viability (Figure 3.4). While treatment with either 0.5 or 1 mM glyphosate did not reduce cell metabolic activity, 2 mM and 5 mM glyphosate significantly suppressed metabolic activity. When taken together with the cell culture growth results (Figure 3.3), it can be concluded that 1 mM glyphosate inhibits cell multiplication without suppression of general cell metabolic activity and that 2 mM glyphosate downregulates cell metabolic activity and cell division. Thus, 1 mM glyphosate is growth-inhibiting but not cytotoxic, while 2 mM glyphosate is cytotoxic and inhibits cell culture growth. Overall, these results demonstrated that glyphosate tolerance is higher in dense cultures (Figure 3.4) than in the low density subcultures (Figure 3.3).

In *Chlamydomonas,* photographs showed strong cell metabolic activity in 0, 1, 2, or 3 mM glyphosate-treated cultures, while 4 and 5 mM glyphosate reduced such activity (Figure 3.5). Quantitative analysis revealed a massive drop in metabolic activity in cells treated with either 4 mM or 5 mM glyphosate (Figure 3.5). The 3 mM glyphosate-treated cultures showed ~50% decrease in cell viability, whilst 1 mM and 2 mM glyphosate had increases in metabolic activity, with the 2 mM samples showing the largest increase. The stimulation of

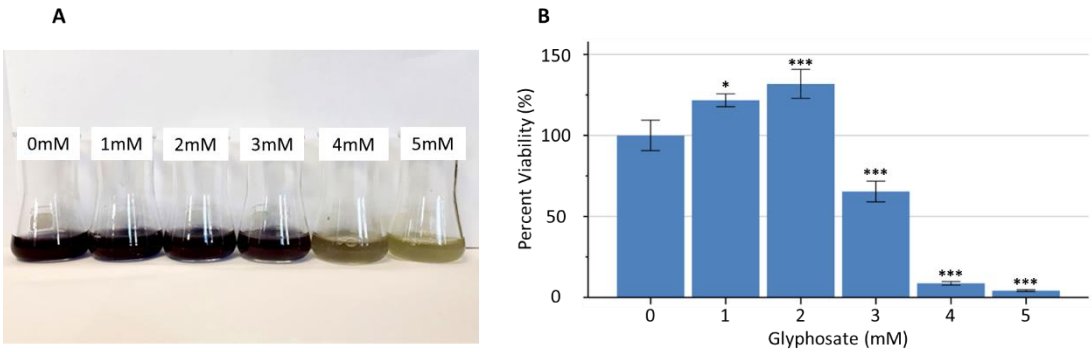

Figure 3.5 Effects of glyphosate on *Chlamydomonas* cell metabolic activity. (**A**) Appearance of *Chlamydomonas* cultures treated with glyphosate for 72 h and then incubated with MTT solution over the subsequent 24 h. Molar concentrations of glyphosate indicated on each flask. (**B**) Quantitative analysis of cell viability using samples from **A**. Bars represent mean ± SD (n = 3). Significant differences between means are denoted by one ($p < 0.05$), two ($p < 0.01$) or three ($p < 0.001$) asterisks.

cell activity demonstrates a hormetic response - where a sub-lethal dose stimulates cell activity. Thus, 2 mM glyphosate is a sub-lethal dose, while 5 mM glyphosate is clearly cytotoxic. Overall, these results provided a useful information on the appropriate glyphosate concentrations required for activation of lethal or hormetic responses in these organisms. The so-called hormetic and lethal glyphosate doses are 1 mM and 2 mM in *Synechocystis*, and 2 mM and 4 mM in *Chlamydomonas*. These concentrations were used in the subsequent proteomics and gene expression analysis experiments.

3.2 Proteomics analysis

3.2.1 iTRAQ analysis

To investigate the mechanism of glyphosate toxicity, a global proteomic analysis of the response of *Synechocystis* to a sublethal (1 mM) and lethal (2 mM) concentrations of glyphosate was conducted. Cells grown to a dense cell culture in the absence of stress were treated with 0 mM, 1 mM, or 2 mM glyphosate and harvested 24 h later for protein extraction. Prior to extraction of proteins, representative flasks of the treated cell cultures were photographed (Figure 3.6). All cultures had a healthy green colour irrespective of the glyphosate concentration and their cell metabolic activity reflected by conversion of MTT to the purple formazan product was not diminished, even in the 2 mM glyphosate treatment. These results show that none of the treatments had caused cell death on the samples subsequently used for protein extraction.

A total of 12 protein samples were generated, consisting of 4-replicate controls, 4-replicate 1 mM glyphosate-treated samples, and 4-replicate 2 mM glyphosate-treated samples. Protein sample quality was checked via SDS-PAGE analysis of CyDye-labelled aliquots and no protein degradation was detected and the relative protein concentration across all samples was correct as shown in protein gel images in Appendix I. After confirmation of protein sample integrity and quality, the samples were labelled with iTRAQ tags and analysed using LC-MS. This generated a list of identified proteins and a separate list of the associated peptides used in protein identification. The hormetic dataset initially had 1009

proteins, while the lethal dataset had 1157 proteins. A filter was applied to exclude all peptides identified with a confidence level below 95% and retain non-redundant proteins identified on the basis of 2 or more peptides passing this threshold. This trimmed the hormetic dataset to 397 proteins and the lethal dataset to 462 proteins. After application of statistical analysis to the datasets, only proteins significantly ($p < 0.05$) changing in abundance in response to treatment were retained for further analysis. The final datasets from the 1 mM (hormetic) and 2 mM (lethal) glyphosate-treated samples are presented in Table S1 (Appendix II).

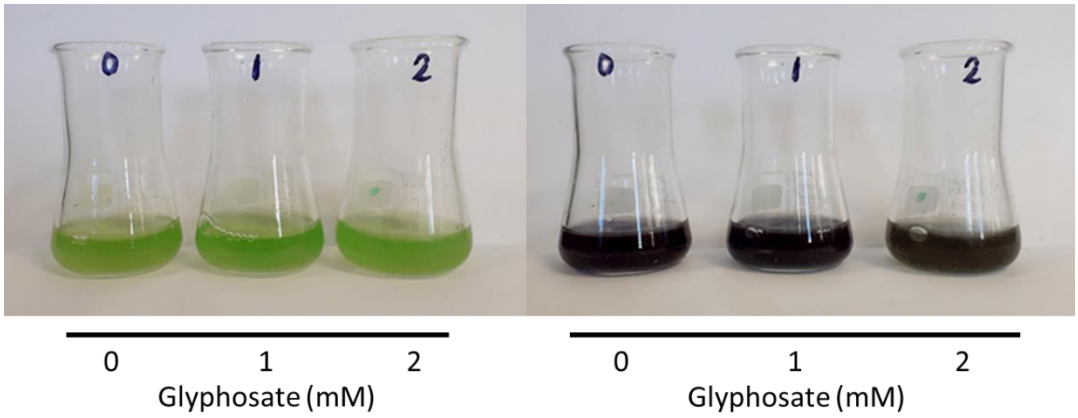

Figure 3.6. Effects of glyphosate treatment on *Synechocystis* within 24 hours. Left panel: Dose-response of glyphosate treated *Synechocystis* cultures 24 h after treatment. Right panel: Same cultures in A 24 h after addition of MTT solution. It is clear that all culture are viable.

Proteins in each treatment group were ranked in descending order of the modulus fold-change and the top 20 proteins protein from the both the 1 mM and 2 mM glyphosate-responsive proteins were selected and combined. Eight proteins of these 40 candidates were duplicated and these are: 33 kDa chaperonin; Allophycocyanin beta chain; General secretion pathway protein G; Inorganic pyrophosphate; Rubisco large chain; RNA binding protein (RRM domain); Slr0244 (like-Universal stress protein); and Fe-Superoxide dismutase. After removing the duplicates, a non-redundant list of 32 proteins was generated and constitute Table 3.1.

Table 3.1. Differentially expressed proteins in *Synechocystis* cell cultures responding to glyphosate treatment.

Accession[a]	Protein name	1mM glyphosate		2mM glyphosate	
		Ratio[b]	*p*-value[c]	Ratio[b]	*p*-value[c]
sp|P73910|HSLO_SYNY3	33 kDa chaperonin	-1.50	0.16	-1.67	0.03
sp|P73826|PHAB_SYNY3	Acetoacetyl-CoA reductase	1.60	0.01	-1.05	0.84
sp|Q01952|APCB_SYNY3	Allophycocyanin beta chain	1.77	0.01	1.81	0.00
tr|P73609|P73609_SYNY3	Anti-sigma factor antagonist	1.26	0.24	1.62	0.00
sp|P72991|FTSH3_SYNY3	ATP-dependent zinc metalloprotease FtsH 3	-1.82	0.21	1.32	0.03
tr|P73287|P73287_SYNY3	Bacterioferritin	1.95	0.04	-1.06	0.77
sp|P73407|CCMK4_SYNY3	Carbon dioxide-concentrating mechanism protein (CcmK) homolog 4	1.54	0.01	-1.25	0.45
sp|P09190|PSBE_SYNY3	Cytochrome b559 subunit alpha (PsbE)	-1.36	0.17	-2.15	0.01
sp|Q55664|ALF2_SYNY3	Fructose-bisphosphate aldolase class 2	1.19	0.06	1.72	0.00
tr|P73704|P73704_SYNY3	General secretion pathway protein G	-1.87	0.01	-2.32	0.00
sp|P80505|G3P2_SYNY3	Glyceraldehyde-3-phosphate dehydrogenase 2 (GADPH)	1.50	0.00	1.61	0.01
sp|P80507|IPYR_SYNY3	Inorganic pyrophosphatase (PPase)	1.50	0.01	2.18	0.00
sp|P73954|Y1513_SYNY3	Membrane-associated protein slr1513	-1.29	0.00	-1.72	0.45
tr|Q6YRU4|Q6YRU4_SYNY3	Sll6060 (N-acetyltransferase domain-containing) protein	-1.02	0.11	-1.89	0.05
sp|P74102|OCP_SYNY3	Orange carotenoid-binding protein (OCP)	1.63	0.11	-1.54	0.00
tr|P72709|P72709_SYNY3	Organic Solute transporter alpha-like (OstA) Slr0250 protein	1.16	0.23	2.13	0.02
tr|Q55387|Q55387_SYNY3	Periplasmic binding protein of ABC transporter for natural amino acids	2.13	0.93	-1.06	0.01
sp|P29256|PSAF_SYNY3	Photosystem I reaction centre subunit III (PsaF)	-1.06	0.01	1.65	0.10

sp|P54691|ILVE_SYNY3	Probable branched-chain-amino-acid aminotransferase	1.50	0.33	1.76	0.00
sp|P72776|PDXJ_SYNY3	Pyridoxine 5'-phosphate synthase	-2.08	0.02	-1.76	0.66
tr|P73405|P73405_SYNY3	Pyruvate dehydrogenase E1 component subunit beta	1.49	0.83	1.65	0.00
sp|P54205|RBL_SYNY3	Ribulose bisphosphate carboxylase large chain	1.76	0.09	2.18	0.00
tr|P73557|P73557_SYNY3	RNA-binding protein (RRM domain)	-1.19	0.34	3.23	0.03
tr|P72700|P72700_SYNY3	Slr0244 (universal stress protein-like) protein	1.54	0.01	-1.08	0.00
tr|P73328|P73328_SYNY3	Slr1900 protein	-1.05	0.54	-1.76	0.01
tr|P74426|P74426_SYNY3	Slr1940 protein	1.56	0.03	-1.11	0.31
tr|P73244|P73244_SYNY3	Slr2025 (ybjN domain containing) protein	-1.20	0.37	-2.33	0.01
sp|P77968|SODF_SYNY3	Superoxide dismutase [Fe]	1.51	0.00	1.78	0.02
sp|Q55511|TIG_SYNY3	Trigger factor	-1.23	0.04	-2.00	0.00
tr|P73592|P73592_SYNY3	Uncharacterized Slr1406 protein	1.53	0.03	-1.40	0.14
tr|P74470|P74470_SYNY3	Uncharacterized Ssl0242 protein	1.54	0.01	-1.13	0.63
sp|P54224|DCUP_SYNY3	Uroporphyrinogen decarboxylase	2.24	0.05	-1.12	0.50

[a] Protein accession number in the UniProt database.
[b] Ratio of the comparison of protein abundance in control to glyphosate-treated samples. This is equivalent to the protein fold-change. Negative values indicate protein down-regulation in glyphosate treatments.
[c] Probability value from Student's t-test analysis for comparing the control mean to the glyphosate sample mean.

Five proteins directly related to photosynthesis and subsequent electron transport feature in the top-32 list (Table 3.1). These proteins are: allophycocyanin β-chain, bacterioferritin, PSII-associated cytochrome b559 subunit alpha (*PsbE*), orange carotenoid binding protein (OCP), and Photosystem I reaction centre subunit III (*PsaF*). All these proteins play a direct role in regulating or facilitating the flow of electrons or harvesting of light energy in the thylakoid membranes. A noticeable observation is the difference in protein changes between cells responding to hormetic versus lethal glyphosate doses.

In the hormetic response (1 mM glyphosate), *PsaF*, allophycocyanin β and bacterioferritin significantly increased in abundance by over 1.5-fold. Bacterioferritin is important in storage of iron, which is highly essential in cyanobacterial photosynthesis. This could be an indication that the general level of photosynthetic activity is increasing. The increase in

allophycocyanin, a protein involved in photosynthetic light-harvesting, suggests that the cells have increased capacity to capture more light energy. Finally, an increase in the abundance of *PsaF*, the plastocyanin docking subunit of PSI suggests an upsurge in PSI activity and thereby an increase in the reduction of $NADP^+$ to NADPH. These results are consistent with increased photosynthetic activity driving the observed hormesis.

In contrast, there were considerable differences in photosynthetic protein responses in the lethal (2 mM glyphosate) dose. The upregulation of bacterioferritin and *PsaF* seen in hormesis was absent from the lethal interaction. Instead, there was a remarkable suppression of OCP and *PsbE* proteins, a response that did not occur in hormesis. As *PsbE* transfers electrons from PSII to plastoquinone, its reduction implies that photochemistry from PSII is impaired and the electrons are likely to be off-loaded to molecular oxygen leading to ROS generation and cell damage. This is particularly problematic for survival of the cells, given that a component of the light-harvesting phycobilisome (allophycocyanin-β) was significantly increased in the lethal response. However, the swinging of suppression OCP (Table 3.1) along with several other phycocyanin proteins (Table S1 in Appendix II) may indicate attempts to remove the outer structure of the phycobilisome as a countermeasure. The overall impact is a reduction in carbon fixation capacity.

The response of Calvin-Benson cycle enzymes to glyphosate showed both similarities and differences between hormesis and lethal datasets. Although the rubisco large subunit (RBCL) and fructose-biphosphate aldolase did not significantly change in hormesis, they were highly upregulated in the lethal response (Table 3.1). This trend was similar for other enzymes, such as transketolase, phosphoglycerate kinase and Rubisco small subunit (Table S1, Appendix II). In contrast, glyceraldehyde-3-phosphate dehydrogenase (GADPH) was significantly upregulated under both conditions (Table 3.1). The response of Calvin-Benson cycle enzymes indicates that shikimate pathway inhibition may activate negative or positive feedback signalling to the major cellular distribution hub of molecular building blocks.

Clues to metabolic adaptations underpinning hormesis emerge when the response of proteins downstream of the Calvin-Benson cycle are considered. Pyridoxine-5'-phosphate synthase increased 2.1-fold in hormesis, suggesting a substantial increase in vitamin B_6 metabolism. This may also indicate increases in lipid metabolism and amino acid production, suggesting that cells counteract sublethal inhibition of the shikimate pathway by increasing overall rates of amino acid biosynthesis. A 1.6-fold increase in acetoacetyl-CoA reductase may reflect an increase in synthesis of polyhydroxybutyrate (PHB), a biopolymer used as a carbon sink by bacteria in the presence of low nitrogen and/or an excess of NADPH and electrons (Koch et al., 2020). This could indicate that cells divert excess fixed carbon away from the restricted shikimate pathway towards biopolymer production in response to glyphosate. Uroporphyrinogen decarboxylase increased 2.20-fold. As this is a key enzyme involved in the biosynthesis of chlorophyll, this suggests that cells are not only thriving in response to mild glyphosate stress, but actively increase their photosynthetic capacity. In contrast, the lethal 2 mM glyphosate dose showed no significant impact on acetoacetyl-CoA reductase, pyridoxine-5-phosphate synthase nor uroporphyrinogen decarboxylase (Table 3.1).

Ferric superoxide dismutase (Fe-SOD) increased in both the hormetic and lethal response by 1.5-fold and 1.7-fold, respectively (Table 3.1). Fe-SOD is the primary enzyme for detoxification of superoxide generated in the thylakoid membrane by the photosystems. This is consistent with the interpretation that glyphosate treatment raises the redox homeostasis and induces photooxidative stress.

3.2.2. Gene ontology analysis

Gene overrepresentation analysis was performed for biological process, cellular component, and molecular function. However, cellular component (CC) was the only analytical function which yielded significant data. Significance of overrepresentation was calculated using Fishers exact test, expected number of significant CC-associated proteins from the raw data was run alongside protein data from the final data table to calculate a *p*-value. Raw *p*-values were corrected by calculating the false discovery rate (see 2.3.5). Table 1 shows results of gene ontology analysis using proteins responsive to 1 mM glyphosate treatment. The 1 mM glyphosate-treated samples showed a significant overrepresentation of bacterial thylakoid proteins (with significant fold changes) present in the iTRAQ data (Appendix II) with a fold enrichment of 3.44. There was also significant overrepresentation of proteins in non-membrane bound organelles related to the bacterial thylakoids, such as Rubisco and structural proteins of the carboxysome. This tell us the proteins of the photosynthetic apparatus were most effected by sub-lethal glyphosate treatment, thus confirming that the mechanism of glyphosate induced stress is present in the photosynthetic electron transport chain and Calvin cycle.

Table 3.2. Gene ontology analysis of *Synechocystis* proteins responsive to 1 mM glyphosate

1mM Glyphosate Gene Ontology						
Cellular component[a]	N. ref prot[b]	N. sig. prot[c]	Expected sig.prot[d]	Fold-enrichment[e]	Raw *p*-value[f]	FDR[g]
Bacterial thylakoid	50	10	2.91	+3.44	0.001	0.040
Thylakoid	55	10	3.20	+3.12	0.002	0.039
Intracellular non-membrane-bound organelle	97	15	5.65	+2.66	0.000	0.053
Intracellular organelle	107	15	6.23	+2.41	0.001	0.054
Organelle	107	15	6.23	+2.41	0.001	0.044
Non-membrane-bound organelle	97	15	5.65	+2.66	0.000	0.027

[a]GO cellular component grouping by Pantherdb.
[b]Number of related proteins in raw data
[c]Number of proteins with statistically significant foldchanges
[d]Number of proteins expected to fold significantly due to chance
[e]Value represents proportion of proteins with significant fold changes versus expected number of fold changes. + indicates a higher value than expected, - indicates a lower value than expected.
[f]Uncorrected probability value from Student's t-test analysis for Fold enrichment. Enrichment is significant when $p < 0.05$.
[g]Corrected *p*-value, calculated via the false discovery rate.

The 2 mM glyphosate-treated samples presented similar significant overrepresentation of 2.38 for proteins in the bacterial thylakoid. This demonstrated an almost identical trend to that seen in the GO analysis of the 1 mM glyphosate-treated samples. The phycobilisome-related proteins also had a significant overrepresentation in the gene ontology, with a fold enrichment of 4.27, likely caused by the large number of significant negative fold-changes in phycocyanin, OCP and phycobilisome structural proteins (Table 3.3). This demonstrates that the lethal mechanism of glyphosate induced cell death is present within the photosynthetic apparatus.

Table 3.3 Gene ontology analysis of Synechocystis proteins responsive to 2 mM glyphosate

2mM Glyphosate Gene Ontology						
Cellular component[a]	N. ref prot[b]	N. sig. prot[c]	Expected sig.prot[d]	Fold-enrichment[e]	Raw *p*-value[f]	FDR[g]
Phycobilisome	13	7	1.64	+ 4.27	0.004	0.032
Cellular anatomical entity	396	69	49.96	+ 1.38	0.000	0.007
Protein-containing complex	104	28	13.12	+ 2.13	0.000	0.007
Thylakoid membrane	46	16	5.80	+ 2.76	0.001	0.011
Photosynthetic membrane	50	16	6.31	+ 2.54	0.002	0.019
Thylakoid	53	17	6.69	+ 2.54	0.001	0.014
Intracellular anatomical structure	281	58	35.45	+ 1.64	0.000	0.002
Light-harvesting complex	13	7	1.64	+ 4.27	0.004	0.030
Plasma membrane-derived thylakoid membrane	43	14	5.42	+ 2.58	0.003	0.031
Plasma membrane-derived chromatophore membrane	43	14	5.42	+ 2.58	0.003	0.036
Plasma membrane-derived chromatophore	43	14	5.42	+ 2.58	0.003	0.033
Cytoplasm	255	50	32.17	+ 1.55	0.001	0.011
Bacterial thylakoid	50	15	6.31	+ 2.38	0.004	0.030
Intracellular non-membrane-bounded organelle	98	27	12.36	+ 2.18	0.000	0.008
Intracellular organelle	108	27	13.63	+ 1.98	0.001	0.014
Organelle	108	27	13.63	+ 1.98	0.001	0.013
Non-membrane-bounded organelle	98	27	12.36	+ 2.18	0.000	0.007
Plasma membrane region	43	14	5.42	+ 2.58	0.003	0.030
Unclassified	351	25	44.28	- 0.56	0.000	0.013

[a]GO cellular component grouping by Pantherdb.
[b]Number of related proteins in raw data
[c]Number of proteins with statistically significant foldchanges
[d]Number of proteins expected to fold significantly due to chance
[e]Value represents proportion of proteins with significant fold changes versus expected number of fold changes. + indicates a higher value than expected, - indicates a lower value than expected.
[f]Uncorrected probability value from Student's t-test analysis for Fold enrichment. Enrichment is significant when $p < 0.05$.
[g]Corrected *p*-value, calculated via the false discovery rate.

There were also many cytoplasmic proteins with significant fold-changes, as evidenced by their 1.55-fold enrichment. However, most of these enzymes operate in diverse metabolic pathways and cellular functions, ranging from structural, transport, antioxidants, and RNA translation and protein synthesis. There was 0.56-fold enrichment in unclassified proteins, this somewhat interesting as the function of these proteins is almost entirely unknown and yet they share a commonality of being underrepresented in response to stress (Table 3.3).

3.3. Gene expression analysis

For gene expression analysis, cell cultures were treated with three different glyphosate concentrations (0 mM, 1 mM, 2 mM) and triplicate samples for RNA extraction harvested at 0-, 3-, 6- and 12-hour (h) timepoints. Using cDNA synthesised from these samples, the specificity of 17 primer sequences (Table S2, Appendix III) were designed to PCR-amplify selected target genes. PCR amplification and DNA gel electrophoresis revealed that 16 of the primers specifically amplified the target genes (Figure S2, Appendix III). Using the verified primers, quantitative RT-PCR analysis was performed on the selected target genes and the results are presented in the sections below.

3.3.1 Shikimate pathway genes

Because the shikimate pathway is an established primary target for glyphosate inhibition, some genes of the pathway were selected for analysis. Figure 3.7 shows the response of *DAHPS*, the enzyme catalysing the commitment step of the pathway. There were no significant *DAHPS* expression changes in control nor 1 mM glyphosate-treated samples across the timecourse. However, exposure to 2 mM glyphosate resulted in suppression of gene expression to less than half at both 3 and 12 hours. The lack of significant suppression of gene expression at 6 hours is likely due to the variability of the replicate samples at this timepoint, probably arising from a technical error. The overall suppression of *DAHPS* indicates that metabolic flux through the shikimate pathway was lowered at the lethal 2 mM glyphosate treatment in contrast to controls and the sublethal 1 mM glyphosate.

EPSPS gene expression showed a very modest increase at the 3 and 12 h timepoints in the 2 mM glyphosate-treated samples (Figure 3.7). No significant changes were observed in the control or 1 mM glyphosate-treated samples. This shows that, although EPSPS protein is the target for glyphosate, its gene expression is only slightly increased by a lethal dose within 12 hours of treatment. chorismate synthase showed no statistically significant changes in any treatment across 12 hours (Figure 3.7). As the lethal glyphosate dose curtails metabolite flux through EPSPS, it is unsurprising that downstream genes, such as the gene encoding chorismite synthase, will remain unchanged due to a greater need to synthesize aromatic amino acids and other shikimate pathway end products.

Overall, the response of *Synechocystis* to lethal and sublethal concentrations of glyphosate causes only minor alteration in gene expression across the shikimate pathway, with the genes encoding the target enzyme EPSPS as well as chorismate synthase showing no changes in expression after glyphosate inhibition. The drop in *DAHPS* gene expression indicates that less fixed carbon is being sent from the Calvin-Benson cycle into the

shikimate pathway. This adds weight to the hypothesis that the main lethal mechanism for glyphosate occurs metabolically upstream.

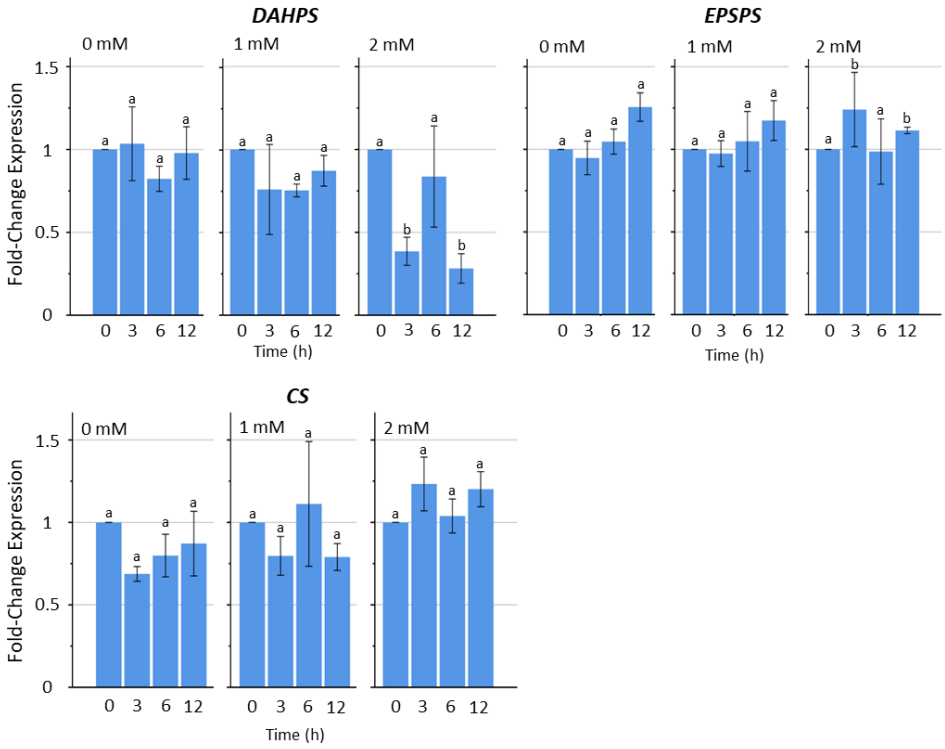

Figure 3.7. Effects of glyphosate on cyanobacterial shikimate pathway gene expression. Cells were treated with indicated concentrations of glyphosate and samples harvested at the indicated timepoints for RNA extraction and qRT-PCR analysis. Bars represent mean ± SD (n = 3). *DAHPS*, 3-deoxy-D-arabino-heptulosonate 7-phosphate synthase; *EPSPS,* 5-enolpyruvylshikimate-3-phosphate synthase; *CS,* chorismate synthase. Means that do not share a letter are significantly different.

3.3.2 Calvin-Benson cycle genes

One of the metabolic pathways directly upstream of the shikimate pathway is the Calvin-Benson cycle. Additionally, several Calvin-Benson cycle enzymes significantly changed (Table 3.1), indicating that this metabolic pathway is indirectly responsive to glyphosate treatment. Gene expression analysis can be used to target selected candidates in the pathway to investigate the extent of its response to glyphosate.

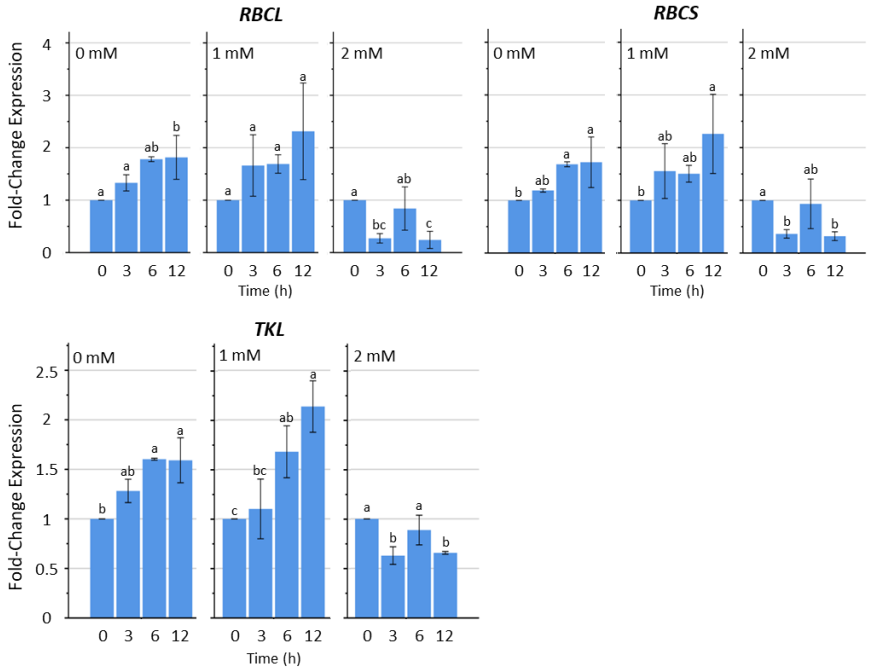

Figure 3.8. Effects of glyphosate on cyanobacterial Calvin-Benson Cycle gene expression. Cells were treated with indicated concentrations of glyphosate and samples harvested at the indicated timepoints for RNA extraction and qRT-PCR analysis. *TKL* denotes transketolase, *RBCL* denotes the Rubisco large subunit, *RBCS* denotes the Rubisco small subunit. Means that do not share a letter are significantly different.

Transketolase (*TKL*) expression increased over the 12 h period in control samples and the hormesis samples (Figure 3.8). However, the lethal 2 mM glyphosate treatment suppressed activation of *TKL* expression (Figure 3.8). Transketolase is a Calvin-Benson cycle enzyme responsible for production of Ethyrose-4-Phosphate , a precursor the shikimate pathway synthesis of 3-Deoxy-D-arabinoheptulosonate 7-phosphate (DAHP). A similar trend was observed for Rubisco large subunit (RBCL) and Rubisco small subunit (RBCS), indicating that the treatments likely affected expression of genes encoding enzymes of the entire pathway in similar fashion. Overall, this demonstrates that the hormesis-inducing 1 mM glyphosate stimulated carbon fixation, while the lethal 2mM dose suppressed the Calvin-Benson cycle even before the cells had died (0-12 h). However, protein measurements taken 24 h after treatment show increases of transketolase and Rubisco in the lethal treatment (Table 3.1). This discrepancy between gene expression and protein expression may reflect the different timepoints of sampling between these experiments or an indication of differential post-transcriptional processes, such as protein turnover. Viewed differently, the rise in Calvin-Benson cycle enzymes in the lethal response is a clear indication of a build-up of metabolites due to inhibition of the shikimate pathway.

3.3.3 Photosystem and phycobilisome related genes

Recent evidence shows that glyphosate toxicity is light-driven (Belbin et al., 2019; Chivasa and Gonzalez-Torralva, 2019) and that glyphosate induces oxidative stress in plant chloroplasts (Radwan and Fayez, 2016; Gomes et al., 2017). The proteomic data also revealed that some of the proteins supporting the photosynthetic light reactions are differentially expressed in response to glyphosate treatment. Therefore, it was necessary to examine the effects of glyphosate on the expression of selected photosystem and phycobilisome proteins.

The heterodimeric cytochrome b_{559} is responsible for transferring electrons from PSII to plastoquinone. Expression of the gene coding for the alpha subunit (*PsbE*) significantly increased from 0-12 h in control and sublethal glyphosate treatments (Figure 3.9). This increase is likely to be stimulated by light incubation since these cultures had just moved out of the dark phase. However, the lethal glyphosate level completely suppressed this light-induced response (Figure 3.9). A similar response profile was observed for *PsaA*, the gene coding for PSI subunit A. Although the D2 subunit (*PsbD*) of PSII had a very modest light-induced increase under control conditions, the changes under glyphosate treatment were not significant as they remained within the background noise of biological and technical variation (Figure 3.9). Overall, these results show that the sublethal 1 mM glyphosate treatment does not impede the photosynthetic electron transfer, while the lethal dose activates a very different response profile. PSII activity is unaffected while PSI activity is shutdown under lethal conditions – this enables PSII to continue generating electrons and diverting them to molecular oxygen when PSI is shutdown.

The orange carotenoid binding protein (OCP) is a key regulatory subunit of the cyanobacterial antenna complex. The orange carotenoid binding protein (OCP) is a key regulatory subunit of the cyanobacterial antenna complex involved in non-photochemical quenching of excess light energy. High light activates conformational changes in OCP, converting it to the bioactive red form (OCPr). This alters the structure of the phycobilisome, reducing its ability absorb and transfer light energy to the photosystems, and allowing excessive amounts of light energy to be dissipated as heat (Kirilovsky et al.,

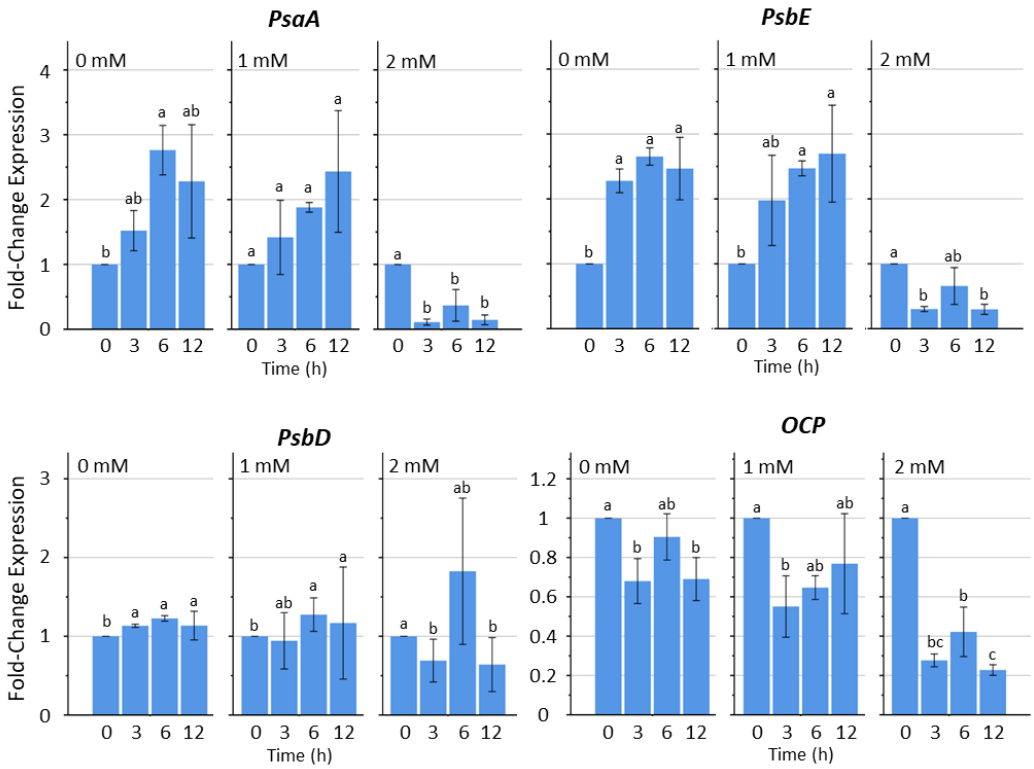

Figure 3.9. Effects of glyphosate on cyanobacterial photosystem and phycobilisome gene expression. Cells were treated with indicated concentrations of glyphosate and samples harvested at the indicated timepoints for RNA extraction and qRT-PCR analysis. *PsaA* denotes Photosystem I subunit A, *PsbE* denotes cytochrome b_{559} subunit alpha, *PsbD* denotes the photosystem II D2 subunit, OCP denotes the orange carotenoid binding protein. Means that do not share a letter are significantly different.

2014). In the control and sublethal glyphosate treatments, OCP gene expression fluctuated across the timepoints, but there was a very clear and consistent suppression by the lethal glyphosate dose (Figure 3.9). This result is consistent with the protein data showing that OCP (Table 3.1), phycocyanin protein, and associated rod proteins decreased in the lethal treatment (Table S1, Appendix II). This implies that the light-harvesting phycobilisome structure is truncated under lethal glyphosate. This also contributes to the growth retardation associated with glyphosate treatments.

3.3.4 Respiratory complexes and ATP synthesis genes

The impact of glyphosate on the respiratory pathway was investigated by targetting selected genes. This was relevant given that cyanobacteria possess a combined photosynthetic-respiratory elctron transport chain due to the absence of delineating organelles. Expression of ATP synthase beta-subunit (*ATPβ*) gene was stimulated by light as activation occurred in untreated control samples without glyphosate (Figure 3.10). At sublethal level (1 mM) glyphosate did not change the light response of the gene (Figure 3.10). However, the lethal 2 mM glyphosate treatment not only blocked the light response, but it significantly suppressed expression (Figure 3.10). Expression of the gene for NAD(P)H-quinone oxidoreductase subunit I (*NDH1*) was responsive to light activation as it increased in control samples without glyphosate (Figure 3.10). This remained unaffected in the sublethal glyphosate dose, while the lethal dose suppressed this response, albeit with high sample variation at 6 h (Figure 3.10). Expression of *SDH2*, the gene encoding Fe-S subunit of succinate dehydrogenase fluctuated with no clear trend in the control and sublethal 1 mM glyphosate treatment (Figure 3.10).

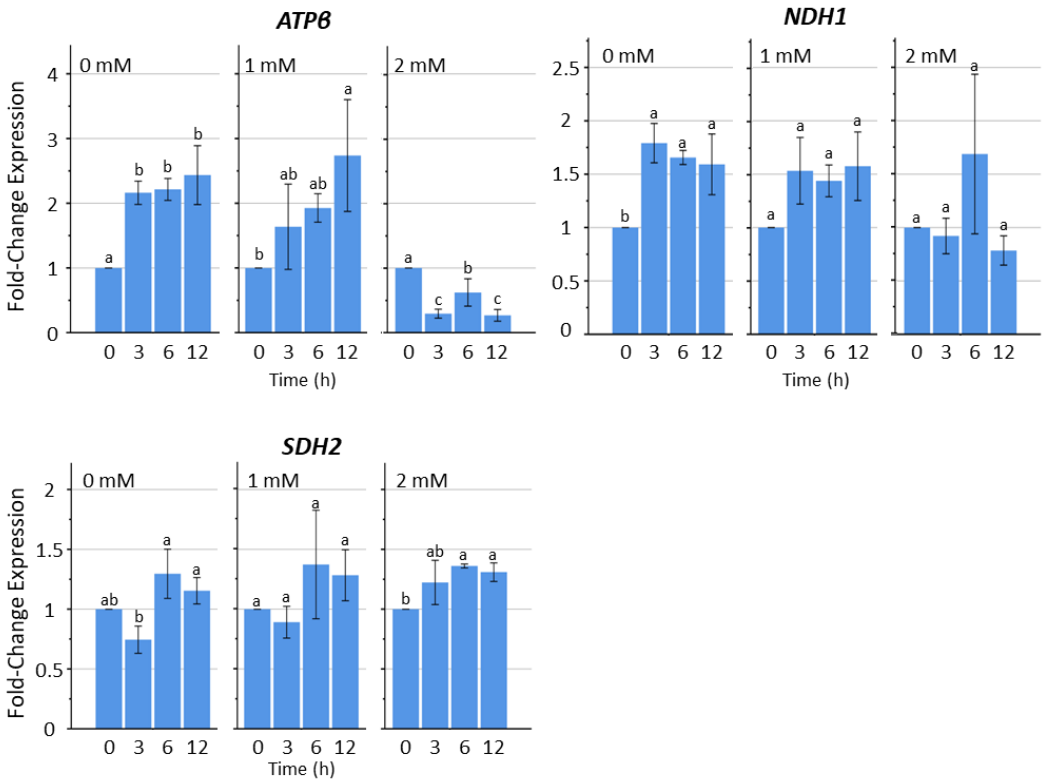

Figure 3.10. Effects of glyphosate on cyanobacterial respiratory electron transport and ATP synthesis associated gene expression. Cells were treated with indicated concentrations of glyphosate and samples harvested at the indicated timepoints for RNA extraction and qRT-PCR analysis. *ATPβ* denotes the ATP-Synthase beta subunit*, NDH1* denotes the NAD(P)H-quinone oxidoreductase subunit I, *SDH2* denotes the succinate dehydrogenase Fe-S subunit. Means that do not share a letter are significantly different.

Sample variation was low in the lethal dose, resulting in a significant upregulation of the gene, but the magnitude of change remained within the range seen in the control and hormesis (Figure 3.10). Overall, changes in *NDH1* and *SDH2* are not convincing. In contrast, the clear suppression of *ATPβ* shows that lethal glyphosate suppresses energy production.

It should be noted that this gene functions in both respiratory and photosynthetic ATP synthesis. Therefore, it can be concluded that glyphosate appears not to affect genes exclusively in the respiratory pathway.

3.3.5 Lipid biosynthesis

We wondered if lipid biosynthesis may also increase during hormesis as happens to the synthesis of vitamin B_6, based on proteomics data. Previous results indicated that sublethal salinity stress increases lipid biosynthesis in *Synechocystis sp.* (Alarcon-Gutierrez, 2020). Therefore, the effects of glyphosate treatment on expression of the gene encoding the enzyme catalysing the commitment step in lip biosynthesis, acetyl coenzyme-A carboxylase (ACCase), was investigated. *ACCase* was stimulated by exposure to light, though the increase was not statistically significant, in the controls and both the hormetic and lethal doses of glyphosate (Figure 3.11). On the basis of this result, glyphosate appears not to activate lipid biosynthetic genes.

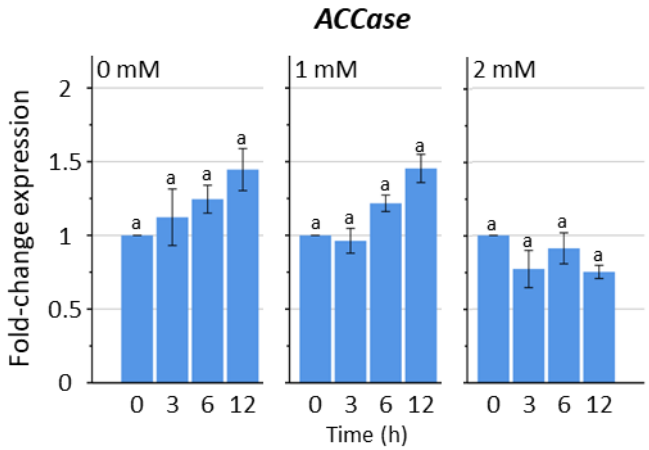

Figure 3.11. Effects of glyphosate on gene expression associated with fatty acid synthesis. Cells were treated with indicated concentrations of glyphosate and samples harvested at the indicated timepoints for RNA extraction and qRT-PCR analysis. *ACCase* denotes Acetyl Coenzyme-A Carboxylase. Cells were treated with indicated concentrations of glyphosate and samples harvested at the indicated timepoints for RNA extraction and qRT-PCR analysis. Means that do not share a letter are significantly different.

3.4 Secreted signals regulate cell response to glyphosate

Secreted signals have been recently shown to regulate the light-dependent cell death response of Arabidopsis cells to a mycotoxin that inhibits chloroplast functions (Chivasa & Goodman, 2020). We wondered whether glyphosate toxicity in *Chlamydomonas* and *Synechocystis* might be similarly regulated. Ten millilitre aliquots from a dense *Chlamydomonas* cell culture were placed in sterile Falcon tubes and centrifuged to aseptically separate the cell pellet from the medium. The cells were resuspended in an equivalent volume of one of 3 types of medium as follows: (i) fresh BG11 medium, (ii) conditioned medium, in which *Chlamydomonas* cells had been growing, and (iii) conditioned medium + nutrients, which is conditioned medium to which nutrients have been added to the same level as in fresh medium. The conditioned medium contains secreted signals, while fresh medium does not have any. After mixing the cells with the respective growth media, they were placed in sterile glass flasks and mock-treated or treated with 2 mM glyphosate. After 72 h incubation, the cultures were assayed for cell viability using the MTT assay and the results are shown in Figure 3.12. Remarkably, glyphosate activated cell death only in cells lacking secreted signals, that is cells incubated in fresh medium. In other words, secreted signals suppressed glyphosate-induced cell death. This response was not driven by the nutrient levels since cells in conditioned medium (full of extracellular signals) blocked death with or without additional nutrients. Thus, glyphosate toxicity is regulated by as yet unidentified extracellular signals.

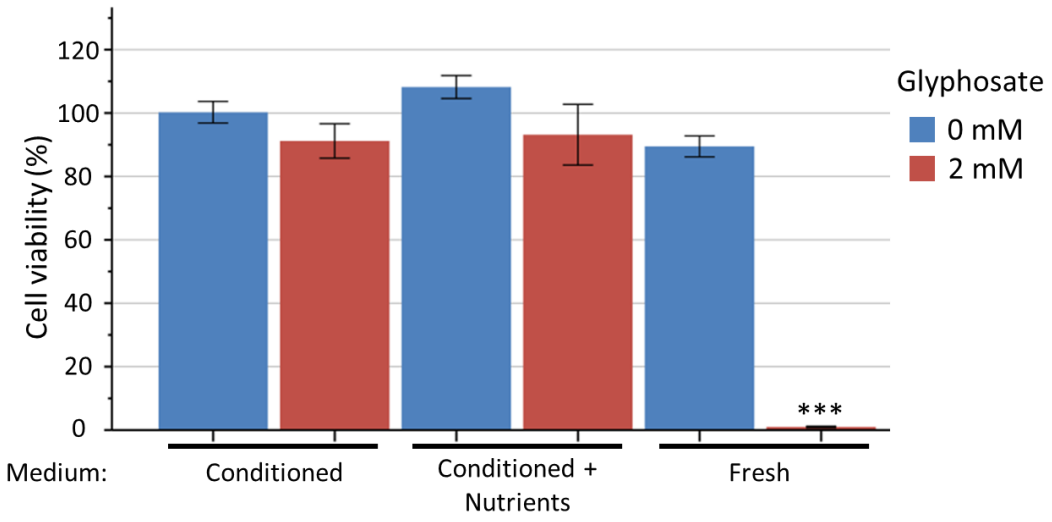

Figure 3.12. Effects of extracellular signals on glyphosate toxicity in *Chlamydomonas*. Cells in the indicated medium were treated with 0 mM (control) or 2 mM glyphosate for 72 h. Cell viability was evaluated using the MTT assay. Bars represent mean SD (n = 3). Asterisks denote significant difference between control and glyphosate-treated means ($p < 0.001$).

For *Synechocystis*, a similar experiment was setup with (i) fresh medium, (ii) conditioned medium, and (ii) conditioned medium fractionated into 0-5 kDa (5K) fraction and a 0-10 kDa (10K) fraction. This was achieved by centrifuging conditioned medium through a 5 kDa or 10 kDa molecular weight cut-off membrane, respectively. Cells resuspended in these types of media were mock-treated or treated with 1mM glyphosate for 72 h. Cell viability was evaluated using the MTT assay. The results are similar to what was observed in

Chlamydomonas. Secreted signals in conditioned medium blocked cell death in *Synechocystis* (Figure 3.13). In fact, the 1 mM glyphosate treatment used here is what we considered sublethal in previous experiments. However, in the absence of secreted signals, that is in fresh growth medium, this glyphosate dose is lethal (Figure 3.17). Medium fractionation indicated that components in the conditioned medium of a molecular weight below 10 kDa are responsible for suppressing glyphosate-induced cell death (Figure 3.13). Remarkably, both the 0-5 kDa and 0-10 kDa fractions strongly stimulated growth in the presence of glyphosate, which is the typical hormesis response. Since this stimulation was not seen with unfractionated conditioned medium, this suggests that secreted components >10 kDa may play a role in downregulating hormesis. This suggest the existence of a complex extracellular stress-regulatory system that may be deployed in biofilms.

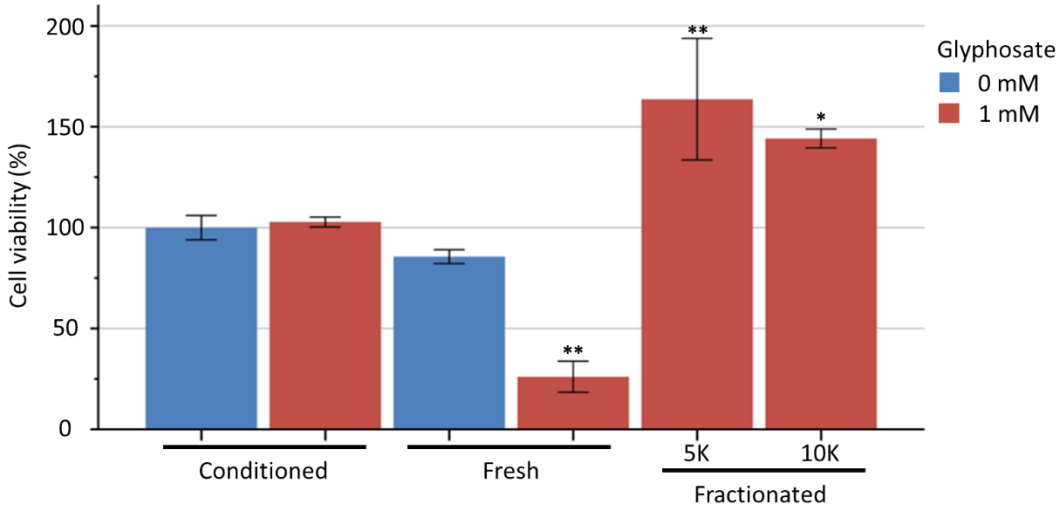

Figure 3.13. Effects of secreted signals on glyphosate toxicity in *Synechocystis sp.* PCC 6803. Cells were mock- or glyphosate-treated for 72 h and cell viability measured using the MTT assay. During treatment, cells were incubated in fresh medium, conditioned medium, or fractionated conditioned medium. For the latter, 5K and 10K refer to conditioned medium spun through 5 kDa or 10 kDa cut-off membranes. Bars represent mean ± SD (n = 3). Significant differences between means are denoted by one ($p < 0.05$) or two ($p < 0.01$) asterisks.

The phenomenon of cell death suppression by secreted factors could arise from glyphosate degradation or metabolism by extracellular enzymes or a result of authentic signalling through peptide signals and autoinducers or autoinducer-like compounds. To determine the mechanism will require several complementary approaches that include proteomics and metabolomic analyses. The size exclusion fractionation provides some clues to the possible molecular weight of the signal(s) involved in this phenomenon.

In the first instance, we wanted to explore the conditioned medium for the presence of proteins. To achieve this, intracellular proteins were extracted from *Synechocystis sp.* PCC 6803 cells and extracellular proteins were recovered from the conditioned medium via protein precipitation (see 2.5.2). The protein samples were labelled with fluorescent Cye-Dyes for visualisation without the use of stains. SDS-PAGE revealed that the extracellular and intracellular protein profiles are distinct and look very different (Figure 3.14). As expected, there are more protein bands in the intracellular fraction compared to the

extracellular fraction. Crucially, there are only a few visible protein bands below 10 kDa, suggesting that isolation of this fraction could lead to identification of proteins and peptides that might have bioactivity in regulating stress-induced death. The exact function or role or function of these extracellular peptides is unknown. All that can be gathered from these results is their presence within the extracellular matrix of *Synechocystis sp*. PPCC 6803.

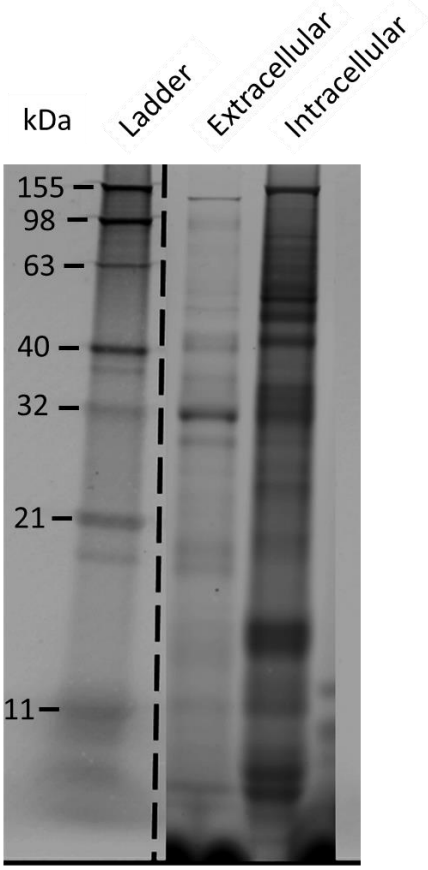

Figure 3.14. SDS-PAGE profile of *Synechocystis* PCC 6803 proteins. Intracellular proteins were extracted from cells and secreted (extracellular) proteins were recovered from the growth medium by precipitation. Protein samples were labelled with Cy5 and resolved by SDS-PAGE. Numbers denote the size of bands in the protein ladder.

Given that the 0-10 kDa range of conditioned medium has proteins, there is a possibility that these may metabolise or degrade glyphosate, thus conferring resistance. To investigate this possibility, 4-replicate cultures of *Synechocystis* were treated with 1 mM glyphosate. Growth medium samples were withdrawn immediately (0 h) and every 24 h subsequently until 72 h later. The amount of glyphosate in the samples was analysed by LC-MS (see 2.5.2). The amount of glyphosate at the start was considered to be 100% and amounts in samples withdrawn across the timepoints expressed relative to this starting value. The level of glyphosate in the medium fluctuated slightly over the 3 days, but there was no significant change (Figure 3.15). This shows that *Synechocystis* did not breakdown or metabolise glyphosate throughout the 72 h experiment. This indirectly points to the possibility that extracellular signals regulate glyphosate tolerance.

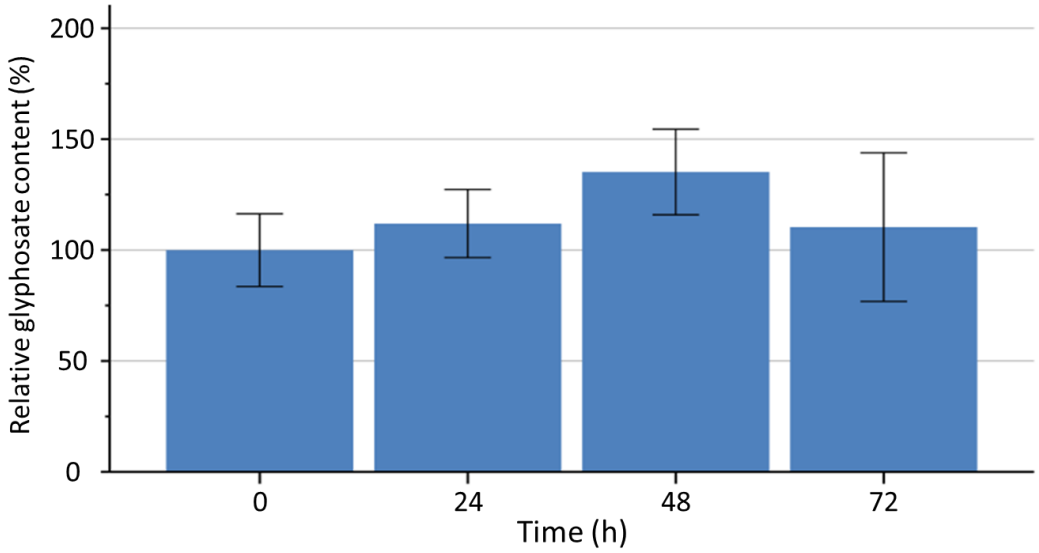

Figure 3.15. Glyphosate concentration in medium of treated cultures. Cultures of *Synechocystis* were treated with 1 mM glyphosate and growth medium samples withdrawn immediately (0 h) and every 24 h thereafter until 3 days later. The amount of glyphosate in the samples was determined by mass spectrometry. Considering the initial amount of glyphosate as 100%, the amounts at subsequent times were calculated relative to this control sample. Bars represent mean ± SD (n = 3). There were no statistically significant differences.

4.0 Discussion

This project aimed to investigate the mechanism by which glyphosate kills cells. That glyphosate targets the shikimate pathway has been known for a long time and there is general consensus that depletion of aromatic amino acids produced by this pathway could be the trigger of cell death. However, the recommended field application rates are unlikely to totally inhibit the shikimate pathway, and some studies have reported that glyphosate fails to kill plant tissues in darkness (Chivasa and Gonzalez-Torralva, 2019). Therefore, this project used proteomics as a tool to elucidate the mechanisms of glyphosate impact on the growth of autotrophs. Two distinct responses dependent on glyphosate concentration were observed viz. hormesis at sublethal concentrations and cell death at higher concentrations. A very clear picture emerged from the proteomics results, which pointed to photosynthesis (rather than the shikimate pathway) as the key metabolic process that seals the fate of cells exposed to glyphosate.

4.1 The hormetic response to glyphosate in cyanobacteria

Cells with a hormetic response to glyphosate had increased expression of several proteins in the photosynthesis electron transport chain and the Calvin-Benson cycle as depicted schematically in Figure 4.1. How these cells escape glyphosate-induced cell death and appear to thrive under such conditions is likely to be underpinned by these changes in protein expression. An interpretation of the gene and protein expression data generated here leads us to envision the scenario depicted in Figure 4.1 and explained below.

Partial inhibition of EPSPS by sublethal glyphosate causes chorismate production to drop and accumulation of immediate upstream metabolites, shikimate-3-phosphate and shikimic acid (Pline et al., 2002). Since over 30% of higher plant organic matter can be derived from shikimate pathway products like L-phenylalanine (Razal et al., 1996), inhibition will cause a metabolic flux 'traffic jam' of metabolites to build up in reverse along the shikimate pathway eventually reaching the Calvin-Benson cycle. The diminished exit of metabolites from the Calvin-Benson cycle slows down carbon fixation, whilst the abundance of ATP and NADPH from the photosynthesis light reactions continues to increase. If unresolved, this can lead to accumulation of protons in the thylakoid lumen, causing it to acidify and inhibit Cyt b_6f complex activity (Tikhonov, 2012). NADPH that is not used by the Calvin-Benson cycle can re-enter the photosynthetic electron transport chain through the cyclic electron flow pathway, thereby maintaining electron transfer. This is achieved through oxidation of NADPH by NDH-1, which then transfers electrons by reducing plastoquinone (PQ). Eventually, the NADP:NADPH ratio becomes unbalanced and electron carriers become saturated, leading to Photosystem II chlorophylls receiving excess energy to produce the triplet chlorophyll (Chl3*) state due to unhindered light harvesting. The excited Chl3* transfers energy to ground state oxygen molecules (O_2), causing the spin of an outer electron to reverse and generate singlet oxygen ($^1O_2$). Electrons in Photosystem II that are not transferred to PQ can also leak and react with oxygen molecules to produce superoxide (O_2^-) anions. These reactive oxygen species (ROS) can damage cellular components and react with protons in the acidified thylakoid lumen to form hydroxyl radicals if they are not quenched by antioxidant enzymes. In response to sub-lethal glyphosate, the cells upregulated Fe-SOD and activated biosynthesis of the antioxidant vitamin B_6 synthesis,

processes which prevent ROS-induced cell damage through removal ROS. To prevent electron leakage, the photosynthetic electron transport chain's capacity for cyclic electron flow is increased through upregulating abundance of electron transferring subunits of NDH-1, Photosystem I, cytochrome b_6f, and Ferredoxin-NADP+ reductase (FNR) (see Figure 4.1). Accumulation of ATP and NADPH is prevented by increasing Calvin-Benson cycle activity through increasing abundance of Rubisco subunits and the other enzymes in the cycle (Figure 4.1).

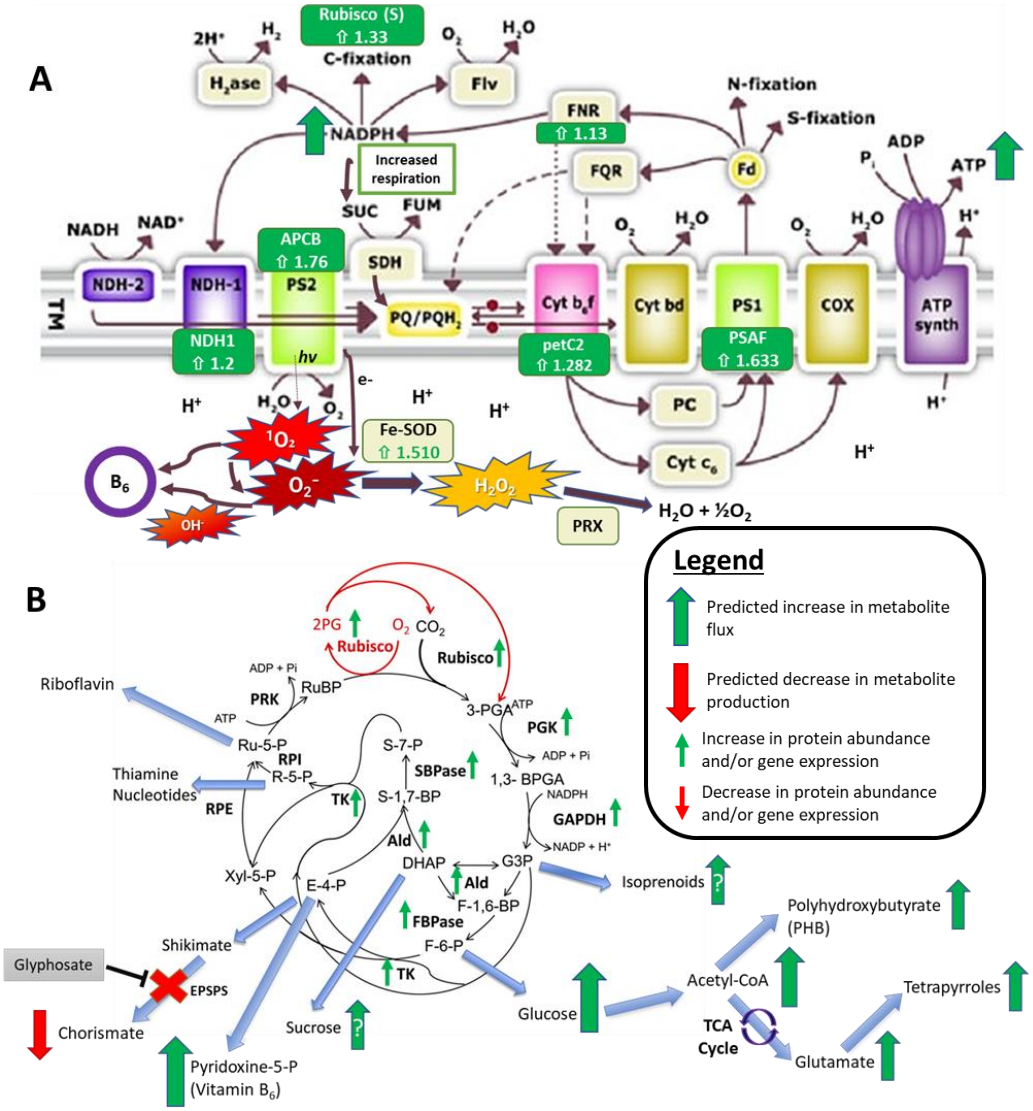

Figure 4.1. Schematic diagram showing the hormetic response of *Synechocystis sp*. PCC6803 to sublethal glyphosate treatment. (A) Representation of photosynthetic electron transport with upregulated proteins identified via proteomics highlighted in green. Fold-change protein expression is shown underneath the protein name. Schematic adapted from Děd, et al. (2016). (B) Predicted response of Calvin-Benson cycle enzymes to sub-lethal glyphosate treatment. Red arrows indicate downregulation; green arrows indicate up-regulation; arrows with question marks denote speculative predictions . Adapted from Raines (2011). Full description of Figure is given in text. List of abbreviations can be found on page VIII.

The protein data showed that the Calvin-Benson cycle plays a key role in preventing cell death. To prevent accumulation of excess ATP and NADPH that would otherwise trigger the generation of damaging ROS, the capacity of the Calvin-Benson cycle to fix more carbon (and consume ATP/NADPH) is increased by upregulating the large and small subunits of rubisco and several other enzymes of the cycle (Figure 4.1). This leads to the increased production of phosphoglycerate-based compounds (PGA, BPGA, G3P), which are accommodated in metabolic reactions via upregulation of downstream enzymes withdrawing compounds from the Calvin-Benson cycle. Under normal high light conditions, one may expect to see a general increase in all Calvin-Benson cycle enzymes.

This redirection of fixed carbon is facilitated by upregulation of enzymes such as GADPH, FBPase/SBPase, aldolase, transketolase, and PGK. These enzymes have essential roles in central carbon metabolism, glycolysis, gluconeogenesis and the oxidative pentose phosphate pathway, indicating that the cells' response to shikimate pathway inhibition is to divert excess metabolites to sugar production, thereby preventing ROS production by the photosystems. The minor down regulation of enzymes processing shikimate pathway metabolites or precursors, DAHPS, PRPPK, and enolase, suggest that the cell does not attempt to increase shikimate pathway activity or nucleotide production. Similarly, a proteomic study of a glyphosate-resistant horseweed (*Conyza canadensis*) biotype noted differential expression of rubisco, ATP synthase subunits and fructose biphosphate aldolase in response to glyphosate treatment (González-Torralva et al, 2017) suggesting metabolic diversion could contribute to horseweed glyphosate resistance.

The notion that hormetic cells use metabolic diversion to prevent catastrophic ROS production and cell damage is evidenced by the dramatic increased production of PHB and pyridoxine-6-phospate (vitamin B_6) as suggested by protein data (Figure 4.1). Vitamin B_6 is an essential co-factor in general cell metabolism and amino acid synthesis. It is also known to efficiently scavenge for singlet oxygen in fungi (Bilski et al., 2007) and higher plants (Havaux et al., 2009) and to increase light stress tolerance (Titiz et al, 2006). Accumulation of vitamin B_6 in response to sublethal glyphosate was also reported in maize (Zhao et al., 2020a). In conjunction, PHB accumulates in cellular vesicles and acts as a mobilizable carbon repository (Müller-Santos et al., 2021), preventing the metabolic congestion of the calvin cycle.

Whilst managing ROS accumulation helps to avoid cell damage, different processes are activated to support the hormetic growth. For the latter, the cells upregulate tetrapyrrole biosynthesis to facilitate production of heme, chlorophylls, phycobiliproteins and cytochrome compounds as suggested by increases in isocitrate dehydrogenase and uroporphyrinogen III decarboxylase enzymes (Figure 4.1). Uroporphyrinogen III decarboxylase is a key mediator of tetrapyrrole biosynthesis (McDonagh et al., 2013). Meta-analysis of chlorophyll biosynthesis in response to sublethal oxidative stress across 33 plant species demonstrated that chlorophyll production is a key stress-adaptive response (Agathokleous et al., 2020). Furthermore, allophycocyanin, an integral protein in the structure of antenna complexes (with light-harvesting functions) increases in abundance. This is a clear indication that cells in a hormesis response are not threatened by ROS

damage and invest energy in increasing light-harvesting capacity and photosynthesis for better growth.

Instances of increased growth due a hormetic response to glyphosate have been reported across several crop species, including common bean (*Phaseolus vulgaris*), safflower (*Carthamus tinctorius*) and sugarcane (*Saccharum sp.)* (Pincelli-Souza et al., 2020; Bortolheiro et al., 2021; Dos Santos et al., 2021). Glyphosate induced hormesis blocked growth reductions caused by water deficit in safflower (Dos Santos et al. 2021). Sugarcane plants treated with a tenth the standard field-recommended dose of glyphosate had better growth (Pincelli-Souza et al., 2020; de Almeida Silva et al., 2022) and increased sugar content (de Almeida Silva et al., 2022). Since sugarcane can store massive amounts of sucrose, it is tempting to speculate that glyphosate injury in this crop is avoided by redirecting fixed carbon redirected towards sucrose production. In the microalga *Scenedesmus vacuolatus*, notable changes in ultrastructure were observed following glyphosate treatment including the thickening of cell walls and the accumulation of starch surrounding the pyrenoids (Iumatto et al., 2019). Both cellulose and starch are derived from glucose, indicating glucose production increased in response to glyphosate. It stands to reason that inhibition of EPSPS triggered diversion of fixed carbon to glucose metabolism. A hormesis response to glyphosate, attended by upregulated photosynthesis, oxidative phosphorylation and chlorophyll biosynthesis proteins, was recently reported in the cyanobacterium *Microcystis aeruginosa* (Xu et al., 2021).

It has been reported that photosynthetic organisms respond to shikimate pathway restriction by heightening sugar production, with higher plants appearing to prefer sucrose whilst microalgae and cyanobacteria prefer glucose (Iumatto et al., 2019; Pincelli-Souza et al 2020; Zhao et al., 2020a; de Almeida Silva et al., 2022;). However, eukaryotic microalgae appear to utilise cellulose and lipids as a combined carbon sink and protective mechanism (He et al., 2015; Iumatto et al., 2019), while the prokaryote *Synechocystis* adopts a different strategy involving biosynthesis of PHB, a biopolymer widely used for carbon storage across multiple families of bacteria (Lodwig et al., 2005; Müller-Santos et al. 2021). Recent studies have also demonstrated PHB production and accumulation can play a protective role against heat-shock and oxidative stress (Müller-Santos et al., 2021).

The increased abundance of bacterioferritin likely plays a role in increasing the availability of iron within the cell, which assists in the production of heme, Fe-superoxide dismutase and Iron-Sulphur complexes. The enzyme systems requiring Fe as a co-factor may play crucial roles is stress tolerance. A similar response has been reported in other bacteria exposed to stress (Tang et al., 2021). For example, *E. coli* increased the abundance of proteins associated with iron uptake, such as enterobactin synthesis enzymes, when exposed to glyphosate and AMPA induced stress (Stenger, 2019). In supporting a role for Fe-dependent molecular systems in escaping glyphosate toxicity, research shows that iron uptake in leaves of glyphosate-sensitive higher plants is impaired by glyphosate (Cakmak et al., 2009). This indicates that iron starvation could be central in destabilising countermeasures to avert glyphosate toxicity.

The increased abundance of iron present in glyphosate-treated cyanobacteria may also be utilised in production of flavodiiron (Flv) proteins, which form heterodimers used in

response to changes in light intensity. The Flv1/3 heterodimer receives electrons from excess NADPH and safely dissipates the energy via electron donation to O_2 to produce H_2O (Allahverdiyeva et al., 2015)(Figure 4.1). The Flv2/4 heterodimer receives electrons from PSII in the place of PQ, after which they are transferred to a poorly understood novel electron sink (Zhang et al., 2012)(see Figure 4.3). Thus, cyanobacteria have diverse Fe-dependent mechanisms to avoid damaging ROS production, hence the success of a hormetic response.

4.2 The lethal mechanism of glyphosate in photoautotrophs

Results of cell viability responses in both cyanobacteria and microalgae demonstrated that the glyphosate lethal mechanism is light driven. This aligns with our original hypothesis that cell death is the result of ROS generation by the photosystems. Evidence for this has appeared in higher plants, microalgae and cyanobacteria (Romero et al., 2011; Gomes et al., 2017; Ye et al., 2019). However, the exact mechanism and events leading up to the lethal generation of ROS has been unknown hitherto. Results of the global proteomic analysis of *Synechocystis sp.* responding to toxic levels of glyphosate suggested that lethal levels of ROS are generated when carbon fixation is severely diminished due to a build-up of metabolites triggered by shikimate pathway inhibition. On the basis of proteomic results obtained from Synechocystis, we propose the following mechanism to operate in activation of cell death (Figure 4.2).

Complete inhibition of EPSP synthase (achievable at high glyphosate concentration) combined with exposure to high light leads to the accumulation of shikimate pathway intermediate metabolites. This metabolic congestion “tails back” to the Calvin-Benson cycle, which then fails to consume ATP and NADPH at the rate they are produced by the photosynthetic light reactions. Accumulation of ATP and NADPH without recycling of the electron acceptors results in a shortage of available $NADP^+$ (and ADP) causing a scenario where electrons cannot transfer out of the photosynthetic-respiratory electron transport chain through normal photochemistry. Initially, a great number of electrons are forced to enter the cyclic electron flow, but the capacity is soon overwhelmed. After the photosynthetic-respiratory electron transport chain becomes over-reduced and decreased availability of ADP lowers ATP synthase activity, the lumen significantly acidifies. However, light harvesting by the photosystems continues unabated and the excess electrons cannot be transferred through photochemistry, resulting in generation of singlet oxygen and superoxide (Wobbe & Remacle 2015; Tian et al., 2019). Increases in superoxide dismutase serve as evidence that cells attempt to detoxify ROS (Figure 4.2). The observed upregulation of inorganic pyrophosphatase, which hydrolyses inorganic pyrophosphate (PP_i), may reflect attempts to avail free phosphate for biosynthesis of the now limiting ADP^+ and $NADP^+$. Studies on *Synechocystis* have suggested a role for this enzyme in inorganic phosphate (P_i) recycling, which is important under phosphate-starved conditions (Gomez-Garcia et al., 2003).

While hormetic cells evade ROS toxicity through activation of broad antioxidant systems, diversion of energy to other pathways, and increasing the capacity of the electron transport chain and Cavin-Benson cycle (Figure 4.1), cells exposed to a lethal dose of glyphosate have weaker or none of these responses (Figure 4.2). The complete inhibition of

the shikimate pathway greatly limiting aromatic amino acid production leads to protein starvation, which makes any response dependent on transcription and translation impossible. The cells have limited options under such conditions. Some of the responses in these cells are similar to responses of hormetic cells, though the magnitude of changes in protein abundance are somewhat diminished in the lethal treatment. For example, Calvin-Benson cycle enzymes are increased in an attempt to relieve the damaging NADPH and ATP accumulation. However, a deviation from the hormetic response is the upregulation of chaperonins, proteases and S-adenosylmethionine (SAM) synthase, which mitigates stress-induced protein misfolding and increases protein recycling, particularly of the now highly valued aromatic amino acids (Hayashi et al., 2018; Heidari et al., 2020).

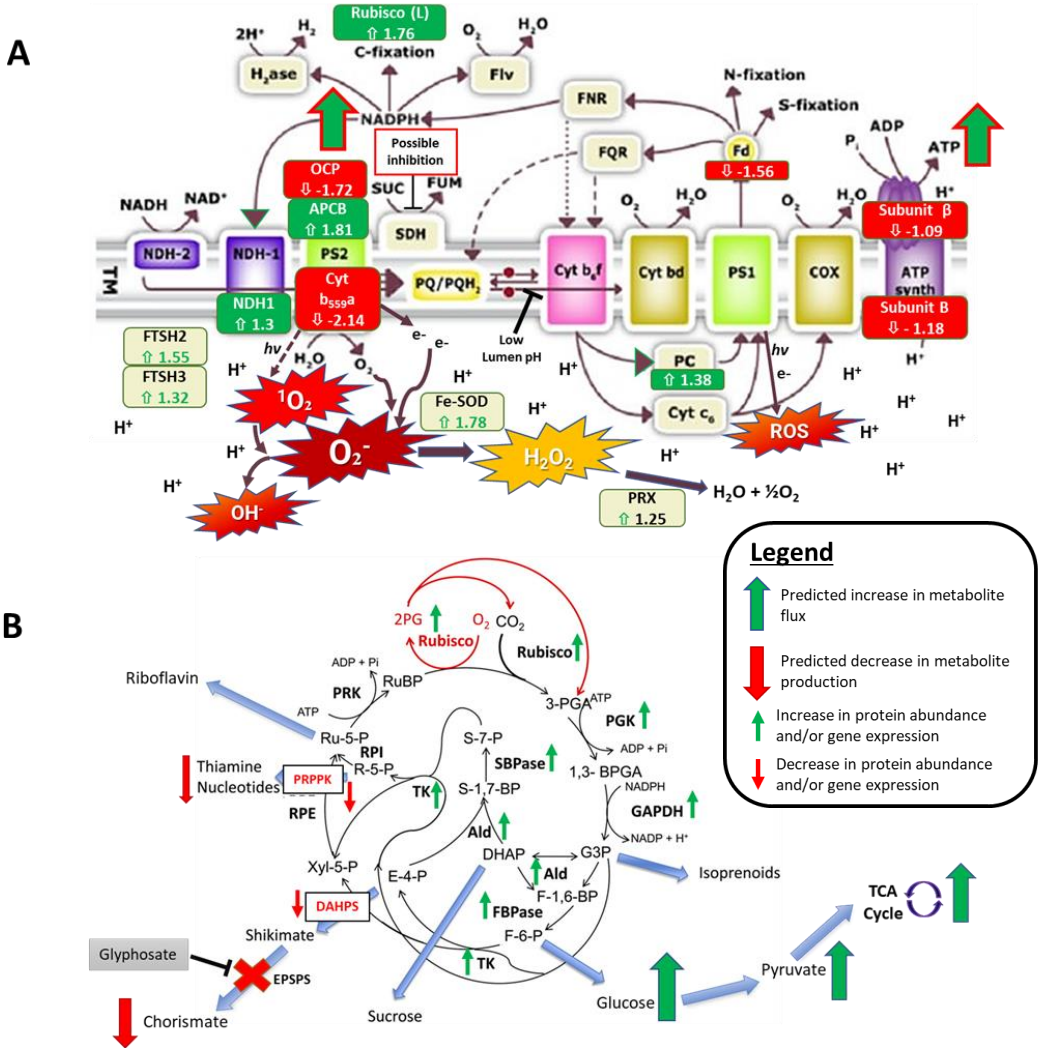

Figure 4.2. Graphic demonstrating the proteomic shifts in *Synechocystis sp.* PCC6803 in response to lethal glyphosate treatment. (A) Representation of photosynthetic electron transport with upregulated proteins identified via proteomics highlighted in green. Fold-change protein expression is shown underneath the protein name. Schematic adapted from Děd, et al. (2016). (B) Predicted response of Calvin-Benson cycle enzymes to lethal glyphosate treatment. Red arrows indicate downregulation; green arrows indicate up-regulation; arrows with question marks denote speculative predictions . Adapted from Raines (2011). Full description of Figure is given in text. List of abbreviations can be found on page VIII.

There are several changes revealing why cells exposed to lethal glyphosate doses die. For example, ferredoxin biosynthesis downregulation (Figure 4.2) reduces electron transfer from PSI, causing it to generate ROS (Giró et al 2011). The orange carotenoid binding-protein (OCP), which is used in protection of PSII is downregulated (Figure 4.2). As shown in Figure 1.4, OCP protects PSII and mitigates photooxidative stress by altering the structure of the phycobilisome upon exposure to high light. Radiation from strong light converts OCP from its ground state (OCP^o) to its active red form (OCP^r) (Kirilovsky et al. (2014). This causes light energy being captured by the phycobilisome to be dissipated as heat instead of being channelled to PSII or PSI. Thus, when the phycobilisome structure is altered by glyphosate stress to exclude both phycocyanin and OCP, this leaves only allophycocyanin (Kirilovsky et al. (2014) (Figure 1.5), leading to heightened ROS generation and cell damage.

While the collapse of key components of the photosynthetic electron transport chain partly accounts for the lethal outcome at higher glyphosate doses, the absence of activation of strong protective measures, as happens in the hormetic response, contributes to cell death. Vitamin B_6 metabolizing enzymes did not feature in the lethal response in contrast to their prominence in the hormetic response. This deprived cells of a valuable singlet oxygen quencher (Bilski et al., 2007). In addition, no tangential pathways to redirect Calvin-Benson cycle metabolites to alternative pathways were activated. Thus, the tetrapyrrole and PHB biosynthesis pathways upregulated in the hormetic response were not activated in the lethal response. Failure to increase tetrapyrrole production restricts the synthesis of new photosystems and cytochrome protein complexes, depriving vital upgrades in the photosynthetic electron transport chain required to prevent over reduction (Hihara et al., 2001). In conjunction with the failure to activate PHB synthesis, this deprives the cell of valuable carbon sinks (Müller-Santos et al., 2021), leading to a surge in ROS and inevitable light-dependent cell death.

4.3 The importance of the extracellular matrix in regulating the response to glyphosate

Our results demonstrated that the presence of extracellular signals in the medium plays a role in modulating cell death and promoting hormesis in glyphosate-treated *Synechocystis* and *Chlamydomonas* cells. Removing these compounds from the medium was shown to almost guarantee cell death in what would otherwise be a sub-lethal treatment in unaltered medium. Additionally, the extracellular compounds associated with glyphosate induced hormesis and stress adaptation were shown to be below 10 kDa in size. The mechanisms, functions and identity of these molecules are so far unknown and require further study, as knowledge surrounding extracellular communication in both microalgae and cyanobacteria is limited.

Non-photosynthetic bacteria, such as *E. coli,* use quorum sensing for collective decision-making within a biofilm. This uses intercellular communication with molecules known as autoinducers, which are usually short chain peptides or homoserine lactones (see reviews by Rutherford & Bassler, 2012; Papenfort & Bassler, 2016). Autoinducers are produced within the cytoplasm and secreted into the extracellular matrix. Upon reaching a critical density, these autoinducers then interact with a corresponding receptor protein that may directly or indirectly induce transcriptional changes to trigger the appropriate response.

Larger autoinducer signals, such as peptides, are assembled in the cytoplasm as precursor peptides known as pro-Auto inducing Peptides (pro-AIP) that have no tertiary structure and/or contain additional amino acid chains which prevent interaction with transcription factors in the cell that synthesized them (reviewed in Rutherford & Bassler, 2012). They exit the cell via an export/processor protein and leave the cell as a mature bioactive peptide or are secreted into the medium and modified via a secreted protease to become active. They enter other cells via outer membrane import proteins and activate cognate transcription factors in cytoplasm of other cells or alternatively interact with receptor proteins on the plasma membrane. Evidence for bioactive extracellular peptides has been found reported in cyanobacteria (Pereira et al., 2014), serving as precedence for the observations and conclusions from the work described in this thesis.

Little research exists on the role or presence of autoinducers in cyanobacteria. However, the existence of extracellular N-octanoyl-homoserine lactones (C8-AHL) has been reported in the cyanobacterium *Gloeothece sp.* PCC6909 (Sharif et al., 2008). C8-AHL induced transcriptional changes of a wide range of proteins, including enzymes in the Calvin-Benson cycle; shikimate pathway; glycolysis; and the tricarboxylic acid cycle (Sharif et al., 2008). This provides strong evidence that a quorum sensing-like signalling is at least partly responsible for transcriptional regulation of metabolic pathways that can be modulated to avoid glyphosate injury. However, the receptors for C8-AHL have not been identified in *Gloeothece sp.* PCC6909 or any other cyanobacteria.

In eukaryotic microalgae, intercellular communication is facilitated through the use of phytohormones and extracellular vesicles (Pichler et al., 2020, Adamo et al., 2021). These mechanisms can also be used for communication between microalgae and cyanobacteria, as has been shown between *Chlamydomonas* and *Synechocystis* (Zhao et al., 2020b). Conversely, microalgae are also capable of interspecies communication via acyl homoserine lactones produced by proteobacteria (Natrah et al., 2011), making it plausible they can also respond to C8-AHLs produced by cyanobacteria. Therefore, more extensive research needs to be conducted to better understand the role of autoinducers and phytohormones in photosynthetic microbial communities.

Another aspect of the extracellular matrix that may prevent cell death in glyphosate-treated cells is the export of electrons. Electron export and trading is a known phenomenon in cyanobacteria and other bacterial species (Gonzalez-Aravena et al. 2018; Light et al., 2018). Research on electron export for photovoltaic and organic electronics devices is growing. However, the mechanisms and evolutionary function of this process, particularly in cyanobacteria, are poorly understood. Both gram negative and positive bacteria are capable of utilising flavin as an electron shuttling molecule, making this a plausible candidate for explaining electron transport between cells and the extracellular environment (Yang et al 2015; Light et al., 2018). Recent research demonstrates that both photosynthetic and respiratory electron transport chains contribute to electron export, and that the respiratory electron chain becomes the primary donor upon the inhibition of photosynthetic apparatus (Saper et al., 2018).

The mechanisms explaining electron export in cyanobacteria are currently hypothetical (reviewed in Lea-Smith et al, 2016). But, in the context of our results, electron donation to

the cytoplasmic membrane during glyphosate would primarily be carried out via NADPH due to its high abundance following the metabolic congestion of the calvin cycle (Wobbe & Remacle, 2015). Secondary donors could include succinate dehydrogenase, though competitive inhibition by glyphosate may mitigate this (Ugarte, 2014; Vanlaeys et al., 2018). Another donor could include the Flv2/4 heterodimer when PSII enters a highly excited state, however the site of electron donation for this protein remains novel and unknown to science (Zhang et al., 2012). Electrons may also be donated directly via ferredoxin, however this would also be carried out via an unknown mechanisms (reviewed in Lea-Smith et al., 2016) and is less likely given its lower abundance in the lethal treatment samples (Figure 4.2). Electrons donated to the outer membrane respiratory complexes NDH-2 and SDH would most likely be used to reduce PQ. These electrons may then be donated to a terminal respiratory oxidase like Cyd or ARTO and used to convert oxygen and protons to water or be used to reduce Fe(II) (Figure 4.3). Alternatively, electrons may be transported to an electron exporting Pilus complex via a hypothetical carrier such as Fe(III), flavin or a flavoprotein. This Pilus complex would then shuttle electrons past the outer membrane and secrete them into the medium via currently unidentified carriers (Figure 4.3)(reviewed in Lea-Smith et al. (2016)). Possible candidates for electron shuttling compounds and mechanisms include redox proteins, flavin, and/or metal ions such as Fe^{3+} (Yang et al 2015; Light et al., 2018)(Reviewed in Lea-Smith et al., 2016). It is unlikely Fe^{3+} was used as an extracellular electron carrier during our experiments however due its abundance in the BG11 medium.

This demonstrates that if an extracellular acceptor for electron export exists, it is synthesised by cells and must be present before the cells are exposed to stress. Some definitive research has been undertaken, where *Synechocysytis sp., Acaryochloris marina MBIC 11017* and *Synechococcus elongatus* PCC 7942 were shown to immediately export NADPH within a photovoltaic mechanism upon exposure to light, and then transport it back into the cell upon oxidation by the anode (Shlosberg et al., 2021). This in turn provides further evidence that electron export via a carrier such as NADPH is utilised during periods of photooxidative stress.

Our results showed that cells can survive a “lethal dose” of glyphosate if secreted “signals” are present. Is it possible that electron export, to relieve the massive excess of cellular NADPH, is the mechanism to prevent over reduction of the photosynthesis electron transport chain? This would buy time for the cell to activate appropriate gene expression, perhaps to mount a shikimate pathway response and other cell-protective metabolic processes. However, simply considering NADPH as the sole electron shuttling molecule would not fully explain our results as NADPH could be exported regardless of what is present in the extracellular medium. It may be possible the mechanism requires activation by an extracellular peptide or autoinducer, which informs the cell of the presence of other organisms. Alternatively, a different electron shuttling compound, such as flavin, may already be present in the medium following the formation of a biofilm, and this mediates stress dependent electron export. Both Flavin and NADPH would be useful for electron trading in a multispecies biofilm as these molecules are universally utilised by all living organisms. It is possible multiple methods of electron trading and export exist within a single species, each one being deployed in specific circumstances. These questions need

further research that could reveal the high tolerance of biofilms to herbicides (Beecraft & Rooney, 2021) as well as provide a greater understanding of microbial communication, cooperation and mutualism.

Although highly speculative, electron export and sharing via mobile extracellular carriers, such as flavin, increase the xenobiotic resistance and survival of cyanobacterial biofilms. Electron export enables cells to offload excess energy and acts as an early warning system for adjacent electron accepting cells to increase their capacity for electron transport. "Solitary" cells which are present in fresh medium have no such compounds to transfer exported electrons to and are therefore susceptible to die at much lower concentrations of glyphosate. The extracellular matrix may also contain signals, such as C8-AHL, which activate gene transcription for stress-adaptive responses, including electron export complexes and antioxidants.

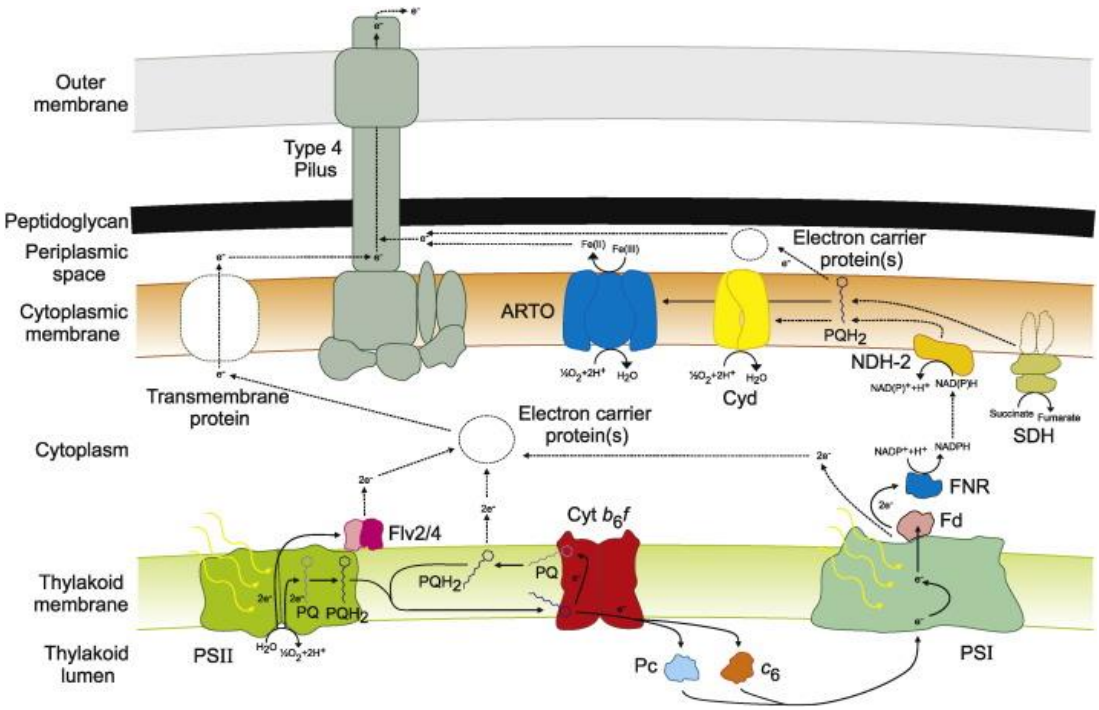

Figure 4.3. **Hypothetical model of electron export mechanisms in cyanobacteria**. Energy derived from photosystems I and II is carried along the Photosynthetic electron transport chain and used to produce NADPH. When NADPH is in excess and cannot be utilised by the calvin cycle, it can instead be oxidised by NDH-2 on the cytoplasmic membrane which will then reduce PQ in conjunction with succinate dehydrogenase. Electrons may then be used to produce water or reduce Fe(II) after being donated to cytochrome d (Cyd) or alternative respiratory terminal oxidases (ARTO). Alternatively, electrons may be shuttled to an electron exporting mechanism (Type 4 Pilus) via Fe(III) or an electron carrier protein. Electrons donated from the Flv2/4 photoprotective mechanism, thylakoid membrane PQH_2 pool and Ferredoxin may also be exported via the same protein complex after being transferred through a hypothetical network of electron carrying soluble and transmembrane proteins. Full description is given in the main text. Solid lines represent known electron transport pathways. Dashed lines represent hypothetical paths of electron transport. Taken from Lea-Smith et al. (2016). For Abbreviations see page VIII.

4.4 Role of alternative glyphosate targets in activation of cell death

It has been proposed that high concentrations of glyphosate can competitively inhibit succinate dehydrogenase (SDH) (Vanlaeys et al., 2018; Burchfield et al., 2019), an enzyme participating in both the TCA cycle and photosynthetic electron transport in cyanobacteria. It is unclear what effect this would have on electron transport in the thylakoid (Figure 4.3). It is possible that, in cyanobacteria, the competitive inhibition of succinate dehydrogenase could reduce transfer of electrons to the outer membrane electron transport chain (Figure 4.3). This will have the effect of increasing the rate of ROS production by the photosystems.

Other studies have suggested that glyphosate also inhibits the cytochrome b_6f complex and possibly complex III of the respiratory electron transport chain (Gomes & Juneau, 2016). There is a possibility that the proposed inhibition of cytochrome b_6f by glyphosate is instead a result of lumen acidification limiting PQH_2 oxidation(Carstensen et al., 2018). Nevertheless, the fact that glyphosate toxicity is light-dependent suggests that mitochondrial targets may not play a significant role.

Finally, a previous study demonstrated that glyphosate toxicity can be induced in darkness when applied concomitantly with exogenous sucrose (Moretti et al., 2018). This led the authors to conclude that sucrose supplies energy to activate glyphosate toxicity, with the implication that cell death in light is activated by sucrose. These authors failed to consider the published signalling role of sucrose in other forms of cell death (Chivasa et al., 2013). This result may indicate the existence of signalling roles for sucrose as a mechanism central to glyphosate toxicity. The current study provides a clear role of photosynthesis in modulating the response to glyphosate.

4.7 Implications of this research to agriculture

The current consensus on the mode of glyphosate toxicity is that depletion of aromatic amino acids caused by inhibition of the shikimate pathway activates death as a result of the inability to make proteins. However, the recommended field rates of glyphosate application do not totally inhibit the pathway, making such an explanation inadequate. New research has demonstrated that glyphosate treatment results in photo-oxidative stress caused by ROS generation in the thylakoid membrane (Gomes et al., 2017). Our results support this notion and we propose that this is the primary mechanism of cell death. The requirement for light, underpinned by the protein changes we observed in the photosynthetic electron transport chain, now provides clear understanding of the molecular basis for the increased effectiveness of glyphosate in weed control when applied at dawn (Belbin et al., 2019). Our research has also revealed the mechanisms behind glyphosate-induced hormesis and can be used to explain the molecular basis for growth-promoting impact of glyphosate in sugarcane farming (Pincelli-Souza et al 2020; de Almeida Silva et al., 2022).

Our results suggest that new modes of effective glyphosate resistance in weeds can arise through changes in any part of the primary metabolic network enabling dissipation of chloroplastic reducing power. This goes beyond previously characterised resistance mechanisms, such as: EPSPS active site mutations (Liu & Cao., 2018), amplifying the gene copy number for EPSPS (Dillon et al., 2017), alteration in transport via reduced uptake,

export from cells and vacuolar storage (Rong-Mullins et al., 2017; Ge et al., 2010), detoxification through modification (Fartyal et al., 2019), aldo-keto reductase induced metabolism (Pan et al., 2019) and other uncharacterised mechanisms (Barua et al., 2021). Some of these unexplained glyphosate-resistance mechanisms in weeds could be conferred through genetic changes enabling plants to reallocate fixed carbon, that would have otherwise been utilised by the shikimate pathway, to other metabolic pathways. In addition, glyphosate-resistant weeds may also have improved antioxidant responses, and a greater capacity for cyclic electron flow to prevent cell death upon light exposure. Our results reveal many new possibilities and options for glyphosate resistance and can therefore be used to aid future studies in this field. In addition, our research has demonstrated the importance of extracellular compounds and their role in preventing glyphosate-induced cell death and hormesis.

4.8 The potential industrial applications of this research

Our results demonstrate that during a hormetic response to glyphosate, photosynthetic organisms redirect fixed carbon away from the shikimate pathway to alternative metabolic pathways. Cells compensate for this disrupted ratio of fixed carbon by boosting overall metabolic and photosynthetic activity and utilising other pathways as a carbon sink. In the case of *Synechocystis sp.* PCC6803, these pathways include both pyridoxine synthesis and glycolysis, which then leads to heightened PHB and tetrapyrrole biosynthesis. A previous study from our lab undertaken by Alarcón-Gutiérrez (2020) demonstrated that salt stress could also be used to increase lipid production in *Synechocystis*. Cell ultrastructural analysis indicated that PHB may have accumulated in intracellular membrane vesicles when comparing the images to those of known PHB vesicles in *Synechocystis* (Klotz et al. 2016).

Polyhydroxybutyrate is an versatile molecule with diverse industrial applications, including but not limited to biofuels, biodegradable plastics, antiadhesives and antifouling agents. In particular, highly efficient, low waste production methods of bio-butanol and other useful products have been formulated using PHB as a source of biomass (Zhang et al., 2021). Bio-butanol production from PHB utilised 99% of the carbon, with over 90% of chemical energy being recovered (Zhang et al., 2021), making it an exciting prospect in the transition to a green economy. Naturally, several studies have been carried out to maximise its production in various bacteria species (Lim et al., 2002; Neddermeyer et al., 2015). The redirection of fixed carbon to increase yields of desirable compounds has been most commonly facilitated through genetic modification (Lim et al., 2002; reviewed in Wu et al., 2021). However, our research demonstrates that metabolism blocking compounds could be utilised to boost growth via hormesis and increase the biomass yield. This would not just apply to PHB but possibly other desirable compounds such as lipids, vitamins or isoprenoids (Alarcón-Gutiérrez, 2020). Although some limitations must be noted, glyphosate usage would be reserved for non-food products due to the hazards posed to consumers. Additionally, further research into the interactions with extracellular compounds could be utilised to boost growth via hormesis in the presence of a stressor or used to promote the activation of target genes, as is currently being explored in extremophiles (Kuar et al., 2019). Other extracellular mechanisms such as electron export and trading have applications in both bioremediation, heavy metal detoxification and photovoltaic devices

(reviewed by Rotaru et al., 2021), hence the need to assess its potential in cyanobacteria and determine the role it may have in the cyanobacterial stress response.

4.9 New understanding of glyphosate impact on the environment

The mechanisms behind the formation of harmful algal blooms are poorly understood. Previous research led to the consensus that the main cause of harmful algal bloom (HAB) events was eutrophication by sewage effluent and fertilisers from agricultural fields. Meta-analysis of studies has shown that cyanobacteria are more likely to survive and outcompete other species when exposed to persistent organic pollutants (POP) in comparison to other phytoplankton (Harris and Smith, 2016). The potential of POPs to promote and provide suitable conditions for harmful agal blooms has also been noted (Harris and Smith, 2016). It is currently thought that cyanobacteria are able to break down POP compounds and harness nutrients locked within them. This implies that herbicides like glyphosate could initiate harmful algal blooms because they are metabolised by cells.

Our results indicate however, that it may be the stress response mechanisms to POPs themselves that trigger bloom events. Cyanobacteria are already highly adaptable to abiotic stressors and as a result, there is a large number of cosmopolitan species (Xiao et al., 2018; reviewed in Andreeva et al., 2020). Previous studies have shown cyanobacteria with a high phenotypic plasticity are more likely to trigger bloom events (reviewed in Xiao et al., 2018). Bloom-inducing hormetic responses have already been documented, for example *Microcystis wesenbergii* in response to exposure to multiple organophosphate herbicides, including glyphosate-isopropylammonium (Sun et al., 2013). Additionally, other authors have proposed hormesis, in response to Cyt b_{599}-inhibiting herbicides, as a trigger mechanism for algal bloom formation (Zhang et al., 2020). We can speculate that the ability of cyanobacteria to survive high stress and use hormesis as an opportunity to capitalise on low-moderate stress enable them to dominate other species in the environment (Lürling & Roessink, 2006; Ma et al., 2006). The complex mechanisms cyanobacteria employ to rapidly redirect fixed carbon, offload electrons, and perform necessary upgrades to the photosynthetic apparatus in response to light dependent stress, may give them the edge over other photoautotrophs (Zhang et al., 2020).

Another important finding is the role extracellular signals play in the microbial community response to glyphosate and other forms of pollution. Our results found that not only are extracellular compounds capable to prevent cell death during glyphosate treatment, but they can also stimulate growth by facilitating a hormetic response. We speculate that these signals also play a role the in the dominance of cyanobacteria in polluted aquatic ecosystems as well as the formation of harmful algal blooms, be it through electron trading, autoinduction and/or other mechanisms. Autoinducer compounds such as acyl-homoserine-lactones have already been identified in cultures of the bloom-forming cyanobacteria, such as *Mycrocystis aeruginosa* and could play a role in establishing stable populations upon introduction to an ecosystem (Zhai et al., 2012).

Additionally, autoinducers play important roles in biofilm formation (Zhai et al., 2012), and whilst these communities often foster mutualistic behaviours, within spatially mixed and newly forming biofilms competition and antagonism is frequent (reviewed in Nadell et al.,

2016). If a biofilm or microbial mat is subject to accumulated glyphosate (Beecraft & Rooney, 2021), it is possible they could become a death trap for more sensitive organisms. If multiple species occupy the biofilm, more tolerant organisms that exhibit a hormetic response following glyphosate treatment may outcompete other species in the biofilm, and subsequently dominate their respective ecosystems (Lürling & Roessink, 2006; Ma et al., 2006).

Additionally, the plethora of different POPs, heavy metals and other pollutants present in aquatic ecosystems could work synergistically at very low concentrations to stimulate hormesis in cyanobacteria alongside glyphosate, its herbicidal adjuvants and degradation products (Harris & Smith, 2016; Séguin et al., 2017; Hébert, Fugère & Gonzalez, 2019; Lori et al., 2020). This would be most frequent in aquatic habitats which have been physically modified by humans or the level of eutrophication is high. The increased frequency of heat waves caused by climate change would also make glyphosate and POP induced algal blooms all the more likely. This demonstrates the role this research could play in furthering our understanding of the mechanisms of HAB formation, and why further research on the synergistic effects of pollutants, extracellular signals and hormetic mechanisms in aquatic ecosystems.

4.10 Conclusions and Future work

We demonstrated that the epicentre of the adaptive response to glyphosate stress is the photosynthetic electron transport chain and Calvin-Benson cycle. In photoautotrophs, all metabolic pathways are connected to the Calvin-Benson cycle, which supplies chemical energy derived from photosystems I and II. Therefore, any form of stress that significantly interferes with the metabolic flow from the Calvin-Benson cycle can potentially upset the redox balance of the photosynthetic electron transport chain. Thus, many stress-adaptive responses involve the redistribution of fixed carbon. In *Microcystis aeruginosa* glyphosate-induced stress works synergistically with antibiotic induced stress, which at low doses triggered a hormetic response driven by the increased abundance of photosystem I, II and cytochrome complex proteins (Xu et al., 2021). Links between the photosynthetic apparatus, fixed carbon redistribution and drought stress-tolerance have been recorded in *Manihot esculenta* (cassava) and *Solanum lycopersicum* (tomato) (Chang et al., 2019; Tamburino et al., 2017). In *Kandelia candel* (mangrove), both Calvin-Benson cycle and light-dependent reactions (photosystems and cytochromes) proteins comprised 64% of the significant fold changes exhibited in response to NaCl-induced stress (Wang et al, 2013). In *Conyza sumatrensis*, dark-incubated plant tissues avoid damage from glyphosate-induced stress (Chivasa & Gonzalez-Torralva, 2019). Additionally, cell death activated by mycotoxins (Asai et al., 2000) and heavy metal ions (Wang et al., 2013) is mitigated by incubation in darkness. Finally, the autoinducers secreted by mutualistic rhizobacteria appear to possess the sole purpose of promoting expression of photosynthesis-related proteins (Hartmann et al., 2021), indicating well-established mechanisms for stress tolerance.

We can hypothesise that the photosynthetic electron transport chain is not only the keystone of all metabolic processes within photosynthetic organisms, but is also the principal site where stress response decisions are integrated and implemented. This in turn implies cell death or adaptive responses to abiotic/biotic stresses rely on chloroplasts (or

thylakoid systems) detecting metabolically distant perturbations by monitoring the balance of Calvin-Benson cycle. An emergent hypothesis from this conclusion is that, above functions in energy metabolism, eukaryotic chloroplasts and prokaryotic thylakoid systems are key integrators of stress and drive adaptive responses leading to tolerance or cell demise. This hypothesis will require future experiments re-examining known light-dependent stress responses where ROS production plays a crucial role.

Several questions raised by this research will need addressing through future research. Firstly, a majority of the proteins differentially expressed in response to glyphosate treatment have no ascribed function. As protein functional databases expand and bioinformatic tools integrated with artificial intelligence (machine learning) become mainstream on proteomics analytical workflows, putative functions for these proteins could refine our understanding of how glyphosate works. The significance of this goes beyond glyphosate, but to our fundamental knowledge of chloroplasts and plastids. Secondly, how do extracellular secretions attenuate glyphosate toxicity? The results showed that this is not through degradation or metabolism, leaving two alternatives of the existence of putative extracellular signals or potential electron acceptors. The identity of these will need to be established. Thirdly, is metabolic diversion from the Calvin-Benson cycle to other sinks enough to protect against glyphosate? This can easily be tested by genetically overexpressing and/restricting flux through selected pathways close to the Calvin-Benson cycle and evaluation sensitivity to glyphosate of the transgenic organisms relative to the wildtype. Finally, does production of PHB or vitamin B6 suffice to attenuate glyphosate toxicity? This can be easily tested using exogenous application of these compounds in the presence of glyphosate.

While in isolation these strategies may not offer full protection against glyphosate, the additive effects could be what the cell combines to survive during the hormetic response. The results will be illuminating in terms of the struggle the agrochemical sector has to contend with in keeping pace with emerging herbicide resistance. This would show that any mutation across many pathways could be enough to knockout the utility of new herbicides. Sustainable strategies of herbicide design will therefore need to thoroughly consider the findings of this research.

5.0 References

Adamo, G., Fierli, D., Romancino, D.P., Picciotto, S., Barone, M.E., Aranyos, A., Božič, D., Morsbach, S., Raccosta, S., Stanly, C. and Paganini, C., 2021. Nanoalgosomes: Introducing extracellular vesicles produced by microalgae. *Journal of extracellular vesicles*, *10*(6), p.e12081.

Agathokleous, E., Feng, Z. and Peñuelas, J., 2020. Chlorophyll hormesis: are chlorophylls major components of stress biology in higher plants?. *Science of the Total Environment*, *726*, p.138637.

Alarcón-Gutiérrez, D.F., (2020). Developing alternative sources of feedstocks for industrial hydrocarbons: optimisation of biomass and stress-induced lipid production in *Synechocystis* SR. Master's Thesis. University of Durham.

Allahverdiyeva, Y., Suorsa, M., Tikkanen, M. and Aro, E.M., 2015. Photoprotection of photosystems in fluctuating light intensities. *Journal of experimental botany*, *66*(9), pp.2427-2436.

Amrhein, N., Deus, B., Gehrke, P. and Steinrücken, H.C., 1980. The site of the inhibition of the shikimate pathway by glyphosate: II. Interference of glyphosate with chorismate formation in vivo and in vitro. *Plant physiology*, *66*(5), pp.830-834.

Andreeva, N.A., Melnikov, V.V. and Snarskaya, D.D., 2020. The role of cyanobacteria in marine ecosystems. *Russian Journal of Marine Biology*, *46*(3), pp.154-165.

Araújo, W.L., Nunes-Nesi, A. and Fernie, A.R., 2011. Fumarate: Multiple functions of a simple metabolite. *Phytochemistry*, 72(9), pp.838-843.

Aristilde, L., Reed, M.L., Wilkes, R.A., Youngster, T., Kukurugya, M.A., Katz, V. and Sasaki, C.R., 2017. Glyphosate-induced specific and widespread perturbations in the metabolome of soil Pseudomonas species. *Frontiers in Environmental Science*, 5, p.34.

Asai, T., Stone, J.M., Heard, J.E., Kovtun, Y., Yorgey, P., Sheen, J., and Ausubel, F.M. (2000). Fumonisin B1-induced cell death in Arabidopsis protoplasts requires jasmonate-, ethylene-, and salicylatedependent signalling pathways. Plant Cell 12, 1823–1835.

Bailey, D.C., Todt, C.E., Burchfield, S.L., Pressley, A.S., Denney, R.D., Snapp, I.B., Negga, R., Traynor, W.L. and Fitsanakis, V.A., 2018. Chronic exposure to a glyphosate-containing pesticide leads to mitochondrial dysfunction and increased reactive oxygen species production in Caenorhabditis elegans. *Environmental toxicology and pharmacology*, *57*, pp.46-52.

Bakhsh, A., Hussain, T., Rahamkulov, I., Demirel, U. and Çalışkan, M.E., 2020. Transgenic potato lines expressing CP4-EPSP synthase exhibit resistance against glyphosate. *Plant Cell, Tissue and Organ Culture (PCTOC)*, *140*(1), pp.23-34.

Barua, R., Malone, J., Boutsalis, P., Gill, G. and Preston, C., 2021. Inheritance and mechanism of glyphosate resistance in annual bluegrass (Poa annua L.). *Pest Management Science*.

Battaglin, W.A., Meyer, M.T., Kuivila, K.M. and Dietze, J.E., 2014. Glyphosate and its degradation product AMPA occur frequently and widely in US soils, surface water,

groundwater, and precipitation. JAWRA Journal of the American Water Resources Association, 50(2), pp.275-290.

Beecraft, L. and Rooney, R., 2021. Bioconcentration of glyphosate in wetland biofilms. *Science of the Total Environment*, *756*, p.143993.

Belbin, F.E., Hall, G.J., Jackson, A.B., Schanschieff, F.E., Archibald, G., Formstone, C. and Dodd, A.N., 2019. Plant circadian rhythms regulate the effectiveness of a glyphosate-based herbicide. *Nature communications*, 10(1), pp.1-11.

Belz, R.G. and Duke, S.O., 2014. Herbicides and plant hormesis. *Pest management science*, *70*(5), pp.698-707.

Benachour, N. and Séralini, G.E., 2009. Glyphosate formulations induce apoptosis and necrosis in human umbilical, embryonic, and placental cells. *Chemical research in toxicology*, 22(1), pp.97-105.

Benbrook, C.M., 2016. Trends in glyphosate herbicide use in the United States and globally. Environmental Sciences Europe, 28(1), p.3.

Bento, C.P., Yang, X., Gort, G., Xue, S., van Dam, R., Zomer, P., Mol, H.G., Ritsema, C.J. and Geissen, V., 2016. Persistence of glyphosate and aminomethylphosphonic acid in loess soil under different combinations of temperature, soil moisture and light/darkness. Science of the Total Environment, 572, pp.301-311.

Berman, M.C., Marino, D.J.G., Quiroga, M.V. and Zagarese, H., 2018. Occurrence and levels of glyphosate and AMPA in shallow lakes from the Pampean and Patagonian regions of Argentina. *Chemosphere*, 200, pp.513-522.

Bilski, P., Li, M.Y., Ehrenshaft, M., Daub, M.E. and Chignell, C.F., 2007. Vitamin B6 (pyridoxine) and its derivatives are efficient singlet oxygen quenchers and potential fungal antioxidants. *Photochemistry and photobiology*, *71*(2), pp.129-134.

Bongaerts, J., Esser, S., Lorbach, V., Al-Momani, L., Müller, M.A., Franke, D., Grondal, C., Kurutsch, A., Bujnicki, R., Takors, R. and Raeven, L., 2011. Diversity-Oriented Production of Metabolites Derived from Chorismate and Their Use in Organic Synthesis. *Angewandte Chemie*, *123*(34), pp.7927-7932.

Bonnet, J.L., Bonnemoy, F., Dusser, M. and Bohatier, J., 2007. Assessment of the potential toxicity of herbicides and their degradation products to nontarget cells using two microorganisms, the bacteria Vibrio fischeri and the ciliate Tetrahymena pyriformis. *Environmental Toxicology: An International Journal*, *22*(1), pp.78-91.

Bortolheiro, F.P.D.A.P., Brunelli-Nascentes, M.C., Boaro, C.S.F. and Silva, M.D.A., 2021. Can low doses of glyphosate stimulate common bean growth?. *Journal of Environmental Science and Health, Part B*, *56*(2), pp.150-162.

Breyton, C., 2000. The cytochrome b6f complex: structural studies and comparison with the bc1 complex. *Biochimica et Biophysica Acta (BBA)-Bioenergetics*, *1459*(2-3), pp.467-474.

Burchfield, S.L., Bailey, D.C., Todt, C.E., Denney, R.D., Negga, R. and Fitsanakis, V.A., 2019. Acute exposure to a glyphosate-containing herbicide formulation inhibits Complex II and increases hydrogen peroxide in the model organism Caenorhabditis elegans. *Environmental toxicology and pharmacology*, 66, pp.36-42.

Cakmak, I., Yazici, A., Tutus, Y. and Ozturk, L., 2009. Glyphosate reduced seed and leaf concentrations of calcium, manganese, magnesium, and iron in non-glyphosate resistant soybean. *European Journal of Agronomy*, *31*(3), pp.114-119.

Carbonera, D., Gerotto, C., Posocco, B., Giacometti, G.M. and Morosinotto, T., 2012. NPQ activation reduces chlorophyll triplet state formation in the moss Physcomitrella patens. *Biochimica et Biophysica Acta (BBA)-Bioenergetics*, *1817*(9), pp.1608-1615.

Carstensen, A., Herdean, A., Schmidt, S.B., Sharma, A., Spetea, C., Pribil, M. and Husted, S., 2018. The impacts of phosphorus deficiency on the photosynthetic electron transport chain. *Plant physiology*, *177*(1), pp.271-284.

Carvalho, G., Balestrino, D., Forestier, C. and Mathias, J.D., 2018. How do environment-dependent switching rates between susceptible and persister cells affect the dynamics of biofilms faced with antibiotics?. *npj Biofilms and Microbiomes*, *4*(1), pp.1-8.

Carvalho, L., McDonald, C., de Hoyos, C., Mischke, U., Phillips, G., Borics, G., Poikane, S., Skjelbred, B., Solheim, A.L., Van Wichelen, J. and Cardoso, A.C., 2013. Sustaining recreational quality of European lakes: minimizing the health risks from algal blooms through phosphorus control. *Journal of Applied Ecology*, *50*(2), pp.315-323.

Castelli, L., Balbuena, S., Branchiccela, B., Zunino, P., Liberti, J., Engel, P. and Antúnez, K., 2021. Impact of Chronic Exposure to Sublethal Doses of Glyphosate on Honey Bee Immunity, Gut Microbiota and Infection by Pathogens. *Microorganisms*, *9*(4), p.845.

Chadwick, G.L., Hemp, J., Fischer, W.W. and Orphan, V.J., 2018. Convergent evolution of unusual complex I homologs with increased proton pumping capacity: energetic and ecological implications. *The ISME journal*, *12*(11), pp.2668-2680.

Chakraborty, S., Tiwari, P.K., Sasmal, S.K., Misra, A.K. and Chattopadhyay, J., 2017. Effects of fertilizers used in agricultural fields on algal blooms. *The European Physical Journal Special Topics*, *226*(9), pp.2119-2133.

Chang, L., Wang, L., Peng, C., Tong, Z., Wang, D., Ding, G., Xiao, J., Guo, A. and Wang, X., 2019. The chloroplast proteome response to drought stress in cassava leaves. Plant Physiology and Biochemistry, 142, pp.351-362.

Chivasa S. and Gonzalez-Torralva, F., 2019. Herbicidal Compositions. Patent application No. WO/2018/069709, PCT/GB2017/053082.

Chivasa, S. and Goodman, H.L., 2020. Stress-adaptive gene discovery by exploiting collective decision-making of decentralized plant response systems. *New Phytologist*, *225*(6), pp.2307-2313.

Chivasa, S., Tome, D.F. and Slabas, A.R., 2013. UDP-glucose pyrophosphorylase is a novel plant cell death regulator. *Journal of Proteome Research*, *12*(4), pp.1743-1753.

Cooley, J.W. and Vermaas, W.F., 2001. Succinate dehydrogenase and other respiratory pathways in thylakoid membranes of Synechocystis sp. strain PCC 6803: capacity comparisons and physiological function. *Journal of bacteriology*, *183*(14), pp.4251-4258.

Crick, L., 2016. 'Molecular Dynamics Simulations of Herbicide Interactions with Clay and Quartz Surfaces', Bsc Dissertation. University of Durham. Durham, UK.

de Almeida Silva, M., Véliz, J.G.E., Sartori, M.M.P. and Santos, H.L., 2022. Glyphosate applied at a hormetic dose improves ripening without impairing sugarcane productivity and ratoon sprouting. *Science of The Total Environment*, *806*, p.150503.

de Melo, M.S., Dos Santos, T.P.G., Jaramillo, M., Nezzi, L., Muller, Y.M.R. and Nazari, E.M., 2019. Histopathological and ultrastructural indices for the assessment of glyphosate-based herbicide cytotoxicity in decapod crustacean hepatopancreas. *Aquatic Toxicology*, *210*, pp.207-214.

Děd, et al. 2016. Formal biochemical space with semantics in Kappa and BNGL. *Electronic Notes in Theoretical Computer Science*, *326*, pp.27-49.

Didier, K.E.K., Cr&epin, P.E.E.B., M&elanie, B.B., Yah, O. and Michel, Z., 2017. Effect of glyphosate used as a sugarcane chemical ripener in Cte dIvoire. *African Journal of Plant Science*, *11*(8), pp.341-350.

Dillon, A., Varanasi, V.K., Danilova, T.V., Koo, D.H., Nakka, S., Peterson, D.E., Tranel, P.J., Friebe, B., Gill, B.S. and Jugulam, M., 2017. Physical mapping of amplified copies of the 5-enolpyruvylshikimate-3-phosphate synthase gene in glyphosate-resistant Amaranthus tuberculatus. Plant physiology, 173(2), pp.1226-1234.

Domínguez, A., Brown, G.G., Sautter, K.D., De Oliveira, C.M.R., De Vasconcelos, E.C., Niva, C.C., Bartz, M.L.C. and Bedano, J.C., 2016. Toxicity of AMPA to the earthworm Eisenia andrei Bouché, 1972 in tropical artificial soil. *Scientific reports*, *6*, p.19731.

Dos Santos, J.C.C., da Silva, D.M.R., Amorim, D.J., Sab, M.P.V. and de Almeida Silva, M., 2021. Glyphosate hormesis mitigates the effect of water deficit in safflower (Carthamus tinctorius L.). Pest Management Science, 77(4), pp.2029-2044.

Druille, M., Cabello, M.N., Omacini, M. and Golluscio, R.A., 2013. Glyphosate reduces spore viability and root colonization of arbuscular mycorrhizal fungi. Applied Soil Ecology, 64, pp.99-103.

Duke, S.O. and Powles, S.B., 2008. Glyphosate: a once-in-a-century herbicide. Pest Management Science: formerly Pesticide Science, 64(4), pp.319-325.

Fartyal, D., Agarwal, A., James, D., Borphukan, B., Ram, B., Sheri, V., Yadav, R., Manna, M., Varakumar, P., Achary, V.M.M. and Reddy, M.K., 2018. Co-expression of P173S mutant rice EPSPS and igrA genes results in higher glyphosate tolerance in transgenic rice. *Frontiers in plant science*, *9*, p.144.

Fernandez, C., Asselborn, V. and Parodi, E.R., 2021. Toxic effects of chlorpyrifos, cypermethrin and glyphosate on the non-target organism Selenastrum capricornutum (Chlorophyta). *Anais da Academia Brasileira de Ciências*, *93*.

Forlani, G., Pavan, M., Gramek, M., Kafarski, P. and Lipok, J., 2008. Biochemical bases for a widespread tolerance of cyanobacteria to the phosphonate herbicide glyphosate. *Plant and cell physiology*, *49*(3), pp.443-456.

Fritz-Wallace, K., Engelmann, B., Krause, J.L., Schäpe, S.S., Pöppe, J., Herberth, G., Rösler, U., Jehmlich, N., von Bergen, M. and Rolle-Kampczyk, U., 2020. Quantification of glyphosate and aminomethylphosphonic acid from microbiome reactor fluids. *Rapid Communications in Mass Spectrometry*, *34*(7), Alberts, B., Johnson, A., Lewis, J., Morgan, D., Raff, M. and

Keith Roberts, P.W., 2018. Molecular biology of the cell. Sixth edition. New York, NY:: Garland Science, Taylor and Francis Group.

Fuchs, M.A., Geiger, D.R., Reynolds, T.L. and Bourque, J.E., 2002. Mechanisms of glyphosate toxicity in velvetleaf (Abutilon theophrasti medikus). *Pesticide Biochemistry and Physiology*, *74*(1), pp.27-39.

Gaines, T.A., Zhang, W., Wang, D., Bukun, B., Chisholm, S.T., Shaner, D.L., Nissen, S.J., Patzoldt, W.L., Tranel, P.J., Culpepper, A.S. and Grey, T.L., 2010. Gene amplification confers glyphosate resistance in Amaranthus palmeri. *Proceedings of the National Academy of Sciences*, *107*(3), pp.1029-1034.

Gan, C.S., Chong, P.K., Pham, T.K. and Wright, P.C., 2007. Technical, experimental, and biological variations in isobaric tags for relative and absolute quantitation (iTRAQ). *Journal of proteome research*, *6*(2), pp.821-827.

Garcia-Muñoz, P., Dachtler, W., Altmayer, B., Schulz, R., Robert, D., Seitz, F., Rosenfeldt, R. and Keller, N., 2020. Reaction pathways, kinetics and toxicity assessment during the photocatalytic degradation of glyphosate and myclobutanil pesticides: Influence of the aqueous matrix. *Chemical Engineering Journal*, *384*, p.123315.

Ge, X., d'Avignon, D.A., Ackerman, J.J. and Sammons, R.D., 2010. Rapid vacuolar sequestration: the horseweed glyphosate resistance mechanism. *Pest Management Science: formerly Pesticide Science*, *66*(4), pp.345-348.

Geiger, D.R., Kapitan, S.W. and Tucci, M.A., 1986. Glyphosate inhibits photosynthesis and allocation of carbon to starch in sugar beet leaves. *Plant Physiology*, 82(2), pp.468-472.

Geiger, D.R., Shieh, W.J. and Fuchs, M.A., 1999. Causes of self-limited translocation of glyphosate in Beta vulgaris plants. *Pesticide Biochemistry and Physiology*, *64*(2), pp.124-133.

Giró, M., Ceccoli, R.D., Poli, H.O., Carrillo, N. and Lodeyro, A.F., 2011. An in vivo system involving co-expression of cyanobacterial flavodoxin and ferredoxin–NADP+ reductase confers increased tolerance to oxidative stress in plants. *FEBS Open Bio*, *1*, pp.7-13.

Gomes, M.P. and Juneau, P., 2016. Oxidative stress in duckweed (Lemna minor L.) induced by glyphosate: is the mitochondrial electron transport chain a target of this herbicide? *Environmental Pollution*, *218*, pp.402-409.

Gomes, M.P., Le Manac'h, S.G., Maccario, S., Labrecque, M., Lucotte, M. and Juneau, P., 2016. Differential effects of glyphosate and aminomethylphosphonic acid (AMPA) on photosynthesis and chlorophyll metabolism in willow plants. *Pesticide biochemistry and physiology*, 130, pp.65-70.

Gomes, M.P., Manac'h, L., Sarah, G., Hénault-Ethier, L., Labrecque, M., Lucotte, M. and Juneau, P., 2017. Glyphosate-dependent inhibition of photosynthesis in willow. *Frontiers in plant science*, *8*, p.207.

Gómez Ortiz, A.M., Okada, E., Bedmar, F. and Costa, J.L., 2017. Sorption and desorption of glyphosate in mollisols and ultisols soils of Argentina. Environmental toxicology and chemistry, 36(10), pp.2587-2592.

Gómez-García, M.R., Losada, M. and Serrano, A., 2003. Concurrent transcriptional activation of ppa and ppx genes by phosphate deprivation in the cyanobacterium Synechocystis sp. strain PCC 6803. Biochemical and biophysical research communications, 302(3), pp.601-609.

Gonzalez-Aravena, A.C., Yunus, K., Zhang, L., Norling, B. and Fisher, A.C., 2018. Tapping into cyanobacteria electron transfer for higher exoelectrogenic activity by imposing iron limited growth. *RSC advances*, *8*(36), pp.20263-20274.

González-Torralva, F., Brown, A.P. and Chivasa, S., 2017. Comparative proteomic analysis of horseweed (Conyza canadensis) biotypes identifies candidate proteins for glyphosate resistance. *Scientific reports*, *7*(1), pp.1-10.

Gopalakrishnan, V., Helmink, B.A., Spencer, C.N., Reuben, A. and Wargo, J.A., 2018. The influence of the gut microbiome on cancer, immunity, and cancer immunotherapy. *Cancer cell*, *33*(4), pp.570-580.

Gorga, A., Rindone, G.M., Centola, C.L., Sobarzo, C., Pellizzari, E.H., del Carmen Camberos, M., Cigorraga, S.B., Riera, M.F., Galardo, M.N. and Meroni, S.B., 2020. In vitro effects of glyphosate and Roundup on Sertoli cell physiology. *Toxicology in Vitro*, *62*, p.104682.

Hammerschmidt, R., 2018. How glyphosate affects plant disease development: it is more than enhanced susceptibility. Pest management science, 74(5), pp.1054-1063.

Harris, T.D. and Smith, V.H., 2016. Do persistent organic pollutants stimulate cyanobacterial blooms?. *Inland Waters*, *6*(2), pp.124-130.

Hartmann, A., Klink, S. and Rothballer, M., 2021. Plant Growth Promotion and Induction of Systemic Tolerance to Drought and Salt Stress of Plants by Quorum Sensing Auto-Inducers of the N-acyl-homoserine Lactone Type: Recent Developments. *Frontiers in Plant Science*, *12*, p.1026.

Hasan, S.S., Yamashita, E., Baniulis, D. and Cramer, W.A., 2013. Quinone-dependent proton transfer pathways in the photosynthetic cytochrome b6f complex. *Proceedings of the National Academy of Sciences*, *110*(11), pp.4297-4302.

Havaux, M., Ksas, B., Szewczyk, A., Rumeau, D., Franck, F., Caffarri, S. and Triantaphylidès, C., 2009. Vitamin B6 deficient plants display increased sensitivity to high light and photo-oxidative stress. *BMC plant biology*, *9*(1), pp.1-22.

Hayashi, T., Teruya, T., Chaleckis, R., Morigasaki, S. and Yanagida, M., 2018. S-adenosylmethionine synthetase is required for cell growth, maintenance of G0 phase, and termination of quiescence in fission yeast. *Iscience*, *5*, pp.38-51.

He, Q., Yang, H., Wu, L. and Hu, C., 2015. Effect of light intensity on physiological changes, carbon allocation and neutral lipid accumulation in oleaginous microalgae. *Bioresource technology*, *191*, pp.219-228.

Heap, I. and Duke, S.O., 2018. Overview of glyphosate-resistant weeds worldwide. Pest Management Science, 74(5), pp.1040-1049.

Heidari, P., Mazloomi, F., Nussbaumer, T. and Barcaccia, G., 2020. Insights into the SAM synthetase gene family and its roles in tomato seedlings under abiotic stresses and hormone treatments. *Plants*, *9*(5), p.586.

Henry, W.B., Shaner, D.L. and West, M.S., 2007. Shikimate accumulation in sunflower, wheat, and proso millet after glyphosate application. *Weed Science*, *55*(1), pp.1-5.

Herbert, S.K., Samson, G., Fork, D.C. and Laudenbach, D.E., 1992. Characterization of damage to photosystems I and II in a cyanobacterium lacking detectable iron superoxide dismutase activity. *Proceedings of the National Academy of Sciences*, *89*(18), pp.8716-8720.

Honda, K. and Littman, D.R., 2016. The microbiota in adaptive immune homeostasis and disease. *Nature*, *535*(7610), pp.75-84.

Iori, S., Dalla Rovere, G., Ezzat, L., Smits, M., Ferraresso, S.S., Babbucci, M., Marin, M.G., Masiero, L., Fabrello, J., Garro, E. and Carraro, L., 2020. The effects of glyphosate and AMPA on the mediterranean mussel Mytilus galloprovincialis and its microbiota. *Environmental Research*, *182*, p.108984.

Iummato, M.M., Fassiano, A., Graziano, M., dos Santos Afonso, M., de Molina, M.D.C.R. and Juárez, Á.B., 2019. Effect of glyphosate on the growth, morphology, ultrastructure and metabolism of Scenedesmus vacuolatus. *Ecotoxicology and Environmental Safety*, 172, pp.471-479.

Iummato, M.M., Sabatini, S.E., Cacciatore, L.C., Cochón, A.C., Cataldo, D., de Molina, M.D.C.R. and Juárez, Á.B., 2018. Biochemical responses of the golden mussel Limnoperna fortunei under dietary glyphosate exposure. *Ecotoxicology and environmental safety*, 163, pp.69-75.

Jardim-Messeder, D., Caverzan, A., Rauber, R. and de Souza, F., E., Margis-Pinheiro, M. and Galina, A.(2015) Succinate dehydrogenase (mitochondrial complex II) is a source of reactive oxygen species in plants and regulates development and stress responses. *New Phytol*, *208*, pp.776-789.

Kao, H.Y., Chung, K.R. and Huang, J.W., 2019. Paraquat and glyphosate increase severity of strawberry anthracnose caused by Colletotrichum gloeosporioides. *Journal of General Plant Pathology*, 85(1), pp.23-32.

Kaur, A., Capalash, N. and Sharma, P., 2019. Communication mechanisms in extremophiles: Exploring their existence and industrial applications. *Microbiological research*, *221*, pp.15-27.

Kirilovsky, D., Kaňa, R. and Prášil, O., 2014. Mechanisms modulating energy arriving at reaction centers in cyanobacteria. In *Non-Photochemical Quenching and Energy Dissipation in Plants, Algae and Cyanobacteria* (pp. 471-501). Springer, Dordrecht.

Kloosterman, H., Hessels, G.I., Vrijbloed, J.W., Euverink, G.J. and Dijkhuizen, L., 2003. (De) regulation of key enzyme steps in the shikimate pathway and phenylalanine-specific pathway of the actinomycete Amycolatopsis methanolica. *Microbiology*, *149*(11), pp.3321-3330.

Klotz, A., Georg, J., Bučinská, L., Watanabe, S., Reimann, V., Januszewski, W., Sobotka, R., Jendrossek, D., Hess, W.R. and Forchhammer, K., 2016. Awakening of a dormant cyanobacterium from nitrogen chlorosis reveals a genetically determined program. *Current Biology*, *26*(21), pp.2862-2872.

Koch, M., Berendzen, K.W. and Forchhammer, K., 2020. On the role and production of polyhydroxybutyrate (PHB) in the cyanobacterium Synechocystis sp. PCC 6803. *Life*, *10*(4), p.47.

Kovalenko, Y.N. and Ulez'ko, A.V., 2020, July. Specific Features in Management of Agro-Food System Development. In *International Conference on Policicies and Economics Measures for Agricultural Development (AgroDevEco 2020)* (pp. 380-384). Atlantis Press.

Ksas, B., Becuwe, N., Chevalier, A. and Havaux, M., 2015. Plant tolerance to excess light energy and photooxidative damage relies on plastoquinone biosynthesis. *Scientific reports*, *5*(1), pp.1-16.

Kushnareva, Y., Murphy, A.N. and Andreyev, A., 2002. Complex I-mediated reactive oxygen species generation: modulation by cytochrome c and NAD (P)+ oxidation–reduction state. *Biochemical Journal*, *368*(2), pp.545-553.

Kwong, W.K., Mancenido, A.L. and Moran, N.A., 2017. Immune system stimulation by the native gut microbiota of honey bees. *Royal Society open science*, *4*(2), p.170003.

Lea-Smith, D.J., Bombelli, P., Vasudevan, R. and Howe, C.J., 2016. Photosynthetic, respiratory and extracellular electron transport pathways in cyanobacteria. *Biochimica et Biophysica Acta (BBA)-Bioenergetics*, *1857*(3), pp.247-255.

Lea-Smith, D.J., Ross, N., Zori, M., Bendall, D.S., Dennis, J.S., Scott, S.A., Smith, A.G. and Howe, C.J., 2013. Thylakoid terminal oxidases are essential for the cyanobacterium Synechocystis sp. PCC 6803 to survive rapidly changing light intensities. *Plant physiology*, *162*(1), pp.484-495.

Lim, S.J., Jung, Y.M., Shin, H.D. and Lee, Y.H., 2002. Amplification of the NADPH-related genes zwf and gnd for the oddball biosynthesis of PHB in an E. coli transformant harboring a cloned phbCAB operon. *Journal of bioscience and bioengineering*, *93*(6), pp.543-549.

Liu, F. and Cao, Y., 2018. Expression of the 5-enoylpyruvylshikimate-3-phosphate synthase domain from the Acremonium sp. aroM complex enhances resistance to glyphosate. Biotechnology letters, 40(5), pp.855-864.

Liu, M. and Lu, S., 2016. Plastoquinone and ubiquinone in plants: biosynthesis, physiological function and metabolic engineering. *Frontiers in Plant Science*, *7*, p.1898.

Lodwig, E.M., Leonard, M., Marroqui, S., Wheeler, T.R., Findlay, K., Downie, J.A. and Poole, P.S., 2005. Role of polyhydroxybutyrate and glycogen as carbon storage compounds in pea and bean bacteroids. *Molecular Plant-Microbe Interactions*, *18*(1), pp.67-74.

Lürling, M. and Roessink, I., 2006. On the way to cyanobacterial blooms: impact of the herbicide metribuzin on the competition between a green alga (Scenedesmus) and a cyanobacterium (Microcystis). *Chemosphere*, *65*(4), pp.618-626.

Ma, J., Lu, N., Qin, W., Xu, R., Wang, Y. and Chen, X., 2006. Differential responses of eight cyanobacterial and green algal species, to carbamate insecticides. *Ecotoxicology and Environmental safety*, *63*(2), pp.268-274.

Mayneord, G.E., Vasilev, C., Malone, L.A., Swainsbury, D.J., Hunter, C.N. and Johnson, M.P., 2019. Single-molecule study of redox control involved in establishing the spinach

plastocyanin-cytochrome b6f electron transfer complex. *Biochimica et Biophysica Acta (BBA)-Bioenergetics*, *1860*(7), pp.591-599.

McDonagh, B., Pedrajas, J.R., Padilla, C.A. and Bárcena, J.A., 2013. Thiol redox sensitivity of two key enzymes of heme biosynthesis and pentose phosphate pathways: uroporphyrinogen decarboxylase and transketolase. *Oxidative medicine and cellular longevity*, *2013*.

Mertens, M., Höss, S., Neumann, G., Afzal, J. and Reichenbecher, W., 2018. Glyphosate, a chelating agent—relevant for ecological risk assessment?. *Environmental Science and Pollution Research*, *25*(6), pp.5298-5317.

Mesnage, R., Arno, M., Costanzo, M., Malatesta, M., Séralini, G.E. and Antoniou, M.N., 2015. Transcriptome profile analysis reflects rat liver and kidney damage following chronic ultra-low dose Roundup exposure. *Environmental Health*, 14(1), p.70.

Mesnage, R., Bernay, B. and Séralini, G.E., 2013. Ethoxylated adjuvants of glyphosate-based herbicides are active principles of human cell toxicity. *Toxicology*, 313(2-3), pp.122-128.

Mesnage, R., Teixeira, M., Mandrioli, D., Falcioni, L., Ducarmon, Q.R., Zwittink, R.D., Amiel, C., Panoff, J.M., Belpoggi, F. and Antoniou, M.N., 2019. Shotgun metagenomics and metabolomics reveal glyphosate alters the gut microbiome of Sprague-Dawley rats by inhibiting the shikimate pathway. *BioRxiv*, p.870105.

Mohr, K., Sellers, B.A. and Smeda, R.J., 2007. Application time of day influences glyphosate efficacy. *Weed Technology*, *21*(1), pp.7-13.

Monsanto-ag. 2019. Roundup Use. [online] Available at: <https://www.monsanto-ag.co.uk/roundup/roundup-agriculture/roundup-use/> [Accessed 3 November 2020].

Moretti, M.L., Van Horn, C.R., Robertson, R., Segobye, K., Weller, S.C., Young, B.G., Johnson, W.G., Douglas Sammons, R., Wang, D., Ge, X. and d'Avignon, A., 2018. Glyphosate resistance in Ambrosia trifida: Part 2. Rapid response physiology and non-target-site resistance. *Pest management science*, *74*(5), pp.1079-1088.

Muller, K., Herrera, K., Talyn, B. and Melchiorre, E., 2021. Toxicological Effects of Roundup® on Drosophila melanogaster Reproduction. *Toxics*, *9*(7), p.161.

Müller-Santos, M., Koskimäki, J.J., Alves, L.P.S., de Souza, E.M., Jendrossek, D. and Pirttilä, A.M., 2021. The protective role of PHB and its degradation products against stress situations in bacteria. *FEMS microbiology reviews*, *45*(3), p.fuaa058.

Muola, A., Fuchs, B., Laihonen, M., Rainio, K., Heikkonen, L., Ruuskanen, S., Saikkonen, K. and Helander, M., 2020. Risk in the circular food economy: Glyphosate-based herbicide residues in manure fertilizers decrease crop yield. Science of The Total Environment, 750, p.141422.

Murata, N. and Nishiyama, Y., 2018. ATP is a driving force in the repair of photosystem II during photoinhibition. *Plant, cell & environment*, *41*(2), pp.285-299.

Nadell, C.D., Drescher, K. and Foster, K.R., 2016. Spatial structure, cooperation and competition in biofilms. *Nature Reviews Microbiology*, *14*(9), pp.589-600.

Natrah, F.M.I., Kenmegne, M.M., Wiyoto, W., Sorgeloos, P., Bossier, P. and Defoirdt, T., 2011. Effects of micro-algae commonly used in aquaculture on acyl-homoserine lactone quorum sensing. *Aquaculture*, *317*(1-4), pp.53-57.

Neddermeyer, F., Rossner, N. and King, R., 2015. Model-based control to maximise biomass and PHB in the autotrophic cultivation of Ralstonia eutropha. *IFAC-PapersOnLine*, *48*(8), pp.1100-1107.

Ngcala, M.G., Goche, T., Brown, A.P., Chivasa, S. and Ngara, R., 2020. Heat stress triggers differential protein accumulation in the extracellular matrix of sorghum cell suspension cultures. *Proteomes*, *8*(4), p.29.

Okada, E., Costa, J.L. and Bedmar, F., 2016. Adsorption and mobility of glyphosate in different soils under no-till and conventional tillage. Geoderma, 263, pp.78-85.

Paerl, H.W. and Huisman, J., 2009. Climate change: a catalyst for global expansion of harmful cyanobacterial blooms. *Environmental microbiology reports*, *1*(1), pp.27-37.

Pan, L., Yu, Q., Han, H., Mao, L., Nyporko, A., Fan, L., Bai, L. and Powles, S., 2019. Aldo-keto reductase metabolizes glyphosate and confers glyphosate resistance in Echinochloa colona. Plant physiology, 181(4), pp.1519-1534.

Papenfort, K. and Bassler, B.L., 2016. Quorum sensing signal–response systems in Gram-negative bacteria. *Nature Reviews Microbiology*, *14*(9), pp.576-588.

Parsek, M.R. and Greenberg, E.P., 2000. Acyl-homoserine lactone quorum sensing in gram-negative bacteria: a signaling mechanism involved in associations with higher organisms. *Proceedings of the National Academy of Sciences*, *97*(16), pp.8789-8793.

Peillex, C. and Pelletier, M., 2020. The impact and toxicity of glyphosate and glyphosate-based herbicides on health and immunity. *Journal of Immunotoxicology*, *17*(1), pp.163-174.

Peixoto, F., 2005. Comparative effects of the Roundup and glyphosate on mitochondrial oxidative phosphorylation. *Chemosphere*, 61(8), pp.1115-1122.

Pereira, Daniel A., and Alessandra Giani. "Cell density-dependent oligopeptide production in cyanobacterial strains." *FEMS microbiology ecology* 88, no. 1 (2014): 175-183.

Perotti, V.E., Larran, A.S., Palmieri, V.E., Martinatto, A.K., Alvarez, C.E., Tuesca, D. and Permingeat, H.R., 2019. A novel triple amino acid substitution in the EPSPS found in a high-level glyphosate-resistant Amaranthus hybridus population from Argentina. Pest management science, 75(5), pp.1242-1251.

Perry, E.D., Moschini, G. and Hennessy, D.A., 2016. Testing for complementarity: Glyphosate tolerant soybeans and conservation tillage. American Journal of Agricultural Economics, 98(3), pp.765-784.

Piasecki, C., Carvalho, I.R., Cechin, J., Goulart, F.A., Maia, L.C.D., Agostinetto, D., Caverzan, A., Stewart, C.N. and Vargas, L., 2019. Oxidative stress and differential antioxidant enzyme activity in glyphosate-resistant and-sensitive hairy fleabane in response to glyphosate treatment. *Bragantia*, *78*, pp.379-396.

Pichler, G., Stöggl, W., Candotto Carniel, F., Muggia, L., Ametrano, C.G., Holzinger, A., Tretiach, M. and Kranner, I., 2020. Abundance and Extracellular Release of Phytohormones

in Aero-terrestrial Microalgae (Trebouxiophyceae, Chlorophyta) As a Potential Chemical Signaling Source1. *Journal of phycology*, *56*(5), pp.1295-1307.

Pincelli-Souza, R.P., Bortolheiro, F.P., Carbonari, C.A., Velini, E.D. and Silva, M.D.A., 2020. Hormetic effect of glyphosate persists during the entire growth period and increases sugarcane yield. *Pest management science*, *76*(7), pp.2388-2394.

Pline, W.A., Wilcut, J.W., Duke, S.O., Edmisten, K.L. and Wells, R., 2002. Tolerance and accumulation of shikimic acid in response to glyphosate applications in glyphosate-resistant and nonglyphosate-resistant cotton (Gossypium hirsutum L.). *Journal of Agricultural and Food Chemistry*, *50*(3), pp.506-512.

Qiu, S., Fu, H., Zhou, R., Yang, Z., Bai, G. and Shi, B., 2020. Toxic effects of glyphosate on intestinal morphology, antioxidant capacity and barrier function in weaned piglets. *Ecotoxicology and environmental safety*, *187*, p.109846.

Radwan, D.E.M. and Fayez, K.A., 2016. Photosynthesis, antioxidant status and gas-exchange are altered by glyphosate application in peanut leaves. *Photosynthetica*, *54*(2), pp.307-316.

Raines, C.A. 2011. Increasing photosynthetic carbon assimilation in C_3 plants to improve crop yield: Current and future strategies. Plant Physiol. 155: 36-42.

Ratcliff, A.W., Busse, M.D. and Shestak, C.J., 2006. Changes in microbial community structure following herbicide (glyphosate) additions to forest soils. *Applied Soil Ecology*, *34*(2-3), pp.114-124.

Ravishankar, A., Pupo, A. and Gallagher, J.E., 2019. Thickening of the cell wall increases the resistance of S. cerevisiae to commercial formulations of glyphosate. *bioRxiv*, p.760694.

Razal, R.A., Ellis, S., Singh, S., Lewis, N.G. and Towers, G.N., 1996. Nitrogen recycling in phenylpropanoid metabolism. Phytochemistry, 41(1), pp.31-35.

Rintamäki, E., Salo, R. and Aro, E.M., 1994. Rapid turnover of the D1 reaction-center protein of photosystem II as a protection mechanism against photoinhibition in a moss, Ceratodon purpureus (Hedw.) Brid. *Planta*, *193*(4), pp.520-529.

Rochaix, J.D., 2011. Regulation of photosynthetic electron transport. *Biochimica et Biophysica Acta (BBA)-Bioenergetics*, *1807*(3), pp.375-383.

Romero, D.M., de Molina, M.C.R. and Juárez, Á.B., 2011. Oxidative stress induced by a commercial glyphosate formulation in a tolerant strain of Chlorella kessleri. *Ecotoxicology and Environmental Safety*, *74*(4), pp.741-747.

Rong-Mullins, X., Ravishankar, A., McNeal, K.A., Lonergan, Z.R., Biega, A.C., Creamer, J.P. and Gallagher, J.E., 2017. Genetic variation in Dip5, an amino acid permease, and Pdr5, a multiple drug transporter, regulates glyphosate resistance in S. cerevisiae. PLoS One, 12(11), p.e0187522.

Rotaru, A.E., Yee, M.O. and Musat, F., 2021. Microbes trading electricity in consortia of environmental and biotechnological significance. *Current Opinion in Biotechnology*, *67*, pp.119-129.

Rutherford, S.T. and Bassler, B.L., 2012. Bacterial quorum sensing: its role in virulence and possibilities for its control. *Cold Spring Harbor perspectives in medicine*, *2*(11), p.a012427.

Sammons, R.D. and Gaines, T.A., 2014. Glyphosate resistance: state of knowledge. Pest management science, 70(9), pp.1367-1377.

Saper, G., Kallmann, D., Conzuelo, F., Zhao, F., Tóth, T.N., Liveanu, V., Meir, S., Szymanski, J., Aharoni, A., Schuhmann, W. and Rothschild, A., 2018. Live cyanobacteria produce photocurrent and hydrogen using both the respiratory and photosynthetic systems. *Nature communications*, *9*(1), pp.1-9.

Schmid, J. and Amrhein, N., 1995. Molecular organization of the shikimate pathway in higher plants. *Phytochemistry*, *39*(4), pp.737-749.

Séguin, A., Mottier, A., Perron, C., Lebel, J.M., Serpentini, A. and Costil, K., 2017. Sub-lethal effects of a glyphosate-based commercial formulation and adjuvants on juvenile oysters (Crassostrea gigas) exposed for 35 days. *Marine pollution bulletin*, *117*(1-2), pp.348-358.

Sharif, D.I., Gallon, J., Smith, C.J. and Dudley, E.D., 2008. Quorum sensing in Cyanobacteria: N-octanoyl-homoserine lactone release and response, by the epilithic colonial cyanobacterium Gloeothece PCC6909. The ISME journal, 2(12), pp.1171-1182.

Shlosberg, Y., Eichenbaum, B., Tóth, T.N., Levin, G., Liveanu, V., Schuster, G. and Adir, N., 2021. NADPH performs mediated electron transfer in cyanobacterial-driven bio-photoelectrochemical cells. *Iscience*, *24*(1), p.101892.

Siegele, D.A., 2005. Universal stress proteins in Escherichia coli. *Journal of bacteriology*, *187*(18), pp.6253-6254.

SigmaAldrich.com. 2020. *Catalog: Glyphosate; Succinic acid.* MERCK, viewed 7 December 2020, <https://www.sigmaaldrich.com/catalog/>

Singh, B.K. and Shaner, D.L., 1998. Rapid determination of glyphosate injury to plants and identification of glyphosate-resistant plants. *Weed Technology*, pp.527-530.

Singh, H., Singh, N.B., Singh, A. and Hussain, I., 2017. Exogenous application of salicylic acid to alleviate glyphosate stress in Solanum lycopersicum. *International Journal of Vegetable Science*, *23*(6), pp.552-566.

Skeff, W., Neumann, C. and Schulz-Bull, D.E., 2015. Glyphosate and AMPA in the estuaries of the Baltic Sea method optimization and field study. Marine pollution bulletin, 100(1), pp.577-585.

Soares, C., Pereira, R., Martins, M., Tamagnini, P., Serôdio, J., Moutinho-Pereira, J., Cunha, A. and Fidalgo, F., 2020. Glyphosate-dependent effects on photosynthesis of Solanum lycopersicum L.–an ecophysiological, ultrastructural and molecular approach. *Journal of Hazardous Materials*, p.122871.

Sparks, T.C. and Lorsbach, B.A., 2017. Perspectives on the agrochemical industry and agrochemical discovery. *Pest management science*, *73*(4), pp.672-677.

Stanier, R.Y., Kunisawa, R., Mandel, M.C.B.G. and Cohen-Bazire, G., 1971. Purification and properties of unicellular blue-green algae (order Chroococcales). Bacteriological reviews, 35(2), pp.171-205.

Steinhauser, D., Fernie, A.R. and Araújo, W.L., 2012. Unusual cyanobacterial TCA cycles: not broken just different. *Trends in plant science*, 17(9), pp.503-509.

Steinrücken, H.C. and Amrhein, N., 1980. The herbicide glyphosate is a potent inhibitor of 5-enolpyruvylshikimic acid-3-phosphate synthase. *Biochemical and biophysical research communications*, *94*(4), pp.1207-1212.

Stenger, K.S., 2019. Identification of the response pathways of Escherichia coli and Enterococcus faecalis to glyphosate and it's major breakdown product Aminomethyl phosphonic acid (AMPA) (Doctoral dissertation, North-West University (South Africa)).

Sun, K., Liu, W., Liu, L., Wang, N. and Duan, S., 2013. Ecological risks assessment of organophosphorus pesticides on bloom of Microcystis wesenbergii. *International Biodeterioration & Biodegradation*, *77*, pp.98-105.

Sura, S., Waiser, M., Tumber, V., Lawrence, J.R., Cessna, A.J. and Glozier, N., 2012. Effects of glyphosate and two herbicide mixtures on microbial communities in prairie wetland ecosystems: a mesocosm approach. Journal of environmental quality, 41(3), pp.732-743.

Sweetlove, L.J., Beard, K.F., Nunes-Nesi, A., Fernie, A.R. and Ratcliffe, R.G., 2010. Not just a circle: flux modes in the plant TCA cycle. *Trends in plant science*, 15(8), pp.462-470.

Sylwestrzak, Z., Zgrundo, A. and Pniewski, F., 2021. Ecotoxicological studies on the effect of Roundup®(glyphosate formulation) on marine benthic microalgae. *International Journal of Environmental Research and Public Health*, *18*(3), p.884.

Tamburino, R., Vitale, M., Ruggiero, A., Sassi, M., Sannino, L., Arena, S., Costa, A., Batelli, G., Zambrano, N., Scaloni, A. and Grillo, S., 2017. Chloroplast proteome response to drought stress and recovery in tomato (Solanum lycopersicum L.). BMC plant biology, 17(1), pp.1-14.

Tan, Y., Zhang, Q.S., Zhao, W., Liu, Z., Ma, M.Y., Zhong, M.Y. and Wang, M.X., 2020. The highly efficient NDH-dependent photosystem I cyclic electron flow pathway in the marine angiosperm Zostera marina. *Photosynthesis research*, *144*(1), pp.49-62.

Tang, J., Zhu, Z., He, H., Liu, Z., Xia, Z., Chen, J., Hu, J., Cao, L., Rang, J., Shuai, L. and Liu, Y., 2021. Bacterioferritin: a key iron storage modulator that affects strain growth and butenyl-spinosyn biosynthesis in Saccharopolyspora pogona. *Microbial cell factories*, *20*(1), pp.1-16.

Tian, L., Nawrocki, W.J., Liu, X., Polukhina, I., Van Stokkum, I.H. and Croce, R., 2019. pH dependence, kinetics and light-harvesting regulation of nonphotochemical quenching in Chlamydomonas. *Proceedings of the National Academy of Sciences*, *116*(17), pp.8320-8325.

Tikhonov, A.N., 2012. Energetic and regulatory role of proton potential in chloroplasts. *Biochemistry (Moscow)*, *77*(9), pp.956-974.

Titiz, O., Tambasco-Studart, M., Warzych, E., Apel, K., Amrhein, N., Laloi, C. and Fitzpatrick, T.B., 2006. PDX1 is essential for vitamin B6 biosynthesis, development and stress tolerance in Arabidopsis. *The Plant Journal*, *48*(6), pp.933-946.

Tohge, T., Watanabe, M., Hoefgen, R. and Fernie, A.R., 2013. Shikimate and phenylalanine biosynthesis in the green lineage. *Frontiers in plant science*, *4*, p.62.

Tzin, V., Galili, G. and Aharoni, A., 2012. Shikimate pathway and aromatic amino acid biosynthesis. *eLS*.

Ugarte, R., 2014. Interaction between glyphosate and mitochondrial succinate dehydrogenase. *Computational and Theoretical Chemistry*, 1043, pp.54-63.

Van Horn, C.R., Moretti, M.L., Robertson, R.R., Segobye, K., Weller, S.C., Young, B.G., Johnson, W.G., Schulz, B., Green, A.C., Jeffery, T. and Lespérance, M.A., 2018. Glyphosate resistance in Ambrosia trifida: Part 1. Novel rapid cell death response to glyphosate. *Pest management science*, *74*(5), pp.1071-1078.

Van Stempvoort, D.R., Roy, J.W., Brown, S.J. and Bickerton, G., 2014. Residues of the herbicide glyphosate in riparian groundwater in urban catchments. Chemosphere, 95, pp.455-463.

Vanlaeys, A., Dubuisson, F., Seralini, G.E. and Travert, C., 2018. Formulants of glyphosate-based herbicides have more deleterious impact than glyphosate on TM4 Sertoli cells. *Toxicology in Vitro*, *52*, pp.14-22.

Vera, M.S., Lagomarsino, L., Sylvester, M., Pérez, G.L., Rodríguez, P., Mugni, H., Sinistro, R., Ferraro, M., Bonetto, C., Zagarese, H. and Pizarro, H., 2010. New evidences of Roundup®(glyphosate formulation) impact on the periphyton community and the water quality of freshwater ecosystems. Ecotoxicology, 19(4), pp.710-721.

Vinyard, D.J., Ananyev, G.M. and Charles Dismukes, G., 2013. Photosystem II: the reaction center of oxygenic photosynthesis. *Annual review of biochemistry*, *82*, pp.577-606.

Wang, L., Liang, W., Xing, J., Tan, F., Chen, Y., Huang, L., Cheng, C.L. and Chen, W., 2013. Dynamics of chloroplast proteome in salt-stressed mangrove Kandelia candel (L.) Druce. *Journal of proteome research*, *12*(11), pp.5124-5136.

Wang, Y., Kroon, J.K.M, Slabas, A.R. and Chivasa, S., 2013. Proteomics reveals new insights into the role of light in cadmium response in *Arabidopsis* cell suspension cultures. Proteomics 13, 1145–1158.

Wobbe, L. and Remacle, C., 2015. Improving the sunlight-to-biomass conversion efficiency in microalgal biofactories. *Journal of biotechnology*, *201*, pp.28-42.

Wu, N., Dong, X., Liu, Y., Wang, C., Baattrup-Pedersen, A. and Riis, T., 2017. Using river microalgae as indicators for freshwater biomonitoring: Review of published research and future directions. Ecological Indicators, 81, pp.124-131.

Wu, T., Kerbler, S.M., Fernie, A.R. and Zhang, Y., 2021. Plant cell cultures as heterologous bio-factories for secondary metabolite production. Plant communications, 2(5), p.100235.

Xiao, M., Li, M. and Reynolds, C.S., 2018. Colony formation in the cyanobacterium Microcystis. *Biological Reviews*, *93*(3), pp.1399-1420.

Xu, S., Liu, Y., Zhang, J. and Gao, B., 2021. Proteomic mechanisms for the combined stimulatory effects of glyphosate and antibiotic contaminants on Microcystis aeruginosa. *Chemosphere*, *267*, p.129244.

Yang, Y., Ding, Y., Hu, Y., Cao, B., Rice, S.A., Kjelleberg, S. and Song, H., 2015. Enhancing bidirectional electron transfer of Shewanella oneidensis by a synthetic flavin pathway. *ACS synthetic biology*, *4*(7), pp.815-823.

Ye, J., Huang, C., Qiu, Z., Wu, L. and Xu, C., 2019. The growth, apoptosis and oxidative stress in Microcystis viridis exposed to glyphosate. *Bulletin of environmental contamination and toxicology*, *103*(4), pp.585-589.

Yu, Y., Zhang, Q., Liu, G., Deng, Y., Kang, J., Zhang, F., Lu, T., Sun, L. and Qian, H., 2021. Proteomic analysis of zebrafish brain damage induced by Microcystis aeruginosa bloom. *Science of The Total Environment*, *795*, p.148865.

Zhai, C., Zhang, P., Shen, F., Zhou, C. and Liu, C., 2012. Does Microcystis aeruginosa have quorum sensing?. FEMS microbiology letters, 336(1), pp.38-44.

Zhang, H., Kang, S., Li, J., Li, Z., Chang, J., Xu, Y., Lu, G.M. and Sun, C., 2021. Near zero-waste biofuel production from bioderived polyhydroxybutyrate. *Fuel*, *286*, p.119405.

Zhang, P., Eisenhut, M., Brandt, A.M., Carmel, D., Silén, H.M., Vass, I., Allahverdiyeva, Y., Salminen, T.A. and Aro, E.M., 2012. Operon flv4-flv2 provides cyanobacterial photosystem II with flexibility of electron transfer. *The Plant Cell*, *24*(5), pp.1952-1971.

Zhang, Q., Qu, Q., Lu, T., Ke, M., Zhu, Y., Zhang, M., Zhang, Z., Du, B., Pan, X., Sun, L. and Qian, H., 2018. The combined toxicity effect of nanoplastics and glyphosate on Microcystis aeruginosa growth. Environmental Pollution, 243, pp.1106-1112.

Zhang, Y., Calabrese, E.J., Zhang, J., Gao, D., Qin, M. and Lin, Z., 2020. A trigger mechanism of herbicides to phytoplankton blooms: From the standpoint of hormesis involving cytochrome b559, reactive oxygen species and nitric oxide. *Water research*, *173*, p.115584.

Zhao, L., Xie, L., Huang, J., Su, Y. and Zhang, C., 2020. Proper Glyphosate Application at Post-anthesis Lowers Grain Moisture Content at Harvest and Reallocates Non-structural Carbohydrates in Maize. *Frontiers in plant science*, *11*, p.2018.

Zhao, L., Zhu, R., Liu, Y., Liu, C., Jiang, P., Song, Y., Luo, Y., Lei, A. and Wang, J., 2020. Extracellular Vesicles: A Novel Messenger of Unicellular Microalgae Communication? (Pre-Print). DOI: 10.21203/rs.3.rs-38027/v1 (Accessed 21/01/2022)

Appendix

I. Protein quality control gel

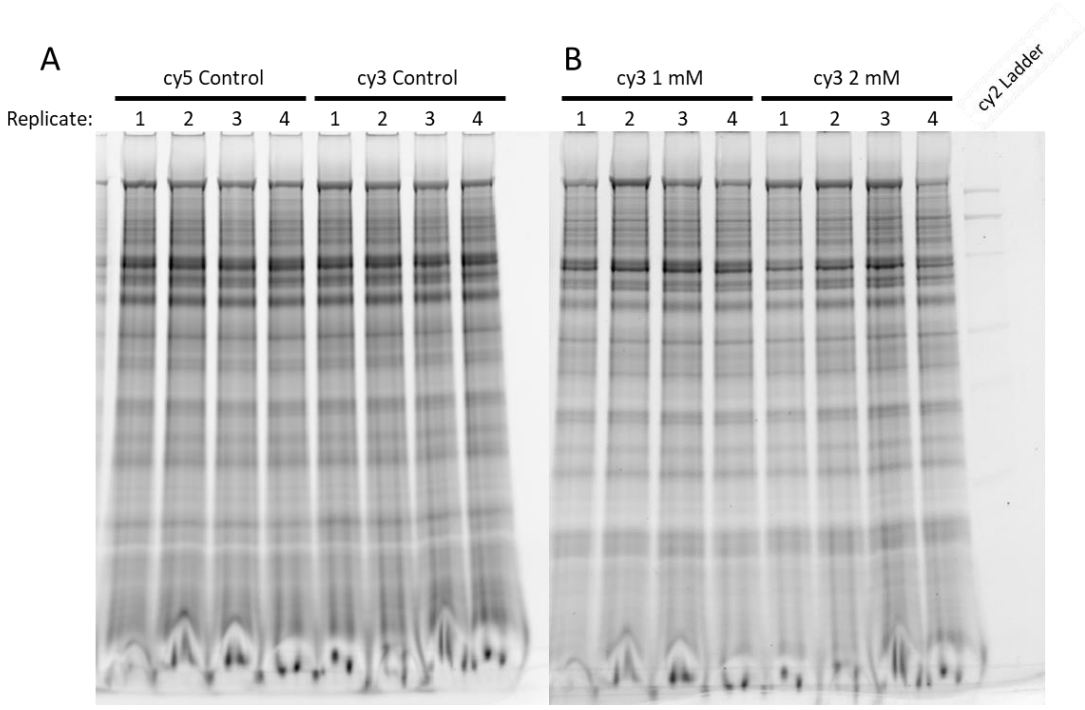

Figure S1. 1D protein gel for quality control check of ITRAQ samples. Protein samples were labelled with fluorescent dyes and separated by SDS-PAGE. (A) Cy3- or Cy5-labelled 4 biological replicate control samples. (B) Cy3-labelled biological replicates from samples treated with 1 mM or 2 mM glyphosate.

II. ITRAQ full data table

Table S1. Full ITRAQ analysis results table. Proteins are arranged alphabetically by submitted name.

Accession [a]	Protein Name	1mM glyphosate		2mM glyphosate	
		Ratio[b]	*p*-value[c]	Ratio[b]	*p*-value[c]
sp|P73530|RS1A_SYNY3	30S ribosomal protein S1 homolog A	-1.11	0.36	-1.30	0.01
sp|P74226|RS10_SYNY3	30S ribosomal protein S10	-1.01	0.93	-1.45	0.02
sp|P74071|RS2_SYNY3	30S ribosomal protein S2	1.29	0.06	1.29	0.00
sp|P73636|RS6_SYNY3	30S ribosomal protein S6	1.22	0.02	1.23	0.03
sp|P73910|HSLO_SYNY3	33 kDa chaperonin	-1.50	0.16	-1.67	0.03
sp|P73294|RL13_SYNY3	50S ribosomal protein L13	-1.14	0.56	-1.61	0.03
sp|P73310|RL14_SYNY3	50S ribosomal protein L14	-1.46	0.01	-1.40	0.04
sp|P73289|RL25_SYNY3	50S ribosomal protein L25	-1.06	0.56	-1.62	0.00
sp|P73320|RL3_SYNY3	50S ribosomal protein L3	-1.27	0.09	-1.53	0.04
sp|P73308|RL5_SYNY3	50S ribosomal protein L5	-1.03	0.83	-1.16	0.01
sp|P23349|RL7_SYNY3	50S ribosomal protein L7/L12	1.22	0.07	1.38	0.00
sp|Q05972|CH601_SYNY3	60 kDa chaperonin 1	1.05	0.57	1.49	0.00
sp|P22034|CH602_SYNY3	60 kDa chaperonin 2	-1.15	0.13	1.25	0.01
sp|P73826|PHAB_SYNY3	Acetoacetyl-CoA reductase	1.60	0.01	-1.05	0.84
sp|P74008|SAHH_SYNY3	Adenosylhomocysteinase	1.12	0.35	1.26	0.00
sp|P73302|KAD1_SYNY3	Adenylate kinase 1	1.20	0.09	1.29	0.00
sp|Q01951|PHAA_SYNY3	Allophycocyanin alpha chain	1.35	0.02	1.33	0.00
sp|Q01952|APCB_SYNY3	Allophycocyanin beta chain	1.77	0.01	1.81	0.00
tr|Q55387|Q55387_SYNY3	ANF_receptor domain-containing protein (Periplasmic binding protein of ABC transporter for natural amino acids)	-1.02	0.93	-1.89	0.01
tr|P73609|P73609_SYNY3	Anti-sigma factor antagonist	1.26	0.24	1.62	0.00
sp|P74122|ARGJ_SYNY3	Arginine biosynthesis bifunctional protein ArgJ	-1.01	0.95	-1.38	0.02
sp|P27181|ATPF_SYNY3	ATP synthase subunit b	-1.16	0.07	-1.18	0.01
sp|P26527|ATPB_SYNY3	ATP synthase subunit beta	1.01	0.93	-1.09	0.05
sp|Q55700|FTSH2_SYNY3	ATP-dependent zinc metalloprotease FtsH 2	1.10	0.81	1.56	0.01
sp|P72991|FTSH3_SYNY3	ATP-dependent zinc metalloprotease FtsH 3	-1.82	0.21	1.32	0.03
tr|P73287|P73287_SYNY3	Bacterioferritin	1.95	0.04	-1.06	0.77
sp|Q55460|CMPA_SYNY3	Bicarbonate-binding protein CmpA	-1.03	0.62	-1.28	0.02
tr|Q55776|Q55776_SYNY3	Biotin_lipoyl_2 domain-containing protein	-1.31	0.11	-1.36	0.01

tr|P73196|P73196_SYNY3	BRCT domain-containing protein	1.16	0.13	1.28	0.01
sp|P72760|CCMK1_SYNY3	Carbon dioxide-concentrating mechanism protein CcmK homolog 1	1.14	0.23	1.19	0.04
tr|P72864|P72864_SYNY3	CcmA Carboxysome formation protein	-1.39	0.01	-1.05	0.33
sp|P73407|CCMK4_SYNY3	CcmK Carbon dioxide-concentrating mechanism protein CcmK homolog 4	1.54	0.01	-1.25	0.45
tr|P72758|P72758_SYNY3	CcmM Carbon dioxide concentrating mechanism protein CcmM	-1.22	0.00	-1.10	0.37
sp|P73456|FTSZ_SYNY3	Cell division protein FtsZ	-1.11	0.36	-1.25	0.04
tr|P73654|P73654_SYNY3	CP12 domain-containing protein	-1.31	0.19	-1.28	0.01
sp|Q54714|PHCB_SYNY3	C-phycocyanin beta chain	1.42	0.44	-1.18	0.00
sp|P09190|PSBE_SYNY3	Cytochrome b559 subunit alpha (PSIIE)	-1.36	0.17	-2.15	0.01
sp|P26290|UCRIB_SYNY3	Cytochrome b6-f complex iron-sulfur subunit 2	1.28	0.01	-1.02	0.91
sp|P73821|SERA_SYNY3	D-3-phosphoglycerate dehydrogenase	-1.13	0.04	1.40	0.00
sp|P73922|FBSB_SYNY3	D-fructose 1,6-bisphosphatase class 2/sedoheptulose 1,7-bisphosphatase	1.27	0.01	1.20	0.01
tr|P73605|P73605_SYNY3	DJ-1_PfpI domain-containing protein	1.45	0.13	1.19	0.04
tr|P73200|P73200_SYNY3	DUF1995 domain-containing protein	1.21	0.03	-1.09	0.78
sp|Q55119|EFP_SYNY3	Elongation factor P	-1.12	0.20	-1.18	0.03
sp|P77972|ENO_SYNY3	Enolase	-1.30	0.10	-1.30	0.00
sp|P73467|Y1223_SYNY3	Epimerase family protein slr1223	-1.15	0.34	1.40	0.04
sp|P27320|FER_SYNY3	Ferredoxin-1	-1.08	0.72	-1.59	0.01
sp|Q55318|FENR_SYNY3	FNR -Ferredoxin--NADP reductase	1.13	0.01	-1.068	0.49
sp|Q55664|ALF2_SYNY3	Fructose-bisphosphate aldolase class 2	1.19	0.06	1.722	0.00
tr|P72586|P72586_SYNY3	GDP-mannose 4,6-dehydratase	1.03	0.70	1.135	0.00
tr|P73704|P73704_SYNY3	General secretion pathway protein G	-1.87	0.01	-2.321	0.00
sp|P52983|G6PI_SYNY3	Glucose-6-phosphate isomerase	1.21	0.08	1.233	0.04
sp|P77961|GLN1B_SYNY3	Glutamine synthetase	1.16	0.34	1.375	0.03
sp|P80505|G3P2_SYNY3	Glyceraldehyde-3-phosphate dehydrogenase 2 (GADPH)	1.50	0.00	1.609	0.01
tr|P73862|P73862_SYNY3	HTH lysR-type domain-containing protein	-1.34	0.11	-1.414	0.01

sp|P80507|IPYR_SYNY3	Inorganic pyrophosphatase	1.50	0.01	2.184	0.00
sp|P72827|FUTA1_SYNY3	Iron uptake protein A1	-1.25	0.02	-1.614	0.00
sp|Q55835|FUTA2_SYNY3	Iron uptake protein A2	-1.34	0.03	-1.178	0.01
sp|P80046|IDH_SYNY3	Isocitrate dehydrogenase [NADP]	1.49	0.00	1.440	0.01
sp|P29107|ILVC_SYNY3	Ketol-acid reductoisomerase (NADP(+))	-1.27	0.01	-1.589	0.00
sp|P73954|Y1513_SYNY3	Membrane-associated protein slr1513	1.54	0.00	-1.083	0.45
tr|P73736|P73736_SYNY3	MurNAc-LAA domain-containing protein	-1.32	0.21	-1.456	0.00
tr|Q6YRU4|Q6YRU4_SYNY3	N-acetyltransferase domain-containing protein	1.49	0.11	1.648	0.05
sp|P26525|NDHI_SYNY3	NAD(P)H-quinone oxidoreductase subunit I	1.26	0.00	1.304	0.01
sp|P74102|OCP_SYNY3	OCP Orange carotenoid-binding protein	-1.29	0.11	-1.721	0.00
tr|P74314|P74314_SYNY3	OmpR subfamily	-1.15	0.05	-1.266	0.05
tr|P74625|P74625_SYNY3	PBS-linker domain-containing protein	-1.35	0.16	-1.565	0.03
tr|P73093|P73093_SYNY3	PBS-linker domain-containing protein	-1.36	0.26	-1.442	0.00
sp|P73789|PPI2_SYNY3	Peptidyl-prolyl cis-trans isomerase slr1251	1.34	0.02	-1.039	0.53
sp|P73728|PRX5_SYNY3	Peroxiredoxin sll1621	1.12	0.16	1.252	0.01
sp|P74421|PGK_SYNY3	Phosphoglycerate kinase	1.05	0.66	1.327	0.01
sp|P29256|PSAF_SYNY3	Photosystem I reaction center subunit III (PSAF)	1.63	0.01	-1.538	0.10
sp|P73203|PYR1_SYNY3	Phycobilisome 32.1 kDa linker polypeptide, phycocyanin-associated, rod 1	1.22	0.19	-1.335	0.00
sp|P21697|PLAS_SYNY3	Plastocyanin	1.21	0.07	1.387	0.00
sp|P72659|PNP_SYNY3	Polyribonucleotide nucleotidyltransferase	-1.06	0.55	-1.257	0.00
sp|P74467|CLPP3_SYNY3	Probable ATP-dependent Clp protease proteolytic subunit 3	-1.14	0.09	-1.470	0.00
sp|P54691|ILVE_SYNY3	Probable branched-chain-amino-acid aminotransferase	1.16	0.33	2.134	0.00
sp|P72704|PPI1_SYNY3	Probable peptidyl-prolyl cis-trans isomerase sll0227	-1.21	0.21	-1.251	0.05
sp|Q55233|DRGA_SYNY3	Protein DrgA	-1.03	0.87	1.216	0.00
sp|P74466|CLPR_SYNY3	Putative ATP-dependent Clp protease proteolytic subunit-like	1.00	0.99	-1.291	0.01
sp|P73790|PHS_SYNY3	Putative pterin-4-alpha-carbinolamine dehydratase	1.19	0.18	1.551	0.04

sp|Q55118|PPI3_SYNY3	Putative thylakoid lumen peptidyl-prolyl cis-trans isomerase sll0408	-1.27	0.01	-1.611	0.00
sp|P72776|PDXJ_SYNY3	Pyridoxine 5'-phosphate synthase	2.13	0.02	-1.058	0.66
sp|P74211|PDXH_SYNY3	Pyridoxine/pyridoxamine 5'-phosphate oxidase	-1.18	0.52	-1.405	0.01
tr|P73405|P73405_SYNY3	Pyruvate dehydrogenase E1 component subunit beta	-1.06	0.83	1.651	0.00
tr|P73348|P73348_SYNY3	Rehydrin	1.19	0.13	1.475	0.00
sp|Q55848|KPRS_SYNY3	Ribose-phosphate pyrophosphokinase	-1.07	0.79	-1.176	0.02
sp|P74518|HPF_SYNY3	Ribosome hibernation promotion factor	1.33	0.03	-1.164	0.08
sp|P54205|RBL_SYNY3	Ribulose bisphosphate carboxylase large chain	1.50	0.09	1.762	0.00
sp|P54206|RBS_SYNY3	Ribulose bisphosphate carboxylase small subunit	1.33	0.03	1.568	0.00
tr|P73557|P73557_SYNY3	RRM domain-containing protein (RNA recognition motif)	-2.08	0.34	-1.764	0.03
sp|P72871|METK_SYNY3	S-adenosylmethionine synthase	-1.20	0.42	1.339	0.01
tr|P73409|P73409_SYNY3	SLH domain-containing protein	1.23	0.29	1.350	0.03
tr|P73488|P73488_SYNY3	Sll1130 protein (Uncharacterised Toxin)	1.15	0.02	-1.228	0.06
tr|P72807|P72807_SYNY3	Sll1663 protein	-1.20	0.26	-1.599	0.01
tr|P73600|P73600_SYNY3	Sll1785 protein	-1.47	0.03	-1.217	0.10
tr|P73111|P73111_SYNY3	Sll1835 protein	-1.01	0.93	-1.239	0.04
tr|P72700|P72700_SYNY3	Slr0244 (Similar to universal stress protein) protein	1.76	0.01	2.183	0.00
tr|P72709|P72709_SYNY3	slr0250 - OstA (Organic Solute transporter alpha)-like_N domain-containing protein	-1.19	0.23	3.231	0.02
tr|Q55590|Q55590_SYNY3	Slr0376 protein	1.44	0.02	-1.333	0.14
tr|P74375|P74375_SYNY3	Slr0442 protein	1.27	0.09	1.395	0.00
tr|Q55436|Q55436_SYNY3	Slr0848 protein	-1.14	0.36	-1.252	0.03
tr|P72839|P72839_SYNY3	Slr1301 protein	1.19	0.08	-1.221	0.00
tr|P73603|P73603_SYNY3	Slr1852 (Specific to synechocystis genus) protein	1.18	0.11	1.471	0.02
tr|P73328|P73328_SYNY3	Slr1900 protein	-1.05	0.54	-1.759	0.01
tr|P74426|P74426_SYNY3	Slr1940 (Collagen like) protein	1.56	0.03	-1.115	0.31
tr|P74500|P74500_SYNY3	Slr1940 protein	1.00	0.98	-1.533	0.02
tr|P73244|P73244_SYNY3	Slr2025 (ybjN domain containing) protein (possible oxidoreductase)	-1.20	0.37	-2.328	0.01
tr|P73489|P73489_SYNY3	Ssl2245 protein	1.24	0.03	-1.413	0.07

tr|P74769|P74769_SYNY3	Ssr1528 protein	1.22	0.01	1.394	0.00
sp|P77968|SODF_SYNY3	Superoxide dismutase [Fe]	1.51	0.00	1.784	0.02
tr|P73091|P73091_SYNY3	TPR_REGION domain-containing protein	-1.47	0.04	-1.233	0.30
tr|P72688|P72688_SYNY3	Transcription termination/antiterminati on protein NusA	-1.08	0.43	-1.184	0.04
tr|P73282|P73282_SYNY3	Transketolase	1.14	0.15	1.286	0.00
sp|Q55511|TIG_SYNY3	Trigger factor	-1.23	0.04	-2.005	0.00
sp|Q55707|Y617_SYNY3	Uncharacterized protein sll0617	-1.14	0.14	-1.334	0.01
sp|P73392|Y1735_SYNY3	Uncharacterized protein sll1735	1.04	0.93	1.508	0.01
sp|P73321|Y1894_SYNY3	Uncharacterized protein slr1894	1.10	0.15	1.321	0.05
tr|P73592|P73592_SYNY3	Uncharacterized Slr1406 protein	1.53	0.03	-1.398	0.14
tr|P74470|P74470_SYNY3	Uncharacterized Ssl0242 protein (Exclusive to cyanobacteria)	1.54	0.01	-1.134	0.63
sp|P54224|DCUP_SYNY3	Uroporphyrinogen III decarboxylase	2.24	0.05	-1.120	0.50

[a] Protein accession number in the UniProt database.

[b] Ratio of the comparison of protein abundance in control to glyphosate-treated samples. This is equivalent to the protein fold-change. Negative values indicate protein down-regulation in glyphosate treatments.

[c] Probability value from Student's t-test analysis for comparing the control mean to the glyphosate sample mean.

III. DNA Primers list and specifity

Table S2. DNA primers used for PCR analysis of Synechocystis genes.

Gene Abbreviations	DNA Sequences	
	Forward Primer (5’ – 3’)	Reverse Primer (3’ – 5’)
OSTA	CTATCCTGCGCGGAATTTGC	CCGTCCTGGAGCACATAGAC
ACCase	AGCGGATCAAAAGTGGACGG	TGACTGCATCTCCCACTTCC
680316s	AGCTCGGGTGATCGACATTG	ATGGGTGGAATCCAACAGGG
ATPbeta	AAGTATCGGCTCTGTTGGGC	GGAACCTTCCTTGGTGGAGG
OCP	GTAAGGACGGCAAACGCATC	AGGACAGTGGCATTGGTCAC
PSIIE	TGGTTGGTTGTTTGTCAGCAC	GAATGGGCAACTCTTGACGG
PsaA	CACCGTGACGCCATCATTTC	GAGAACATGTCCTGGGGACG
PsaF	TGACCCCCTGTAGCGAAAAC	GTTCCGCCCGAATTTTACCG
PSIID2	CCGCTGGTTCCAAATTGGTG	GGGACGAATGCCTACCAGAC
SDH2	TTCTGGGACGACTTGGAACG	GTTTTTCCCTTTCCGCTGGG
NDH1	ACTGTCCCACAAACTGCCTC	CTTCCCAAAGCCACGTTGTC
ENOL	TGCCGGTACCGATGATGAAC	TAAAGGTTTCTGCCCCCACC
TKL	CAACCCATTGAAGTGCTGGC	TTGTAGGCACCGGAGGTTTC
RBCL	GTTTCACTGCCAACACCACC	TTCTGACGGTCAACTACGGC
RBCS	ACTTTACCCAAAGAGCGCCG	CCGGGAATAAAGCCCTGGTC
DAHPS	CATGATTGTGGAAACGGCCC	TCCCCATGACCTTGGAAAGC
EPSPS	CGATGATTCCCTCCGTCACC	GCAAACTTGCCGTTACTCCG

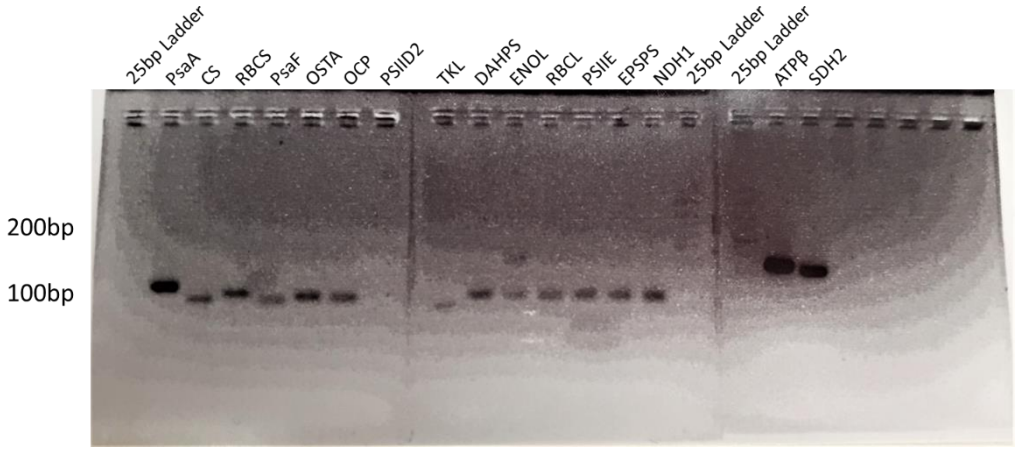

Figure S2. Gel image of PCR product from multiple primer pairs. Synechocystis cDNA was used as a template in endpoint PCR reactions using the primer pairs in Table S2 in each separate reaction. The products were separated by DNA electrophoresis in a 3.5% agarose gel. Th 25 bp DNA ladder and product from the PSIID2 primers are faint in this gel because the really high level of PCR product in the other samples necessitated use of a very short exposure in the imaging camera. With the exception of enolase (ENOL), all reactions show specific bands within the range (75-150 bp). Each PCR product matched the expected size from the cDNA sequences. Numbers and arrows on the left indicate the size (in base pairs) and position of DNA ladder bands. Primers for 16S rRNA and ACCase were excluded from this analysis as they had already been tested and used in our laboratory in a previous project. snENOL was excluded from further study due to nonspecific

binding. All other primers produced sufficient solid bands between 150 and 75 base pairs, albeit PSIID2 was too faint to be visible in the presence of other primers. The ladder solution was also difficult to see due to faintness in comparison to other primers. Upon QPCR analysis (see 2.4.5), snPSAF was unable to produce consistent data, foldchanges of 9.6 and 0.4 occurred on the same timepoint and was thereby excluded from the results.

IV. RNA Sample quality control

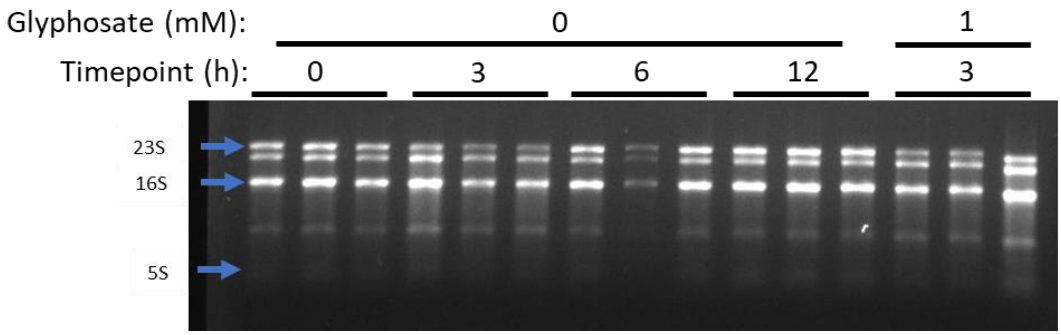

Figure S3. Representative gel image of Synechocystis total RNA. RNA samples were separated by electrophoresis in a 1% agarose gel and the ethidium bromide-stained RNA visualised by imaging under UV-illumination. The particular samples in this image were derived from *Synechocystis sp.* PCC6803 cells harvested at 0, 3, 6 and 12 hours after mock-treatment. Number indicates size of RNA in Svedberg units.